Technological University Dublin

ARROW@TU Dublin

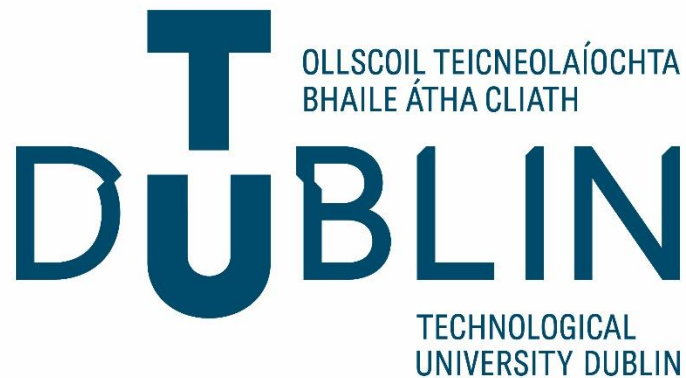**Doctoral**   **Science**

2019

Development and Diagnostics of Novel Non-Thermal PlasmaTreatment Systems

Laurence Scally
Technological University Dublin

Development and Diagnostics of Novel Non-Thermal Plasma Treatment Systems

Laurence Scally

This thesis is submitted in fulfilment as part of the requirements of a PhD

Supervisors

Prof. Patrick J. Cullen

Prof. Hugh J. Byrne

Dr Vladimir Milosavljevic

Technological University Dublin
School of Food Science and Environmental Health
2019

Abstract

Non-thermal plasma (NTP) has been a point of interest in many areas over the last few decades. Much research has been, and continues to be undertaken, to understand the fundamentals of plasma discharges. This is such a broad topic due to the very nature and variable dependencies that set the conditions for plasma discharge to occur. This can come in the form of electrode geometry and spacing, dielectric barrier thickness, humidity of environment, material selection for electrodes and dielectric barriers, the power supply used, and the operating gas(es) used. A lot of these influencing factors can be set and kept constant, but still result in variation from system to system. However, the most important aspect comes from the power supply used and the gas(es) employed as the operating environment for plasma discharge. The power supply is important as there can be multiple variables applied to generate plasma and varying each one can have a significant impact on how it behaves. Examples of such parameters include the frequency, duty cycle, voltage, current, and the number of pulses per unit time for the associate power. Gas supplies create the potential for certain chemistries to arise that allow for the processing of many types of samples. For these reasons, it is crucial that diagnostics and monitoring continue to be carried out on the many plasma systems available and currently under development so that the understanding of the multitude of possibilities that arise when using NTP for application purposes can be furthered and set with more confidence. By doing this, not only are the processes and physical properties of plasma better understood, but the mechanisms and reasons for the changes in surface properties, food modification, or biological responses are better elucidated, enabling more efficient application methods to be developed.

Chapter 3 highlights how the use of different gases for plasma generation impacts the surface morphology of polyethylene terephthalate. The use of ambient air, argon and CO_2 shows how different gas chemistries interact and change the surface properties of the polymer being treated and that those with the largest oxygen content provide the highest changes in surface characteristics. Chapter 4 delves more deeply into the physics of the gas chemistry of a helical dielectric barrier discharge system. What was found in This Study was that a gas mixture of Ar and He at a ratio of 10:1 respectively generated the most amount of nitrogen at a voltage of 27 kV when compared to other ratios of Ar and He in ambient air within the contained system. This gave a better understanding of the energetics, reaction mechanisms, and transfer pathways that occur within the plasma discharge. Chapter 5 showed, through the use of optical and Raman spectroscopy, the main reactive species responsible for enhancing the degradation of low-density polyethylene. The treatment of low-density polyethylene was carried out with plasma that used ambient air and a gas mixture of ambient air that contained ~4% CO_2. The results from the optical spectroscopy and Raman measurements led to the conclusion that an increase in reactive oxygen species created a more polar surface that gave rise to better bacterial cell adhesion post-treatment due to formation of more open sites on the polymer surface. The studies of Chapter 6 show that there is a strong dependency on the plasma gas chemistry and the discharge frequency being used. By altering the discharge frequency, the level of reactive nitrogen species can be controlled without altering the atmospheric conditions of the system. The optimum setting to generate high levels of reactive oxygen and reactive nitrogen species are, a power supply setting of 240 V, 91 μs, and a discharge

frequency of 1000 Hz. By treating human cancer cell lines with the plasma discharge, an increased level of cytotoxicity was found to be induced.

Declaration

I declare that this thesis which I now submit for the examination is entirely my own work and has not been taken from the work of others, save to the extent that such work has been cited and acknowledged within the text of my work. I also declare that I have adhered to all principles of academic's honesty and integrity and have not misrepresented or fabricated or falsified any idea/data/fact/source in any submission.

This thesis was prepared according to the regulations for postgraduate study by research of Technological University Dublin and has not been submitted in whole or in part for another award in any institute.

The work reported on in this thesis conforms to the principles and requirements of the Institute's guidelines for ethics in research.

The Technological University Dublin has permission to keep, lend or copy this thesis in whole or in part, on condition that any such use of the material or the thesis is duly acknowledged.

Laurence Scally   Date: 31/01/2018

Acknowledgement

I wish to express my gratitude to my supervisors Prof. Hugh Byrne and Dr Patrick J. Cullen for their continuous and excellent guidance and support throughout my research work, and also for allowing me to have the freedom to follow various ideas.

I am also very grateful to Mr. James Lalor for sharing his knowledge and for helping me with my laboratory work and taking the time to train me on various fabrication processes of materials. I would also like to extend my gratitude to Mr. Miroslav Gulan who answered many of my questions about electrical analysis and setups.

On a more personal note I would like to thank my parents, family members, and friends. They have always supported and encouraged me with their best wishes and lending their ears to listen to me whenever I had a problem or doubted myself. Finally I would like to convey my deepest gratitude to my partner, Róisín, who has stood by me and supported me continuously throughout everything and has put up with my many late nights and busy schedule with the understanding and patience of a saint.

Table of Contents

List of Figures

List of Tables

Abbreviations

AC	Alternating Current
AFM	Atomic Force Microscopy
APPJ	Atmospheric Pressure Plasma Jet
BTF	Bio-Trickling Filtration
CCD	Charge-Coupled Device
CFU	Colony-Forming Unit
CNC	Computer Numerical Controlled
CRC	Colorectal Cancer
DBD	Dielectric Barrier Discharge
DC	Direct Current
DI	Deionised
DMEM	Dulbecco's Modified Eagle's Cell Culture Medium
DNA	Deoxyribonucleic Acid
DSC	Differential Scanning Calorimetry
EEDF	Electron Energy Distribution Function
FBS	Fetal Bovine Serum
FNS	First Negative System
FTIR	Fourier-Transform Infrared Spectroscopy
HDPE	High Density Polyethylene
HV	High Voltage
IC	Inhibitory Concentration
LDPE	Low Density Polyethylene
LIF	Laser-Induced Fluorescence
MRSA	Methicillin-Resistant *Staphylococcus Aureus*
NIR	Near-Infrared
NIST	National Institute of Standards and Technology
NTP	Non-Thermal Plasma
OAS	Optical Absorption Spectroscopy
OES	Optical Emission Spectroscopy
PAW	Plasma-Activated Water
PBS	Phosphate Buffered Saline
PCL	Polycaprolactone
PE	Polyethylene
PET	Polyethylene Terephthalate
PGA	Polyglycolic Acid
PLA	Polylactic Acid
PP	Polypropylene
PTFE	Polytetrafluoroethane
PVA	Polyvinyl Acetate

PVC	Polyvinyl Chloride
RF	Radio Frequency
RNS	Reactive Nitrogen Species
ROS	Reactive Oxygen Species
SBD	Surface Barrier Discharge
SDS	Sodium Dodecyl Sulfate
SFE	Surface Free Energy
SPS	Second Positive System
UV	Ultraviolet
VIS	Visible
VOC	Volatile Organic Compound
WCA	Water Contact Angle

Chapter 1 – Introduction to Non-Thermal Plasma Applications

1.1 Introduction

Multiple industries in the fields of, for example, medicine, agriculture, and materials processing, have had to revise their manufacturing, fabrication, and treatment processes over recent years and have shown interest in devices that can operate at more efficient and greener capacities (Peng 2018). This has put an unprecedented amount of pressure on the development of new and innovative technologies to create more efficient, greener, and competitively advantageous systems for use in various processing procedures. As is most often the case, research and development has been conducted continuously to strive for better methods that can be studied and diagnosed within the laboratory, such that they can then be safely scaled up for industrial and commercial needs. One of the leading subject areas that has aided in the betterment and updating of current systems, methodologies, and procedures is plasma physics, more specifically, non-thermal plasma (NTP) generation. The use of NTP has allowed various applications to achieve more efficient and dynamic heights. However, the use of NTP must be monitored to ensure that the performance is tailored for each intended use. One of the most common and powerful methods to ensure this is optical spectroscopy. This comes in the form of optical emission and optical absorption spectroscopy. These two optical techniques are suited for non-intrusive diagnostic purposes and they provide insights into the characteristics of the plasma and the gas chemistry that is responsible for various effects that arise from NTP treatments (Ono 2016).

NTPs are being increasingly sought after to enhance, improve, and even generate new procedures and treatment methods for multiple applications. The use of

non-thermal treatments has been applied to medical, agricultural, material, and technological industries (Uhm 2015, Moriguchi 2018, Holzer 2018, Toyokawa 2018, Adımcı 2018, Ceriani 2018). It has been shown to generate sufficient reactive oxygen and reactive nitrogen species to sterilise and disinfect sample surfaces (Alkawareek 2009). This leads to the eradication of bacterial films, fungal growths, mould, and also kill off small insects and their eggs (Bhatt 2018). By utilising these effects, many systems have been created to generate non-thermal plasma to clean wounds, accelerate their healing, decrease the use of pesticides and harsh chemical washes, sterilise medical instruments, prolong the lifetime of various foods, create morphological properties on various materials, pollution control, and for use in selective processes such as etching and deposition (Mizuno 2007, Mizuno 2009, Alkawareek 2009, Zelzer 2009).

This project focuses on the importance of tailoring the gas chemistry of non-thermal plasmas to optimise treatment parameters for application purposes. To do this, optical emission and optical absorption spectroscopy are employed, along with electrical diagnostics. By carrying out optical diagnostics of different non-thermal systems and highlighting the gas chemistries present in each system, the reaction mechanisms and most probable pathways of interaction with samples can be discerned. In order to ensure that a better understanding is derived from each study, different gases are used. Different gases, when compared to one another, show how different sentinel species can impact samples being treated, and thus allow for a more fine-tuned treatment process that can be tailored for different sample sensitivities. The route towards optimisation of the plasma parameters is demonstrated, in this work, according to their performance in treating polymer surfaces and increasing the

cytotoxic response of human cancer cells after mapping the gas chemistry of plasma discharges with optical emission and optical absorption measurements.

1.2 Plasma

The term plasma refers to a state of matter that is gaseous in nature, but creates an environment of energetic and/or reactive species by breaking down a gas and can be seen in Figure 1.1 (Conrads 2000). Generating plasma can be carried out in multiple ways, but one of the most common method used in multiple applications is through the ionisation of atoms and molecules in a gas through the interaction of strong electric fields and collisional processes (Lieberman 2005). These interactions would excite and dissociate gases (air, argon, helium, carbon dioxide etc.) and would produce an environment that contains energetic electrons, atoms and molecules; creates reactive species and ions; emits light in the ultraviolet, visible, and infrared region (Yousfi 2011, Osmokrovic 2007). The study of plasmas has been carried out for decades, but the real-world application of them has driven it towards a more practical sense in terms of end user needs and full system diagnostics for better safety protocols. Since plasmas have been studied intensely on a theoretical and purely physics based level, there are many techniques already in place that allow for a full understanding of the kinetics and mechanisms that occur within each plasma system to specifically tailor it for applications as required. The term most commonly used to refer to the plasma used in many applications, which will be discussed further in this work, is non-thermal plasma (NTP). Some of the areas that these innovative NTP systems are being introduced to include: food processing, medical implementation, agricultural methods, material fabrication, and microbiological treatments.
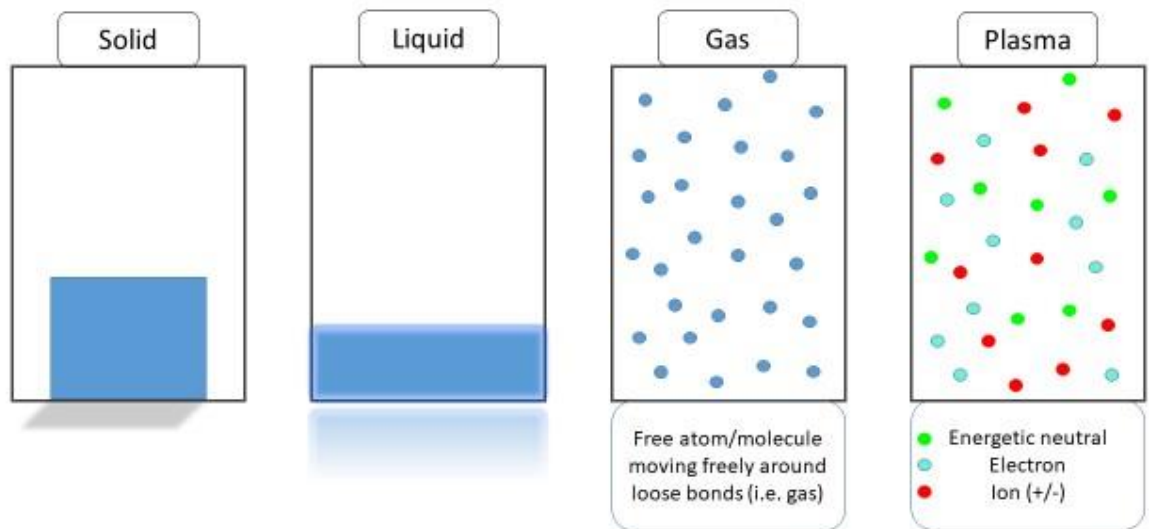
Figure 1.1: Depiction of different states of matter showing the differences between a simple gas and a plasma.

Although there are many different types of plasmas that are being used across various areas, the task that the system will be set to complete is the main determining factor as to what kind of plasma will be generated. Plasmas are generally broken down into two groups: thermal and non-thermal plasmau. Both of these classifications are based on whether or not the electrons, neutrals, and ions present within the plasma are in equilibrium with one another. When the electrons, neutrals, and ions within a plasma are at equilibrium with each other the electron and ion temperatures are close to matching throughout the plasma i.e. $T_e = T_{gas} = T_i$. When a plasma is said to be non-thermal, then the electron temperature is much higher than that of the ion temperature when averaging out all values throughout the plasma volume i.e. $T_e \gg T_{gas} = T_i$. The temperature of thermal plasmas is generally in the order 10^3-10^4 K whereas non-thermal plasmas can have a temperature equivalent to room temperature when in operation. For this reason, non-thermal plasmas are often employed when carrying out

treatment processes as many materials and samples can be sensitive to high temperatures and completely degrade when only a surface effect or modification are wanted. Furthermore, to the simplified explanation of the difference between thermal and non-thermal plasma, the following are needed to be understood when working with and analysing such technologies. For thermal plasmas the collision processes of the energetic electrons and the ions and neutrals within the gas become more frequent over time due to the cascade effect which sustains the plasma (Samal 2017). Over time, the constant kinetic transfer of energy from the electrons colliding with the heavier particles causes the energies of the ions and neutrals (T_{gas} and T_i) to be equivalent to that of the electrons (T_e). As a result, the gas temperature (T_g) becomes raised to the point where it is the same as T_e and thus the plasma reaches thermal equilibrium for the electrical power that is being input into the system (Donaldson 1991). This is more clearly expressed in Table 1.1 along with an example of where thermal plasma could be found. To generate non-thermal plasma, there are some criteria that must be met. Non-thermal plasmas could be generated at low pressures and have a significant difference between the temperature/energy of the electrons and the energy of the ions and neutrals present within the gas (Burkhard 1994). The differences in these energies give rise to partial ionization, non-equilibrium states of thermal energies (no local thermodynamic equilibrium), and a lower gas temperature (Schriver 1998, Moreau 2008). This is more clearly described in Table 1.1 and shows the difference when compared with thermal plasma and the various applications they are used in.

Table 1.1: Plasma description, systems, and applications.

Plasma equilibrium	Operational gas temperature (K)	Example System	Application
Thermal	8,000 – 25,000	Plasma torch	Arc welding (Selvan 2015)
	~1500	Steam plasma gasification using V-type plasma torch	Waste treatment (Polyethylene decomposition) (Hyun 2006)
	1,000 – 13,000	Non-transferred arc plasma flame	Nanoparticle synthesis (Kim 2013)
Non-thermal	300	DBD	Polymer treatment (Felixa 2017, Seidelmann 2017)
	300 – 450	Plasma jet	Etching and deposition (Yang 2004, Leduc 2009)
	300	Plasma jet	Wound treatment and healing (Kubinova 2017)
	300	DBD	Food decontamination (Rød 2012)
	Below 300	SBD	Sterilisation of surfaces from bacterial growths (Matthes 2013)

Terrestrial plasmas are widely sought after for many applications and the can be split into two broad and commonly used terms: thermal plasma and non-thermal plasma. NTP can be used for many applications that thermal plasma cannot, and can be generated through the use of high DC or AC power supplies. Significant work has gone into developing methods to utilize NTPs due to their relative ease of generation and the large amount of chemical interactions and gas kinetics that can be incurred with their creation. Since the inception of NTP applications in the real world, many devices have been developed to create NTP for various treatments. There is, however, a secondary condition that further divides the NTP and that is the operating temperature of the plasma. Although the descriptors of NTP within physics and engineering can place it in a domain that would be much higher than ambient temperature (potentially thousands of degrees higher than ambient temperature), the term 'cold plasma' has been used to describe NTPs that operate at close to ambient temperature and to categorise non-thermal condition plasmas into slightly more accurate profiles (Cullen 2017). Some of the most common methods to generate non-thermal plasma (NTP) includes: dielectric barrier discharge (DBD), surface barrier discharge (SBD), atmospheric air plasma jet (APPJ), and micro-plasma arrays. Each of these systems can be used by dissociating ambient air for the treatment and processing of various materials and samples including polymers, foods, medical treatment, and etching and deposition through ion bombardment. Some NTP systems can be seen in Figure 1.2.
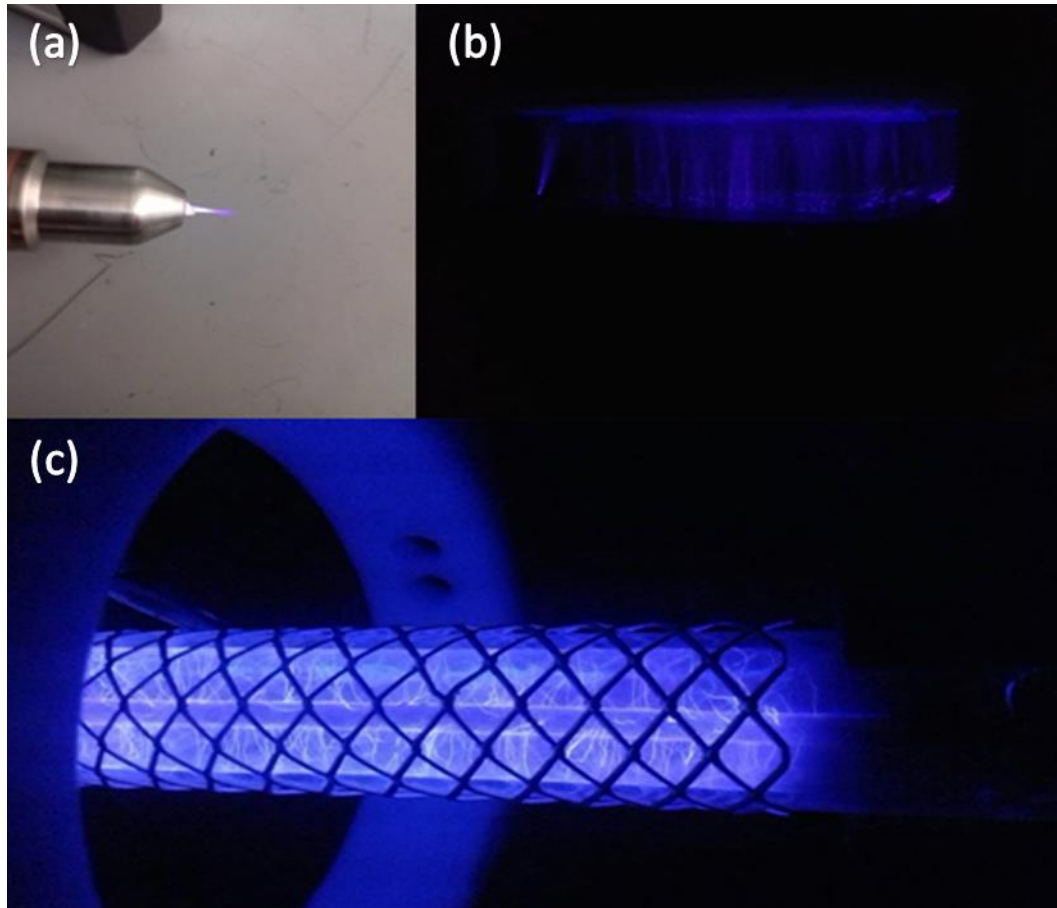
Figure 1.2: Pictures of NTP systems under operation. (a) shows a commercial non-thermal plasma jet named the kINPen® that was developed by Neoplas Tools (b) shows a dielectric barrier discharge plasma device that could operate at pressures below atmospheric (c) shows discharge in a cylindrical dielectric barrier discharge system that allow for different gases to flow through it. In this picture, argon is used.

1.3 Methodology and Thesis Layout:

The overarching topic for this thesis is the use of optical spectroscopy to diagnose NTP systems to distinguish which chemical species within the gas chemistry of the various discharges have an influence on sample treatments and modifications. To do this, different gases are used at varying flow rates and in different mixtures to show with greater confidence how specific species are generated, and thus draw a comparison as to which species and mechanisms are prevalent in modifying treated samples. The use of optical emission and optical absorption spectroscopy is employed to provide a greater understanding on how to better tailor NTP systems for optimised and efficient treatment. Utilising an Edmund Optics CCD spectrometer, the emission intensity different species, such as OH, O, N_2, N_2^+, and NO_2 could be measured with arbitrary units. From this, the integral of the total intensity for the main band head can be measured and plotted as a singular point and compared over time, or plotted spatially so as to give the spatial and temporal evolution of the plasma discharge with respect to different parameters. Using the line intensity of N_2 at 337 nm and N_2^+ at 391 nm, a ratio can be used to show whether the distribution of electron energies is more dominant in the low energy or high energy region (18.8 eV and 11.1 eV respectively)(Fantz 2012). The work carried out in each chapter was devoted to this process and descriptions of these can be seen in the following:

Chapter 2 provides a review of the current literature that shows how the use of non-thermal plasmas are becoming more prevalent. This also highlights the importance of this study and how optical techniques are needed to monitor the specific gas chemistries that reflect the energy transfer mechanisms, gas reaction schemes, and chemical interactions for better sample treatment.

Chapter 3 has been published as a peer-reviewed research paper. The work carried out in it highlights how the use of different gases for plasma generation impacts the surface morphology of thin polymer food packaging material called polyethylene terephthalate. The use of ambient air, argon and CO_2 shows how different gas chemistries interact and change the surface properties of the polymer being treated.

Chapter 4 has been published as a peer-reviewed research paper. The work that was carried out during this study was to delve more deeply into the physics of the gas chemistry of non-thermal plasma discharges. This was done to show the importance that optical measurements have in plasma diagnostics and the necessity of monitoring different gas mixtures and ratios to better tailor different systems to the needs of various applications. Many works base their studies on the fact that plasmas generate reactive nitrogen and reactive oxygen species and associate these with the effects they find on their samples. It is, however, prudent to show the weight each species may have on the results found during treatments to optimise the use and efficiency of non-thermal plasma systems. What was found in this study was that a gas mixture of Ar and He at a ratio of 10:1 respectively generated the most amount of nitrogen at a voltage of 27 kV when compared to the other gas ratios used. This gave a better understanding of the energetics, reaction mechanisms, and transfer pathways that occur within the plasma discharge.

Chapter 5 has been published as a peer-reviewed paper that highlights the use of optical spectroscopy to monitor and establish the main reactive species responsible for enhancing the degradation of low-density polyethylene. The treatment of low-density polyethylene was carried out with plasma that used ambient air and a gas mixture of ambient air that contained ~3.8% CO_2. During plasma discharge, optical emission and optical absorption spectroscopy measurements were undertaken to monitor the

formation and stability of various reactive species spatially and temporally. This, along with Raman spectroscopy, allowed for the conclusion that an increase in reactive oxygen species (OH, atomic oxygen, and ozone) created a more polar surface that gave rise to better bacterial cell adhesion post-treatment due to formation of more open sites on the polymer surface.

Chapter 6 is still being worked on to submit for publication. The results, however, show that there is a strong dependency on the plasma gas chemistry and the discharge frequency being used. By altering the discharge frequency the level of reactive nitrogen species can be controlled without altering the atmospheric conditions of the system. From the results that have been analysed, the optimum setting to generate high levels of reactive oxygen and reactive nitrogen species is to have the Leap100 power supply settings at 240 V, 91 μs, and set the discharge frequency to 1000 Hz. By treating human cancer cell lines with the plasma discharge, an increased level of cytotoxicity was found to be induced.

References

P. Adımcı, F. İbiş, U. K. Ercan, & B. Bagis, "Evaluation of effects of non-thermal plasma treatment on surface properties of CAD/CAM materials", Journal of Adhesion Science and Technology, 1–15, (2018). doi:10.1080/01694243.2018.1493834

M.Y. Alkawareek, Q. T. Algwari, S. P. Gorman, W. G. Graham, D. O'Connell, B. F. Gilmore, "Application of atmospheric pressure nonthermal plasma for the *in vitro* eradication of bacterial biofilms", FEMS Immunology & Medical Microbiology, 65, 381-384, (2009).

Hetal K. Bhatt, R. V. Prasad, D. C. Joshi, and N. Sagarika, "*Non-Thermal Plasma System for Decontamination of Fruits, Vegetables and Spices: A Review*", International Journal of Chemical Studies, **6**, (2018)

R. Burkhard, W. Hoffelner, and R. C. Eschenbach, 'Recycling of metals from waste with thermal plasma', Resources, Conservation, and Recycyling, Volume 10, Issues 1-2, pages 11-16, April (1994). https://doi.org/10.1016/0921-3449(94)90033-7

E. Ceriani, E. Marotta, V. Shapoval, G. Favaro, & C. Paradisi, "Complete mineralization of organic pollutants in water by treatment with air non-thermal plasma" Chemical Engineering Journal, 337, 567–575, (2018). doi:10.1016/j.cej.2017.12.107

H. Conrads, and M. Schmidt, "Plasma generation and plasma sources", Plasma Sources Science and Technology, volume 9, 441 (2000).

P. J. Cullen, J. Lalor, L. Scally, D. Boehm, V. Milosavljević, P. Bourke, and K. Keener, "Translation of plasma technology from the lab to the food industry", Plasma Processes and Polymers, e1700085, (2017).

D. A. Donaldson, R. R. Apa, T. L. Eddy and J. E. Flinn: 'Heat transfer in thermal plasma processing', HTD-161, ASME, 1991, 41–51.

U. Fantz, H. Falter, P. Franzen, D. Fantz, U., Falter, H., Franzen, P., D. Wünderlich, M. Berger, A. Lorenz, W. Kraus, P. McNeedy, R. Rield, and E. Speth, "Spectroscopy—a powerful diagnostic tool in source development", Nuclear Fusion, 46(6), S297–S306, (2006).

T. Felixa, F. A. Cassinia, L. O. B. Benetolia, M. E. R. Dottob, and N. A. Debachera, 'Morphological study of polymer surfaces exposed to non-thermal plasma based on contact angle and the use of scaling laws', Applied Surface Science, Volume 403, 57-61 (2017).

F. Holzer, F.-D. Kopinke, & U. Roland, "Non-thermal plasma treatment for the elimination of odorous compounds from exhaust air from cooking processes", Chemical Engineering Journal, 334, 1988–1995, (2018). doi:10.1016/j.cej.2017.11.079

P. S. Hyun, C. G. Kim, and S. J. Kim, 'Characterisation of PE gasification by steam plasma', Journal of Industrial Engineering and Chemistry, Volume 12, 216-223 (2006).

T. H. Kim, S. Choi, and D. W. Park, 'Effects of NH3 flow rate on the thermal plasma syntheiss of AlN nanoparticles', Korean Ohysical Society, Volume 63, Issue 10, Novemeber (2013).

S. Kubinova, K. Zaviskova, L. Uherkova, V. Zablotskii, O. Churpita, O. Lunov, and A. Dejneka, 'on-thermal air plasma promotes the healing of acute skin wounds in rats', Scientific Reports, volume 7, 45183 (2017).

M. Leduc, S. Coulombe, and R. L. Leask, 'Atmospheric Pressure Plasma Jet Deposition of Patterned Polymer Films for Cell Culture Applications', IEEE Transactions on Plasma Science, volume 37, 927-933 (2009).

M. A. Lieberman, A. J. Lichtenberg, Principles of Plasma Discharges and Materials Processing, publ. John Wiley & Sons, Inc. (2005).

R. Matthes, C. Bender, R. Schlüter, I. Koban, R. Bussiahn, S. Reuter, J. Lademann, K. D. Weltmann, and A. Kramer, 'Antimicrobial Efficacy of Two Surface Barrier Discharges with Air Plasma against In Vitro Biofilms', Kaufmann GF, ed. PLoS ONE. 2013;8(7):e70462. doi:10.1371/journal.pone.0070462.

A. Mizuno, "Industrial applications of atmospheric non-thermal plasma in environmental remediation" Plasma Physics and Controlled Fusion. 49, A1, (2007).

A. Mizuno, "Recent progress and applications of non-thermal plasma" International Journal of Plasma Environmental Science and Technology, 3, (2009).

M. Moreau, N. Orange, and M. G. J. Feuilloley, ' Non-thermal plasma technologies:New tools for bio-decontamination', Biotechnology Advances, Volume 26, Issue 6, pages 610-617, November-December (2008).

Y. Moriguchi, D.-S. Lee, R. Chijimatsu, K. Thamina, K. Masuda, D. Itsuki, A. Myoui, "Impact of non-thermal plasma surface modification on porous calcium hydroxyapatite ceramics for bone regeneration", PLOS ONE, 13(3), e0194303, (2018). doi:10.1371/journal.pone.0194303

R. Ono (2016). Optical diagnostics of reactive species in atmospheric-pressure nonthermal plasma. Journal of Physics D: Applied Physics, volume 49, 083001, (2016).

P. Osmokrovic, M. Vujisic, K. Stankovic, A. Vasic, and B. Loncar, "Mechanism of electrical breakdown of gases for pressures from 10^{-9} to 1 bar and inter-electrode gaps from 0.1 to 0.5 mm", Plasma Sources Science and Technology, volume 16, 643 (2007).

P. Peng, P. Chen, C. Schiappacasse, N. Zhou, E. Anderson, D. Chen, J. Liu, Y. Cheng, R. Hatzenbeller, M. Addy, Y. Zhang, Y. Liu, and R. Ruan, "*A Review on the Non-Thermal Plasma-Assisted Ammonia Synthesis Technologies*", Journal of Cleaner Production, **177**, (2018).

S. K. Rød, F. Hansen, F. Leipold, and S. Knøchel, 'Cold atmospheric pressure plasma treatment of ready-to-eat meat: Inactivation of Listeria innocua and changes in product quality', volume 30, 233-238 (2012).

S. Samal, 'Thermal plasma technology: the prospective future in material processing', Journal of Cleaner Production, Volume 142, Part 4, pages 3131-3150, 20 Jan (2017).

D. Schriver, M. Ashour-Abdalla, R.L. Richard, 'On the origin of the ion-electron temperature difference in the plasma sheet., J. Geophys. Res., volume 103, pp. 14879-14895 (1998).

L. J. W. Seidelmann, J. W. Bradley, M. Ratova, J. Hewitt, J. Moffat, and P. Kelly, 'Reel-to-Reel Atmospheric Pressure Dielectric Barrier Discharge (DBD) Plasma Treatment of Polypropylene Films', Applied Sciences, volume 7, 337 (2017).

M. C. P. Selvan, N. Rammohan, and S. S. Sampath, 'Plasma arc welding (PAW) – A literature review', American International Journal of Research in Science, Technology, Engineering, and Mathematics, pages 181-186, Volume 11, Issue 2, June – August (2015).

Y. Toyokawa, Y. Yagyu, R. Yamashiro, K. Ninomiya, & A. Sakudo, "Roller conveyer system for the reduction of pesticides using non-thermal gas plasma - A potential food safety control measure", Food Control, 87, 211–217, (2018). doi:10.1016/j.foodcont.2017.12.030

S. H. Uhm, J.-S. Kwon, E.-J. Lee, J.-H. Lee, K.-M. Kim, K.-N. Kim, & E. H. Choi, "Applications of non-thermal atmospheric pressure plasma in prevention and regeneration of oral diseases", IEEE International Conference on Plasma Sciences (ICOPS), (2015). doi:10.1109/plasma.2015.7179718

X. Yang, M. Moravej, S.E. Babayan, G.R. Nowling, and R.F. Hicks, 'Etching of uranium oxide with a non-thermal, atmospheric pressure plasma', Journal of Nuclear Materials, volume 324, 134-139 (2004).

M. Yousfi, N. Merbahi, J. P. Sarrette, O. Eichwald, A. Ricard, J.P. Gardou, O. Ducasse and M. Benhenni, "Biomedical Engineering - Frontiers and Challenges", edited by R. Fazel-Rezai, INTECH, Chapter 5 (2011).

M. Zelzer, D. Scurr, B. Abdullah, A. J. Urquhart, N. Gadegaard, J. W. Bradley, & M. R. Alexander, "Influence of the Plasma Sheath on Plasma Polymer Deposition in Advance of a Mask and down Pores", Journal of Physical Chemistry B, 113, 8487-8494, (2009).

Chapter 2 – Introduction to Plasma Physics Theory and Current Applications

2.1 Introduction

Plasma discharges are classically separated into two separate identifying categories: thermal and non-thermal. Some of the first observations of this fourth fundamental state of matter would include lighting, auroras, the stars, and the sun itself. Given our long history of interaction of plasma from various sources, both man-made and natural, it is only in recent years that we have truly investigated ways of using it to our benefit for a multitude of purposes. This chapter will give the reader an overview of the underlying theory behind plasma dynamics, the impact of system design and geometry, and how these have begun to be applied in real-world methodologies. Covered in this chapter are the quantitative descriptors for gas breakdown, plasma discharges, sheath boundaries, atomic interactions, discharge types and classifications, system designs, and current uses in applications. By doing this, a foundation will be laid that highlights the potential of non-thermal uses and to what extent they may be expanded upon, and improved, with the works shown in chapters 3 – 6 of this thesis. Systems of note that will be used in the experimental chapters of this work, and altered for novel treatment processes, include a commercial plasma jet (Chapter 3), an inhouse dielectric barrier discharge system of a cylindrical geometry (Chapter 4), and an optimised pin-to-plate design for more efficient ambient air discharge creation (Chapters 5 and 6). These novel technologies have been designed, altered, and then characterised using optical emission and optical absorption spectroscopy methods that will be technically detailed in section 2.3.

2.1.1 Gas Breakdown and Electrical Discharge

The use of gas discharge breakdown for the generation of NTP creates a complex, active, and energetic multi-step system. By exciting a gas, electrons become more energetic and can become free and unbound. Further interaction with an electric field causes these electrons to accelerate and becomes "seed" electrons. These then go on to interact with atoms and molecules within the gas by means of collisional processes which gives energy to promote other electrons and cause a chain of interactions to occur. This process induces a sustained plasma discharge for as long as the power supplied to the system remains the same. Reducing the power decreases the energetics of these electrons and the plasma discharge dissipates. Overall, the discharge is considered to be quasi-neutral. Conversely, an increase in electric field strength would create a more energetic environment and increase the concentration and density of the plasma volume. This has been known for many years and one of the earliest demonstrations of plasma discharge systems was an ozone generation tube developed by W. Siemens in 1857 (Kogelschatz 2002). Currently, there are many other technologies that are being implemented and developed that generate NTPs and shown in Figure 2.1 is a simple diagram of a DC electrical gas discharge generator. The electric field E is described in equation (2.1.1.1) where ΔV is the potential difference between the two plates of a capacitor and d is the distance between the electrode plates (Knight 2008).

$$E = \frac{\Delta V}{d} \tag{2.2.1.1}$$
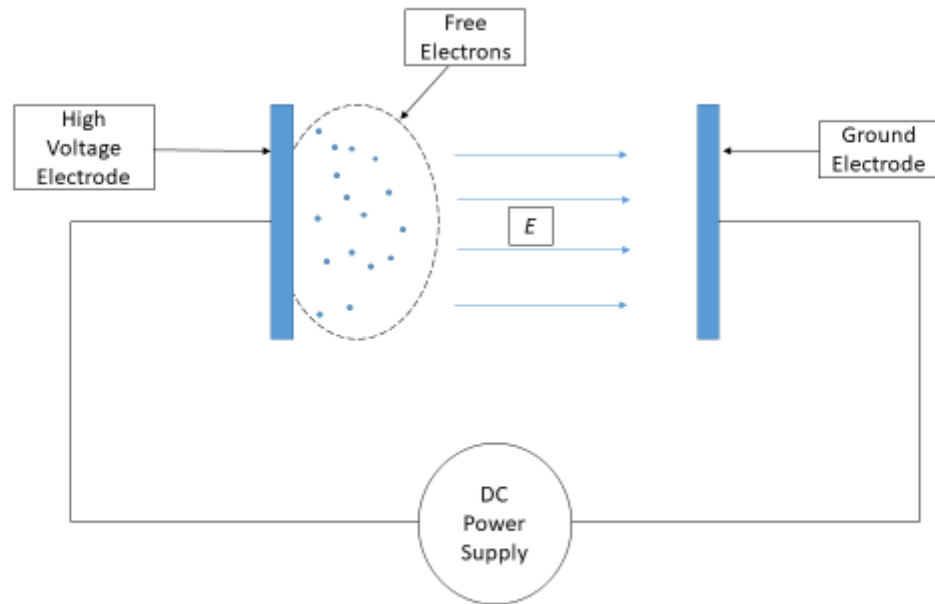
Figure 2.1: An idealistic DC electrical gas discharge system. *E* represents the electric field lines which excites and accelerates electrons towards the ground electrode.

Given that the free electrons present within the gas are acted upon and accelerated towards the ground electrode and interact with other atoms and molecules through collisional processes, it is important to know at what energy levels they exist at and whether there is a higher population of low energy electrons or high energy electrons. Due to their light mass, the electrons present are acted upon much more so than the heavier atomic and molecular ions within the electric field. Because of this, they are the source of energy transfer to these particles with regards to collisional processes with their net velocity calculated with equation (2.1.1.2) where v_d is the drift velocity and μ is the mobility of the electron.

$$v_d = -\mu E$$

(2.1.1.2)

The mobility of the electron is dependent on the density of the background gas of the plasma discharge. This can be seen in equation 2.1.1.3 (where k is the Boltzmann constant, T is energy, m is electron mass, v_m is the momentum transfer frequency, and n is the density) (Lieberman 2005).

$$\mu = \left(\frac{V_d}{E}\right) + \left(\frac{KT}{mV_m}\right) \cdot \left(\frac{\nabla n}{n}\right) \tag{2.1.1.3}$$

By considering that the electron travels through a volume of atoms and molecules to which it can interact with through collision processes, there arises a probability for these to occur. Assuming that there is a homogenous spread of these neutral particles throughout the plasma volume and that these neutrals remain stationary compared to the comparatively high velocity electrons, the collisional processes occur due to electrons impacting the neutrals. Describing the plasma volume in space as *xyz*, the number of atoms available for interaction is the density by the volume as seen in equation (2.1.1.4) with n_0 being the neutral density (Lieberman 2005)..

$$n_0 xyz \tag{2.1.1.4}$$

By creating a potential difference between the cathode and anode there arises, as mentioned previously, an interaction with the electrons in the gas. These free electrons travel from the anode to the cathode and the positively charged ions to travel towards the anode. From this, a positively charged region occurs at the anode that causes a sheath at the surface interface that compensates for the energetic electrons escaping the region. These energetic electrons have a thermal velocity much greater

than that of the ions present as the electron mass $m_e \ll M$, the ion mass (equation 2.1.1.5. with T_e being the electron temperature and T_i being the ion temperature).

$$\sqrt{\frac{eT_e}{m_e}} = v_e \ll v_i = \sqrt{\frac{eT_i}{M}} \qquad (2.1.1.5)$$

Due to the quasi-neutral nature of plasmas, these sheaths are generally only a few Debye lengths in size. Equation (2.1.1.6) shows the Debye length (where λ_d is the Debye length, ε is the permittivity, e is the electron charge, and n_e is the electron density) (Lieberman 2005 and Loureiro 2016).

$$\lambda_d = \sqrt{\frac{\varepsilon T_e}{e n_e}} \qquad (2.1.1.6)$$

2.1.2 Townsend Breakdown

As mentioned previously, the multiplication of electrons occurs from ion collisions with the cathode and ionization from inelastic collisions between electrons and neutrals. First, the ionization process may be described by using the Townsend equation (2.1.2.1) to calculate the number of ionization events as a function of distance (Lieberman 2005). Here α is the Townsend ionization coefficient, p is the gas pressure, with A and B being constants that are gas dependent (Loureiro 2016).

$$\alpha = Ap \exp^{\left(-\frac{Bp}{E}\right)} \qquad (2.1.2.1)$$

The multiplication factor is the sum of all electrons entering the anode from a primary electron. By including the generation of the primary electrons from the gas

rather than the cathode. Relating the calculations for these two possibilities, a simplified criterion to describe the breakdown of the gas can be given by equation (2.1.2.2) which is dependent on the cathode and is relatively constant for the cathode used (Loureiro 2016).

$$\gamma(\exp^{(ad)} - 1) = 1 \tag{2.1.2.2}$$

Meeting these criteria allows for the generation of a self-sustaining plasma. Since the coefficient α is shown in equation (2.1.2.1) to be dependent on the electric field applied to the gas between the electrodes, the criteria needed from equation (2.1.2.2) can be met by varying the applied voltage (Loureiro 2016). From this it can be given that there is a point where the gas breaks down; this point is the breakdown voltage V_b and is shown in equation (2.1.2.3) which is the Paschen Law for gas discharges (Lieberman 2005 and Loureiro 2016).

$$V_b = \frac{Bpd}{\ln(Apd) - \ln[\ln(1 + \frac{1}{\gamma})]} \tag{2.1.2.3}$$

As can be seen from this, V_b is dependent on the pressure of a system and the distance between the electrodes. When the pressure is too low or too high, the minimum value of V_b needed to create plasma is increased. This is due to the changes in collisional processes undergone between the first electron and a neutral atom. When the pressure is too low, the mean free path becomes large and the amount of interactions becomes lower than what would be necessary to create plasma discharge. By having the pressure too high the mean free path decreases and the electrons that become free do not have enough time to become accelerated by the electric field to generate enough ionization events. This then causes the energy in the system to

dissipate throughout the volume without creating a cascade of electrons to allow for a self-sustaining plasma (Loureiro 2016).

2.1.3 Streamer Breakdown

The description of the Townsend discharge and the dependence the plasma has an ion dominated interactions does not, however, fully take into consideration the use of systems with larger pressures. There was found to be an inconsistency with the plasma development time when comparing the breakdown to the gas to the formation of the conducting gas when plasma discharge was achieved. It was then, in 1940, that J. M. Meek theorized that the creation of these higher-pressure discharges needed to have the potential difference created by the electron multiplication taken into consideration. By considering the changes in the field as the electron avalanche occurs throughout the electric field, a space charge disturbance can be represented by equation (2.1.3.1) where E_{sc} is the space charge (electric) field, Q_{sc} is the number of charges in the space charge head, r, is its radius, and ε is the relative permittivity of the gas (Loureiro 2016).

$$E_{sc} = \frac{Q_{sc}e}{4\pi\varepsilon r^2}$$
(2.1.3.1)

As this space charge head is created and changes spatially, it also changes temporally throughout the gas and so the radius of it also varies as the charges fluctuate. This diffusion can be described using equation (2.1.3.2) where D is the diffusion coefficient and t is time after the electron avalanche initiation (Hillborg 1991).

$$r = \sqrt{4Dt}$$
(2.1.3.2)

Given that the space charge of the avalanche head progresses and fluctuates over time, if it gains enough charge and becomes comparable to or greater than the electric field applied, then further, secondary, avalanches can be created in front of the initial avalanche head. This dynamic creation of streamer heads can cause a very fast development of highly conductive channels which allow for streamer (or filament) discharges. Given that the distance travelled by the electrons accelerated by the applied field affects how much energy it carries and therefore impacts the formation of a plasma discharge, there is an impact from the density and pressure of the gas used. Therefore, each gas has its own critical distance (d_c) that the space charge head must travel. This represented in equation (2.1.3.3) (Hillborg 1991).

$$\frac{\alpha}{p} d_c = 20 + \ln(d_c) \qquad (2.1.3.3)$$

Given that the electrons are much lighter than the ions produced, the formation of the streamer breakdown is close to the drift velocity of the electrons. This is three orders of magnitude higher than the velocity of the ions associated with Townsend breakdown. By specifying the conditions of a plasma, it can be ascertained which regime the plasma is operating under.

2.2 Atmospheric Pressure Plasma Discharge

2.2.1 Glow Discharge

Although there are two pathways for gas breakdown (Townsend and streamer), there are different regimes of plasma discharge. These are defined by the electrical characteristics of the gas and are termed dark glow, glow discharge, and arcing. Dark glow exists in the Townsend regime and the others are products of streamer breakdown. By plotting the voltage of the applied field through a gas, the current of it

can be obtained which indicates the changes in electron density (Loureiro 2016). These shifts in electron density represent the different regimes and discharge types as the electron flux influences the interactions that occur and thus modify the plasma discharge created with variation of the applied electric field and/or current (Loureiro 2016).

Glow discharge occurs due to the changes in the electric field from the variation in electron kinetics and positions. By applying a voltage to two parallel electrodes that are within a contained environment (e.g. quartz tube), the electrons and ions within undergo the processes outlined previously. However, in this instance the electrons collide with the surface of the environmental boundary and their kinetics are dampened (Lieberman 2005 and Loureiro 2016). Over time they begin to adhere to the surface of this containment barrier. Ions within the system interact and neutralise a partial amount of them, but the majority are still influenced by the applied field and are carried away. This leaves a negative charge over its surface, and from this, a radial electrical field is created. This then impacts the formation of different processes within the gas centre as the ions become more dominant within the core of the gas. They both still travel in accordance with the applied electric field, but the separation of charged particles that creates the radial field affects and distorts the axial field (Loureiro 2016). When applying an even stronger axial field by increasing the supplied voltage, charges build up on the anode and cathode and reach sufficient energies to go beyond Townsend breakdown and undergo glow discharge. With the radial field still being generated, the number of electrons lost to the boundary collision decreases and the applied/axial voltage needed to cause gas breakdown decreases, but the current increases as there are more electrons available for conduction (Loureiro 2016). The name for this type of discharge arises from the visible glow seen during plasma

generation. From the larger range of electron energies and the larger amount of electron densities more collisional processes arise. Inelastic collisions become more prevalent and from this, more excited atoms are generated which then go through a relaxation process and emit varying wavelengths of light (Loureiro 2016). The creation of a glow discharge can be seen in Figure 2.2 below which represents a simple description of the phenomena.
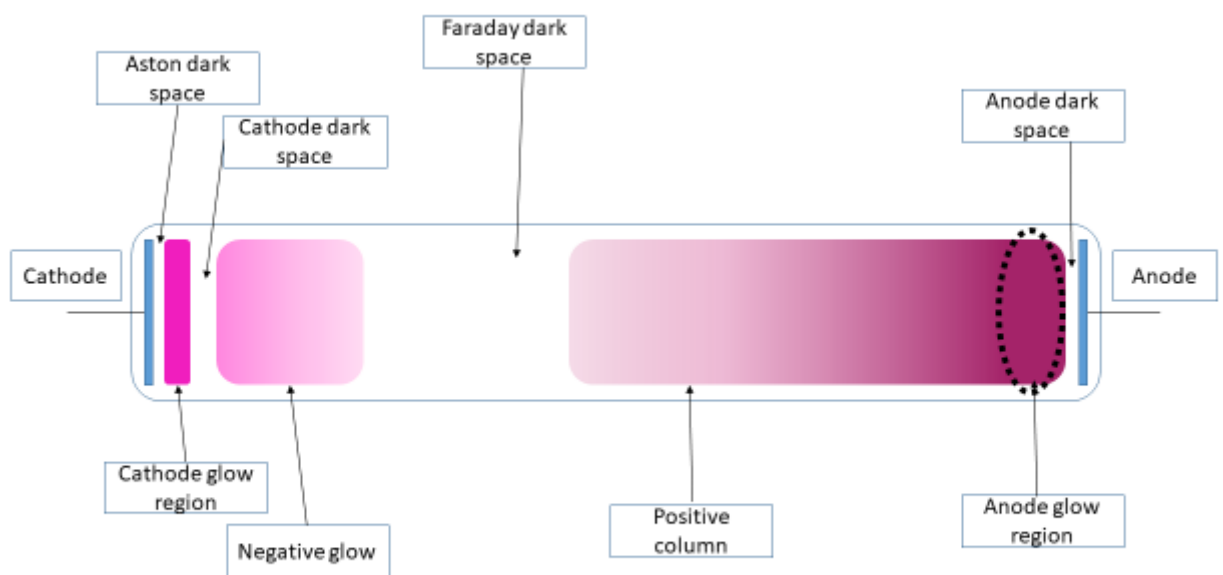
Figure 2.2: Simple representation of DC glow discharge.

2.2.2 Corona Discharge

A second type of plasma discharge to consider is corona discharge. Assume that a system of cylindrical nature was set up with an inner wire electrode and a surrounding plate electrode with gas between them, parallel coaxial wires, or even a planar electrode with a parabolic point perpendicular to it; these electrode geometries form large and non-uniform electric fields at point regions of the anode (Hutchinson 1987). A region of low intensity emissions occurs at the anode or cathode depending on

whether the corona is negatively or positively charged (Hutchinson 1987). Corona discharges can be created by one of two methods: 1) continuous applied high voltage to the system or 2) pulsed voltage for electric field attenuation. In the case of continuous high voltage discharge, there is a chance of generating spark discharges between the electrodes (Hutchinson 1987). The use of a pulsed applied voltage offers a much more versatile scenario in which the voltage being applied can be varied by tuning it to different pulse frequencies that can create streamer formations without the generation of electron cascades that cause sparking (Hutchinson 1987). The formation of a corona discharge can be seen in Figure 2.3 below.
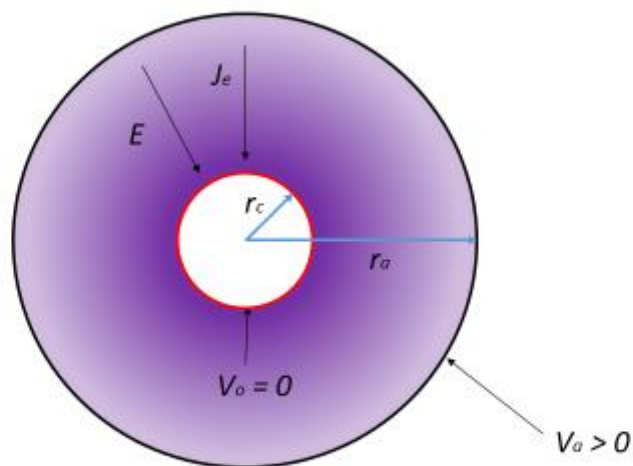
Figure 2.3: Coaxial wire corona discharge model with the HV source on the outer circle and the ground electrode kept in the centre. J_e is the electron current.

The description of the electric field for any point in a coaxial wire corona discharge system (E_r) can be given with equation (2.2.2.1). In this equation r is the radial coordinate within the discharge gap and it is given that $r_c \ll r_a$ and $r_c \leq r \leq r_c$.

μ_i is the ion mobility, L is the length of the cylinder of the coaxial wire design, and V_a is the onset voltage of the corona discharge (Hutchinson 1987 and Loureiro 2016).

$$E_r = \sqrt{\frac{1}{2\pi\varepsilon_o \mu_i L}\left[1-\left(\frac{r_c}{r}\right)^2\right] + \left[\left(\frac{V_a}{r\ln\left(\frac{r_a}{r_c}\right)}\right)^2\right]}$$ (2.2.2.1)

With corona discharge, an approximation is made that asserts that all upward transitions are collisional and all downward transitions from excited states are radiative. This is assumed given that the radiation and electron density are relatively low (Hutchinson 1987). The description of these excitation and relaxation processes can be seen in equation (2.2.2.2) where n_i is the ground population density, n_j is the excited population density, and n_e is the electron density. A_{ij} and A_{ji} are the spontaneous transition probabilities. The terms shown describe the processes that are undergone within a corona discharge and show how the population densities within the discharge can occur. The last two terms $n_e n_i <\sigma_{ij}v>$ and $n_e n_j <\sigma_{ji}v>$ represent the collisional excitation and recombination respectively (Hutchinson 1987).

$$0 = \sum_{j=1}\left[n_i A_{ij} - n_j A_{ji} + n_e n_i <\sigma_{ij}v> - n_e n_j <\sigma_{ji}v>\right]$$ (2.2.2.2)

2.2.3 AC Plasma Discharge

When utilising NTP systems, it must be noted that the use of the power supply affects the outcome of the characteristics and properties of the system. When using a DC power supply, one uses strong electric fields to create energetic species by interacting with the more loosely bound electrons and cause an electron cascade due to acceleration from interacting with the electric field (Loureiro 2016). This allows for

conductance from one electrode to another. By using a DC power supply, a more direct approach to surface etching and sputtering can be created. However, if there is a need to treat samples which are sensitive enough to warrant a decrease in surface bombardment and high energy etching, then one may place an insulating material over the electrode regions to decrease these interactions and allow for other mechanisms of processing (Loureiro 2016). By creating an insulating barrier between the electrodes used in a DC power supply, it becomes impossible to generate plasma without causing arcing and material breakdown as would occur within a capacitor (Loureiro 2016). Therefore, an AC power supply should be used. By doing this, an alternating applied electric field would be created. When using an AC supply, there are multiple aspects that can change the characteristics of the plasma discharge and they are very versatile when the need for fine-tuning a plasma discharge is needed for different processing methods. For example, since the electric field supplied alternates and causes a switch in the polarity of the electrodes, an impact on the plasma sheath boundary, reaction mechanisms, and ion and electron mobility arise, the changes in the electric field causes an impact on the electrons and ions present since they contain charges that interact with the shifting field. However, if the frequency of the discharge is high enough (in the kHz region), then the electrons will end up becoming the most affected as they have a much smaller mass than the ions present (Lieberman 2005). This allows them to change momentum much faster. This causes an increase in electron collisions with other atoms and molecules within the gas and the electron energy distribution function may be affected. With field switching frequencies kept at a low value (e.g. 50 Hz) the time averaged impact that this has on the plasma discharge means that the ions present are affected (Lieberman 2005). The low switching speed allows enough time for the movement of the ions to be impeded and may create a higher temperature

plasma as the kinetic energy of the plasma will then be affected by the momentum of the ions being moved by the electric field oscillation.

2.3 Plasma Kinetics and Optical Diagnostics

2.3.1 Collision Cross-Section Probability

The collisional processes that occur are considered to be either elastic or inelastic. Collisions that do not change the internal energies of the collision partners and conserve the sum of the kinetic energies are termed elastic collisions (Hutchinson 1987). Those collisions that impart an amount of the kinetic energy from the electron to the neutral atom allow the neutral atom to undergo excitation or ionization and so do not conserve the kinetic energy of both species, but rather increase the potential energy of the neutral atom (Hutchinson 1987). When this occurs, the collision is termed inelastic.

The probability of collisions in an idealised hard-sphere case is described by the cross section of the particles in question. Given that the area of the electron is extremely small compared of that of an atom, it can be ignored and the area of the atom in question is used to calculate the cross section σ as shown in equation (2.3.1.1) (r is the atomic radius) (Lieberman 2005).

$$\sigma = \pi r^2 \tag{2.3.1.1}$$

The cross section is used to calculate the mean free path λ_m of electrons, which is shown in equation (2.3.1.2) and describes the distance travelled by the electron before colliding with an atom. Predicting the electron path along one plane at a time, the reference for the mean free path becomes $\lambda_m = z$ with respect to its x and y coordinates (Lieberman 2005).

$$\lambda_m = \frac{1}{\sigma n_o} \tag{2.3.1.2}$$

If the kinetic energy of the electron is above the ionization energy of a neutral atom that it interacts with, then there may be an electron emitted from that the atom. These ejected electrons then interact with the electric field of the system and become accelerated and can go on to ionize more neutral atoms (Loureiro 2016). This multiplication process is termed "electron avalanche" and the dynamics of this can vary throughout the plasma volume and over time. As the electron multiplication takes place, more and more ions are created which are accelerated towards the cathode. As they are accelerated, these ions can bombard the cathode and create the emission of secondary electrons. This leads to more collisions that causes the plasma to be self-sustaining by creating a number of electrons equal to the number of ions lost (Hutchinson 1987). This process aids in the breakdown and discharges previously mentioned.

Other considerations for collisional processes include the point that when particles undergo collisional interactions, there is a scattering of these particles through some angle. By working only with the interactions that scatter the particle by an angle $\theta = 90^o$ or more for a hard sphere model, the angle of incidence is the same as the angle of reflection. This concludes that a 90° collision would occur on through a radian 45° ($\chi = 45^o$) diagonal incident line. From this, the cross section can be written as is seen in equation (2.3.1.3) (Lieberman 2005).

$$\sigma_{90} = \frac{\pi r^2}{2} \tag{2.3.1.3}$$

The possibility of many other collisions at smaller angles will eventually cause scattering of particles through 90°. Because of this, a better determination of the cross section is needed. Born from this is the differential scattering cross section $I(v, \theta)$. Describing this value requires knowledge of the impact parameter b, and the scattering angle θ. Defining these values and how to use them to calculate the scattering cross section can be seen in equation (2.3.1.4) (Lieberman 2005).

$$I(v,\theta) = \frac{b}{\sin\theta}\left|\frac{db}{d\theta}\right| \qquad (2.3.1.4)$$

Integrating (2.3.1.4) we can obtain the total scattering cross section as shown in equation (2.3.1.5). However, it is frequently more prudent to be able to define a single cross section. This can be done by using the average particle velocity to obtain the momentum transfer cross section σ_m which is used to calculate the frictional drag caused by the loss in momentum of the incident particle when undergoing a collisional process. The momentum transfer cross section can be seen in equation (2.3.1.6). The value represented by $(1 - \cos\theta)$ is the fraction of the initial momentum mv lost by the incident particle (Lieberman 2005).

$$\sigma_{sc} = 2\pi\int_0^\pi I(v,\theta)\sin\theta d\theta \qquad (2.3.1.5)$$

$$\sigma_m = 2\pi\int_0^\pi (1-\cos\theta)\, I(v,\theta)\sin\theta d\theta \qquad (2.3.1.6)$$

It can be found, however, that for the hard sphere model that $\sigma_{sc} = \sigma_m = \pi r^2$, but for other scattering forces $\sigma_{sc} \neq \sigma_m$. As previously stated, the electron radius can be considered negligible compared to the atomic radius of the neutral or ionic species involved in electron-atom and electron-ion collisions.

2.3.2 Collisional Processes

Numerous techniques have been tested in order to characterize and identify the various plasma discharges that have been created over the years. One of the most common of these is optical spectroscopy due to the non-invasive nature it exhibits and the ease of its implementation. Optical emission spectroscopy (OES) and optical absorption spectroscopy (OAS) have been used to determine the collisional process pathways, reaction mechanisms, and energy distributions of electrons and ions. In this section, the rates of collisional processes and radiative processes that may occur within a plasma are discussed. These include radiative recombination, collisional ionization, and collisional excitation (Hutchinson 1987).

For the process of radiative recombination, the collision cross section (σ_{rr}) is used to express the power radiated from the recombination mechanism that occurs as an electron transition from one level to another. This can be seen in equation (2.3.2.1) where α_{fs} is the fine structure constant, G_n is the Gaunt factor, $\dfrac{c^2}{v_1^2}$ is the ratio between electron rest energy and kinetic energy, Z is the associated particle charge, r_e is the classical electron radius, and ω is the angular frequency of the electron (Hutchinson 1987).

$$\sigma_{rr} = G_n \frac{16\alpha_{fs}}{3\sqrt{3}} \pi (Zr_e)^2 \frac{c^2}{v_1^2} \frac{\Delta\omega_n}{\omega_n} \qquad (2.3.2.1)$$

It can be asserted and substituted into equation (2.3.2.1) that the ionization potential χ_i for a given state n_s (state ionization potential χ_n) can be equated to the kinetic energy through equation (2.3.2.2) (Hutchinson 1987).

$$\hbar\Delta\omega_n = \frac{2\chi_n}{n_s} \tag{2.3.2.2}$$

Given this and also equation (2.3.2.3) where W_k is the kinetic energy

$$\hbar\omega = W_k + \chi_n \tag{2.3.2.3}$$

it can be shown that, integrating over a Maxwellian electron distribution, equation (2.3.2.4) can be given with $\bar{g}_n$ being the averaged Gaunt value (Hutchinson 1987).

$$\langle\sigma_{rr}v\rangle = \overline{g}_n \frac{16\alpha_{fs}}{3\sqrt{3}} \pi(Zr_e)^2 c^2 \frac{2}{n}\left(\frac{m_e}{2\pi T}\right)^{\frac{3}{2}} \int_0^\infty \frac{e^{\left(-\frac{W_k}{T}\right)}4\pi v dv}{1 + \frac{W_k}{\chi_n}} \tag{2.3.2.4}$$

To simplify this slightly, $\alpha_{fs}c$ may be substituted with $(2R_y/m_e)^{1/2}$ with R_y being the Rydberg energy. Rearranging equation (2.3.2.4) with this new identity equation (2.3.2.5) is obtained.

$$\langle\sigma_{rr}v\rangle = \overline{g}_n \frac{64}{3}\left(\frac{\pi}{3}\right)(r_e)^2 cZ\left(\frac{Z^2 R_y}{n^2 T}\right)^{\frac{1}{2}} \exp\left(\frac{\chi_n}{T}\right)E_i\left(\frac{\chi_n}{T}\right) \tag{2.3.2.5}$$

When trying to determine or describe the rate coefficient for this process, it is needed that the existence of partially filled states is taken into account. By correcting the radiative recombination rate by a factor of $\frac{\xi}{2n^2}$ equation (2.3.2.5) is changed to compensate for a partially filled state and gives equation (2.3.2.6). The identity $\frac{\xi}{2n^2}$ gives a description of the number of electrons in a state and how this impacts the free

space for recombination processes and ξ is the argument of dispersion function (Hutchinson 1987).

$$\langle \sigma_{rr} v \rangle = \overline{g_n} 5.2 \times 10^{-20} Z \left(\frac{\chi_n}{T} \right)^{\frac{3}{2}} \exp\left(\frac{\chi_n}{T} \right) E_i \left(\frac{\chi_n}{T} \right) \tag{2.3.2.6}$$

Another collision type to consider is collisional ionization. The most rudimentary assumption for the description of collisional ionization is that of the interaction between a bound atom and a free energetic electron colliding with one another. The bound electron is assumed to be stationary with respect to the incoming energetic electron. As the incoming electron with energy W_{ce} collides with the stationary electron of energy and changes the stationary electron energy by ΔW_{ee}. If the change in energy through this collisional transfer is greater than the ionization potential χ_i, then the atom or molecule in question will become ionized. The cross section for ionization recombination σ_{ir} is the integrated value of all impact parameters b. For this collision process, which considers two electrons colliding, a Coulomb collision is considered. This allows us to represent the change of energy from the electron collision with equation (2.3.2.7) (Hutchinson 1987).

$$\Delta W_{ee} = \frac{W_{ce}}{[1 + \left(\frac{4\pi\varepsilon_o}{e^2} \right)^2 W_{ce}^{\,2} b^2]} \tag{2.3.2.7}$$

Since we cannot assume that both of the particles are stationary, a centre of mass frame is needed to be used in order to calculate the ionization recombination cross section. Equation (2.3.2.7) brings light to the dependence of ΔW_{ee} on the impact parameter b, that is, that if the impact parameter is too high, ionization will not occur

and so there is a threshold for ionization with respect to b. From this, an estimate of σ_{ir} can be shown with equation (2.3.2.8) (Hutchinson 1987).

$$\sigma_{ir} = \pi b^2 = \pi \left(\frac{e^2}{4\pi\varepsilon_o} \right)^2 \frac{1}{W_{ce}^2} \left(\frac{W_{ce}}{\chi_i} - 1 \right) \qquad (2.3.2.8)$$

which can be rewritten to take into consideration the Bohr radius a_o and gives a classical collisional ionization cross section per active bound electron as shown in equation (2.3.2.9) (Hutchinson 1987).

$$\sigma_{ir} = 4\pi a_o^2 \left(\frac{R_y}{W_{ce}} \right)^2 \left(\frac{W_{ce}}{\chi_i} - 1 \right) \qquad (2.3.2.9)$$

This assumes that there is one electron in the bound state for interaction, but if there are a number of electrons present then the cross section must be multiplied by the factor equivalent to the number of present bound electrons (Hutchinson 1987). This then gives the total cross section for the atom. However, this only considers high energy electron collisions and not those where the incident electron energy is close to the ionization energy. This is due to the omission of the potential energy an electron has in a Bohr orbit, which is $-2\chi_i$ in the Coulomb field of the ion. From this it is assumed that a lower energy (slow moving) incident electron is accelerated by an ion potential field which gives the incident kinetic energy as $(W_{ce} + W_+)$ where W_+ is the added energy from the ion potential field energy and $W_+ \sim -2\chi_i$. Another point to consider is that if the colliding electron transfer too much energy, then it may become bound and give rise to no net ionization (Hutchinson 1987). Going forward with these two new assertions, equation (2.3.2.9) can be modified to reflect them as shown with equation (2.3.2.10) (Hutchinson 1987).

$$\sigma_{ir} = 4\pi a_o^2 \left(\frac{R_y^2 \left(\frac{W_{ce}}{\chi_i - 1} \right)}{W_{ce}(W_{ce} + W_+)} \right) \quad (2.3.2.10)$$

$$\langle \sigma_{ir}, v \rangle = 4\pi a_o^2 \left(\frac{R_y}{\pi n_e} \right)^{\frac{1}{2}} \left(\frac{R_y}{\chi_i} \right) \left(\frac{R_y}{T} \right)^{\frac{1}{2}} \exp\left(\frac{\chi_i}{T} \right)$$
$$\times \left[1 - \left(\frac{\chi_i + W_+}{T} \right) \exp\left(\frac{\chi_i + W_+}{T} \right) E_i\left(\frac{\chi_i + W_+}{T} \right) \right] \quad (2.3.2.11)$$

By including the average Gaunt value to this, one can create a more accurate expression as the use of equation (2.3.2.11) does not take into consideration the change in the cross section with higher energies which sit above the classical estimate. Introducing the average Gaunt value creates a more accurate representation of the behaviours seen at low and high temperatures. This slight amendment can be seen in equation (2.3.2.12) below which represents the rate per atomic electron and should be summed over all significant electrons in the atom (Hutchinson 1987).

$$\langle \sigma_{ir}, v \rangle = \overline{g}_n 4\pi a_o^2 \left(\frac{8T}{\pi n_e} \right)^{\frac{1}{2}} \frac{R_y}{\chi_i(\chi_i + W_+)} \exp\left(\frac{-\chi_i}{T} \right) \times \left[1 - \exp\left(-\frac{(\chi_i + W_+)}{T} \right) \right] \quad (2.3.2.12)$$

For collisional excitation the excited state populations within a coronal situation needs to have the discrete quantum states taken into consideration. The transitions between these states can be described using the perturbation theory which takes the electric field of the colliding electron into consideration. A way to describe this is to relate the collision electric field frequency and the Einstein coefficient of the transition in question to get the rate of excitation. The field of the electron at the atom/ion is described as $\frac{1}{z}$ multiplied by the field of the atom at the electron. A Fourier

analysis can be used to obtain the colliding electron acceleration due to the ion field. The probability of the transition that occurs due to the collisional excitation from i to j can be seen in equation (2.3.2.13) where B_{ij} is the Einstein coefficient of induced transition probability and $\rho(v_{ij})$ represents the energy density of the perturbed electric field (Hutchinson 1987).

$$P_{ij} = \int_{-\infty}^{\infty} B_{ij} \rho(v_{ij}) \qquad (2.3.2.13)$$

and more specifically, for a particular transition can be shown with equation (2.3.2.14)

$$P_{ij} = 8\pi^2 \varepsilon_o B_{ij} \left| E(\omega_{ij}) \right|^2 \qquad (2.3.4.14)$$

Before going further with this, the relation between the spectral power of the radiation and the transition probability must be given In order to do this the spectral power must be described in some sense, and this can be seen in equation (2.3.4.15) where W is the radiated power and E' is the colliding electric field (Hutchinson 1987).

$$\frac{dW}{d\omega} = \frac{e^2}{6\pi^2 \varepsilon_o c^2} \frac{e^2}{m_e^2} B_{ij} \left| E'(\omega) \right|^2 (2\pi)^2 \qquad (2.3.2.15)$$

The relation between the radiated power to the transition probability can be seen in equation (2.3.2.16).

$$P_{ij} = B_{ij} \left(\frac{4\pi\varepsilon_o}{e^2} \right)^2 \frac{3m_e^2 c^3}{4} \frac{1}{z^2} \frac{dW}{d\omega} \qquad (2.3.2.16)$$

By integrating equation (2.3.2.16) over the impact parameter b, one can obtain the excitation cross section for collisional excitation from one state to another. This is shown in equation (2.3.2.17) where the excitation cross section is represented by σ_{ij} (Hutchinson 1987).

$$\sigma_{ij} = B_{ij} \left(\frac{4\pi\varepsilon_o}{e^2} \right)^2 \frac{3m_e^{\ 2}c^3}{4} \frac{\hbar\omega}{z^2} \frac{d\sigma_c}{d\omega} G \qquad (2.3.2.17)$$

In order to obtain the rate coefficient for this collisional excitation process, the integration of equation (2.3.2.17) must be done with respect to the velocity. When this is carried equation (2.3.2.18) can be obtained and shows the rate coefficient $\langle \sigma_{ij} v \rangle$ with j being the bremsstrahlung emissivity (Hutchinson 1987).

$$\langle \sigma_{ij}, v \rangle = B_{ij} \left(\frac{4\pi\varepsilon_o}{e^2} \right)^2 \frac{3m_e^{\ 2}c^3}{4} \frac{4\pi j(\omega_{ij})}{n_e n_i z^2} \qquad (2.3.2.18)$$

This can be further revised and developed into equation (2.3.2.19) when taking the constants and oscillator strength f_{ij} into consideration (Hutchinson 1987).

$$\langle \sigma_{ij}, v \rangle = 3.15 \times 10^{-13} f_{ij} \left(\frac{R_y}{E_{ij}} \right) \left(\frac{R_y}{T} \right)^{\frac{1}{2}} \exp\left(\frac{-E_{ij}}{T} \right) \overline{g}_n \qquad (2.3.2.19)$$

2.3.3 Optical Spectroscopy

Optical spectroscopy has been used for many years as a diagnostic technique to characterize plasma discharges. The occurrence of emission profiles in plasmas is due to the transfer of energy through collisional and radiative means. These transfers of energy can cause an electron to undergo excitation to another state, which it then falls from due to the relaxation back to a lower and more stable state. By undergoing this relaxation transition, a photon is emitted to preserve the conservation of energy. This emission is of light energy which corresponds to a particular wavelength (Lieberman 2005). Wavelengths are dependent on the energy emitted and varies between every atom and molecule and allows the use of optical emission spectroscopy to identify the species present within a plasma discharge. If the spectrometer used for the emission

spectroscopy measurement is calibrated, then the power or energy of the emitted wavelength can be recorded, but if it is not, then the intensity of the emissions is recorded with arbitrary units (a.u.). A simple representation of the excitation and emission process can be seen in figure 2.4. The emission wavelength λ is calculated using equation (2.3.3.1) were ω is the emission frequency (Lieberman 2005).

$$\lambda = \frac{2\pi c}{\omega} \qquad (2.3.3.1)$$
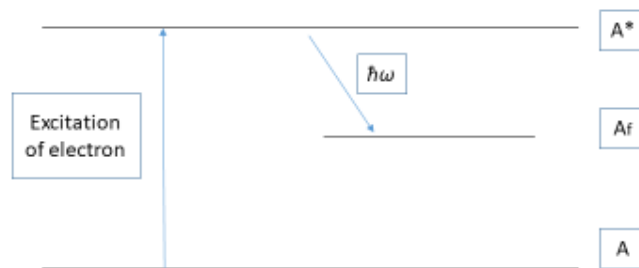
Figure 2.4: Simple representation of excitation and relaxation of an electron in a bound state which leads to light emission for optical spectroscopy measurements. A is the ground state, A* is the excited state, and A_f is the relaxed state. $\hbar\omega$ is the emitted wavelength energy.

When looking at the line intensities of optical emission spectroscopy measurements, it can easily be seen how certain species are affected by changes in voltage, current, frequency, gas mixture, and flow rates. However, it can sometimes be difficult to determine precise paths of energy transfer between different species.

After implementing OES, the data that is acquired can be analysed to give the absolute emission intensity (I_A) for each spectral line observed. Each of these emission lines have their own constant associated with their emission. This constant is the Einstein coefficient of spontaneous emission (A_{ij}) and it gives the probability of an electron radiatively transitioning from an excited state to a lower one. By manipulating equation (2.3.3.2), the population density (N_p) of each species and their corresponding excitation level can be found (Lieberman 2005).

$$I_A = A_{ij} N_p h\nu \qquad (2.3.3.2)$$

If one divides the absolute intensity I_A by the spontaneous emission coefficient A_{ij} for each spectral line and getting n_p for each species, this can then be plotted against the excitation energy level. This gives a spread of the population densities and shows more clearly how each species can influence the generation or quenching of another and if there are any preferential pathways for this to occur. From this it can be illustrated that the spread of energies follows a Maxwellian distribution. Although N_p is dependent on multiple plasma parameters such as electron temperature (T_e), gas temperature (T_g), electron density (n_e), and neutral density (n_n), there are a few points to take into consideration (Lieberman 2005). Firstly, the distribution of excited atoms is generally affected by T_e, T_g, and n_e. Secondly, when using atmospheric-pressure low-temperature plasma the effective electron temperature can be found to be in a particularly narrow range of 1-2 eV. Lastly, the gas temperature of nonthermal plasmas generally lies within a range of 300-600 K . So, with these points taken into consideration, it can be assumed that changes in the electron density have the largest impact on N_p compared to T_e and T_g. Therefore, any changes seen in N_p can be attributed to changes in n_e (Fantz 2006, Friedl 2012). By amending equation (2.3.3.2)

to give equation (2.3.3.3), the relative population density of excited species as a function of electron density can be obtained. By plotting N_p against the excitation energy levels, it is made much clearer how population increases and decreases show the relationship of energy transfer between atoms and molecules and how excited species are quenched and generated through collisional processes with neutral species i.e. N_2. To go further with this, it would be possible to estimate n_e by calculating the population ratio (N_{p1} /N_{p2}) and comparing it to the line ratio (I_1/I_2) of spectral lines relating to 2p levels of Ar (Zhu 2009). X. M. Zhu *et al* used a collisional radiative model to calculate the electron density using the line ratio method for an atmospheric-pressure low-temperature argon discharge.

$$\frac{I_A}{A_{ij}} = N_p\left(n_e\right)$$
(2.3.3.3)

The use of OES measurements can also give an insight into the electron energy distribution function (EEDF) of a plasma discharge. By using a line intensity ratio method, one can determine whether the electrons present exist more so in the high energy tail or the low energy bulk of their distribution of energies. In order to carry out this line ratio technique, a species that is excited by direct electron collision at high energy and an atom at low energy is needed, such as N_2 at 337 nm and N_2^+ at 391 nm (Fantz 2012). By dividing the absolute intensity of the high energy atom by the absolute intensity of the low energy atom, one can get a ratio spread to show the spread of electron energies. If the vale is above one, then the processes are dominated by low energy electron collisions, and vice versa. By obtaining this information, the gas kinetics and mechanisms that are undergone to generate the excited species that are recorded by OES can be understood with more clarity.

As well as using OES, the use of absorption spectroscopy fives a wider scope into the gas chemistry of a plasma discharge. By using a spectrometer with a UV-VIS-NIR light source, a full range of recordings can generally take place between 200-900 nm. By recording the signal from the light source across an optical path that encompasses the volume where plasma will be generated, one can use the decrease in light intensity during plasma discharge to determine the changes in intensity due to being decreased by absorption. For example, ozone emits light above 900 nm and is difficult to detect with many spectrometers, but it absorbs light in the UV range. This absorption technique then becomes crucial to detect more species that could be present when creating a plasma discharge. The use of equation (2.3.3.4) below shows how the spatial average density of a species can be calculated by using optical absorption spectroscopy. $D(t)$ is the spatial average density, $\sigma(\lambda)$ is the wavelength dependent absorption coefficient, L is the optical path length, $I(0)$ is the reference signal intensity, and $I(t)$ is the measured intensity (Scally 2018(a)).

$$D(t) = \frac{1}{\sigma(\lambda) \cdot L} \ln \frac{I(0)}{I(t)}$$
(2.3.3.4)

2.4 Plasma Applications

As mentioned, there are many areas that are being updated and innovated with new technologies that have been designed to generate non-thermal plasma to treat various samples. The following are outlines of each area mentioned previously to give a better insight into the specific processes that have made plasma technologies popular in recent years and why it is emerging as novel approach to create new and better treatment methodologies.

2.4.1 Food and Biological Implementation

Current agricultural produce protocols include the use of pesticides, crop rotation, produce storage, thermal treatment, drying, freezing, protective packaging, and chemical washes (Cullen 2017). These examples are set up more as intervention steps to reduce the growth and spread of contaminants such as bacteria and pests. Certain factors dictate the implementation of these steps and these include: the impact it will have on the quality of the product, is the produce for human or livestock consumption, will the produce be used for plantation of crops, and will the step impact health and safety standards in industry or cause greater harm to the end user. These factors are taken into consideration when developing new innovative technologies, so the steps taken to treat various samples need to be optimised and brought to a minimum. From this, the latest generation of systems and technologies have been developed to create a treatment process which will efficiently create protocols that yield a more "natural" and greener process for multiple products along the production line for different produce samples. By implementing NTP systems, it has been shown that the germination of grains can be improved, the shelf-life of foods can be prolonged, bacterial and fungal growths can be controlled, and pesticides can be broken down into less toxic constituents (Jiafeng 2014, Phan 2017, Attri 2016, Pankaj 2013, Panngom 2016, Ulbin-Figlewics 2013).

The use of NTP systems creates a unique environment that allows for a wide range of mechanisms and reactions to occur. These can be utilised to decontaminate food produce while minimising the use of harsher procedures such as thermal and radiation treatment or chlorine washes. In recent studies it has been found that although the treatment of samples using NTP impact and inhibit the growth of bacteria, moulds, and fungi and degrade the pesticide coating on the external layers, there may be impacts on food in terms of taste, quality, and rheological properties which need to

be studied further (Lee 2016, Bauer 2017, Lee 2017). Produced from the discharge of NTP systems are reactive oxygen species (ROS) and reactive nitrogen species (RNS). These species include hydroxyl radicals, nitrates, nitrites, atomic oxygen, ionic nitrogen, peroxides, and nitrous oxides (i.e. O, O_2, OH, H_2O_2, N_2^+, NO, NO_2, NO_3^-, N_2O_4, O_3) (Graves 2012, Kim 2016, Chauvin 2017). Studies carried out by Misra *et al* (2014), Wang *et* al (2016), and Han *et al* (2016) show that the treatment of food samples with NTP systems can cause decontamination across the sample surfaces and increase the shelf-life of the product. By creating abundant ROS and RNS and allowing them to interact with the surface of food produce, different interactions and mechanisms can occur with the biological media (bacteria). Interaction of reactive oxygen and nitrogen species to bacteria cells causes a bactericidal effect that kills many microbial contaminants (Bermúdez-Aguirre 2013). ROS causes an oxidation process that may destroy the bacteria cell wall by breaking down the C-O, C-N, and C-C bonds of peptidoglycans and oxidising the lipids within the cell (Lee 2017). This leads to the death of the cell and can cause apoptosis in multicellular organisms if the dosage of oxidative species is high enough to cause stress on the media (Turrini 2017). By carrying out this decontamination process on food stuffs, a much more viable environment is created that reduces the biological mechanisms that would cause the foods to spoil faster as a result of the retardation of bacteria growth such as, *Escherichia coli*, *Listeria monocytogenes* and *Staphylococcus aureus*.

2.4.2 Material Processing

Many materials need to undergo processes to give them properties that are more favourable for specific uses. One may want to create a more hydrophobic or hydrophilic surface, to increase the tensile and bonding strength of the material, to create a coating on the surface that will act as an antibacterial barrier, or to allow for

a more bio-acceptable surface. As with any product, the dependence on the end use of the material dictates what characteristics are warranted and therefore, what fabrication and treatment processes are used to create the materials. Polymers are a commonly used material in many industries. They can be used as packaging materials for food, scaffolding for surgical sutures, surface coatings, and electrical components. Some polymers of note include polyethylene (PE), polyethylene terephthalate (PET), polytetrafluoroethane (PTFE), high density polyethylene (HDPE), and low-density polyethylene (LDPE).

Cold plasma is widely used to functionalise material surfaces and to alter their properties during their synthesis to give more desirable characteristics for their end use. The methods used when employing NTP systems to modify material surfaces include etching or cleaning, deposition or sputtering. Utilising different gas chemistries when creating a plasma discharge give the ability to vary and control the outcome of plasma treatments and allow one to tailor the treatment in order to gain the wanted effects and changes on material's surface. In the case of Fatyeyeva *et al* (2014), the use of CF_4 caused the surface of polyamide samples to become more hydrophobic while the use of N_2 and O_2 gases contributed to the hydrophilic surface functionalisation of the polyamide samples. Work carried out by Sanchis *et al* (2006) showed, through the use of Fourier transform infrared spectroscopy (FTIR), atomic force microscopy (AFM), and differential scanning calorimetry (DSC), that the polarity of treated LDPE samples had an increase in the surface polarity. The results that they obtained show that the wettability of the treated samples is greater than the reference due to the formation of carbonyl, carboxyl, and hydroxyl groups on the surface when using a low pressure O_2 plasma discharge. They also found that short treatment times promote the formation of the aforementioned polar groups and that

longer treatment times caused slight abrasions on the samples surface with little impact on the surface roughness. This functionalisation and increase in wettability of LDPE and other polymers that undergo plasma treatment is attributed to discharges containing oxygen. Modifying the surfaces of polymers may be carried out through etching or bombardment from high energy particles or deposition of reactive species. Atomic oxygen is commonly associated with having one of the highest influences on creating polar groups on polymer surfaces. Inert species such as Ar or He would be associated with bombardment of the surface and create binding sites and atomic crevices on the surface which increases the surface energy and wettability of the sample. The results of using various gases can be seen in works carried out by Kostov *et al* (2010) and Scally *et al* (2017) where the use of ambient air for plasma discharges impact the surface metrology of treated samples due to the O_2 and N_2 content found in air. It can also be seen in the work carried out by Scally *et al* (2017) *(Shown in Chapter 3 of this thesis)* that the use of inert gases still interact with ambient air to produce reactive species, but sue to the high energy atoms that are created, the etching of the surface and transfer of energy from these atoms cause the surface energy of the samples to increase and therefore increase their wettability. This shows that the use of different systems and gases impact the outcome of treated samples and that the plasma discharge chemistry must be fully understood and controlled before going through treatment protocols with the system. By creating discharges that bombard and etche the surface of polymers, the binding sites that are created improve the binding strength when two polymers are overlapped and sealed together (Poncin-Epaillard 1999). This bombardment and etching effect is also used to modify and fabricate other materials, such as electronics or circuitry. Instead of using chemicals to wet etch a substrate, Ar gas can be used to create a discharge that generates energetic atomic Ar that will

remove layers of the substrate and will do so without deviating into the boundary set by the mask and without creating contaminations through the creation of reactive by-products.

2.4.3 Medical Treatment

The use of NTPs has spread to multiple industries due to the qualities it possesses as mentioned in previous sections. Not too dissimilar from the use of reactive species generated from plasma discharges in the food industry, the medical sector are testing the latest plasma technologies as alternative medical treatments. By incorporating NTP treatment methods into different stages of medical procedures, the growth of various bacteria and viruses may be destroyed or inactivated by means of interaction with ROS and RNS and allow for a more sterile environment for recuperation (Poor 2014, Whittaker 2004). Most importantly for the medical sector is the current antibiotic crisis which is attributed to the overuse and misuse of antibiotics and the lack of funding into the development of new and effective drugs (Ventola 2015). New plasma systems aim to tackle this problem and overcome the immune response that has made it more difficult to treat various bacteria and infections such as methicillin-resistant *Staphylococcus aureus* (MRSA).

A paper based on the works that Kubinova *et al* (2017) carried out show that the use of NTP can aid in the healing of acute open wounds. Using a single jet NTP system they treated open wounds on rats. They found that the ROS generated not only had a bactericidal effect that sterilised the wounds, but also identified an accelerated healing time of the wounds. It was shown in this work and work carried out by Luk *et al* (2005) and Pérez-Gómez *et al* (2014) that NO species have been shown to be a large importance for accelerated wound healing with low levels of NO bioavailability

impairing wound healing. This shows that the characterisation and monitoring of the plasma gas chemistry is vital as the correct mixture, reactive species concentration and density need to be known to optimise the treatment of biological samples. If the dosage is too high then necrosis and apoptosis may occur on healthy cells mammalian and negatively impact the overall recovery (Kubinova 2017). For this reason, care is needed when treating samples to fully treat any wounds or infections on living tissue without damaging healthy tissue. By varying the gas chemistry, cold plasma can be potentially overcome the resistance and immune responses of bacterial and viral cells.

Other works have shown that the use of non-thermal plasma can aid in the treatment of cancerous cells and tumours. This has been investigated in procedures carried out by Nguyen *et al.* (2016), Chen *et al.* (2016), and Kang *et al.* (2014), in which it was demonstrated that implementation of NTP systems have yielded apoptosis and decreased proliferation in cancer cell lines due to DNA mutation. This mutation has been associated with oxidative stress caused by a cascade effect because of overproduction of ROS within the cancerous cells and damage of DNA causing a cell cycle arrest that led to early and late stage apoptosis. However, it has also been found that the use of NTP for the treatment of tumours has a penetrative effect and can cause apoptosis throughout the tumour even if the surface was the only area treated. This is possibly due to the reactive radical species penetrating the surface of the tumour, inducing a bystander effect as seen in ionising radiation treatments, a systemic breakdown of intracellular signalling, or even synergistic influences from the other components of the plasma discharge such as UV radiation (Vandamme 2011). Yagi *et al.* (2015) drew a correlation between the cell death of melanoma cells in mice and the reactive species associated with water vapour (mainly OH, but also possibly H_2O_2, HO_2, HNO_x etc.) has the largest impact on the resulting apoptosis of the melanoma

cells after plasma treatment. The densities of OH, NO, and O were monitored by using laser-induced fluorescence (LIF).

The results that have been found in the works presented are quite promising and show the potential that NTP systems have in replacing or supporting current treatment procedures. However, it is obvious that more research needs to be carried out to understand the limitations of the technology and what long-term effects could arise from these treatments. As well as this, it must be fully understood what reactive species are required to optimise these treatments and those carried out in other industries, and for this reason it is important to carry out measurements such as OES and OAS to characterise the gas chemistry and kinetics of the plasma being generated.

2.5 Plasma Systems in Use

As the use of NTP systems is becoming more prevalent in different areas as described in the application section of this review and in many other works not mentioned, the need for system design and fabrication optimisation is of high priority. Achieving this requires diagnostic testing of the system when being developed to ensure that the plasma being generated is tailored for the specific needs required for its end use. Optical spectroscopy and electrical measurements are often used to determine the parameters required to generate a plasma discharge in the system and allow one to discern what gas chemistry can be created and what parameters impact this the most. Described in detail are the developments and optimisation of DBD, APPJ, and micro-plasma array systems that could potentially be utilised to further different areas.

2.5.1 Dielectric Barrier Discharge

Dielectric barrier discharge (DBD) systems are possibly one of the most basic plasma discharge set ups that can be created. By placing a high voltage (HV) and ground electrode parallel to one another with a gas between them, gas breakdown can occur when enough electrical power is supplied to the system to create plasma discharge. A simple schematic can be seen in Figure 2.5 below. However, when using an AC power supply an insulating dielectric material is needed to dampen the electric field and prevent conductance and arcing from one electrode to another. This is not necessary for DC power supplies. If the dielectric material is too thin or the power supplied is too great, then electrical breakdown of the material can arise and damage the system and any samples being treated. This is a cause of concern when developing such systems and why the end use constantly needs to be kept in mind. DBD systems are often used to treat the surfaces of samples or to treat liquid samples. This is due to the atmospheric pressure discharge environment having low flow rates interacting and disrupting the sample surface and allow for larger areas of treatment when compared to other systems such needle jet plasma generators. Such works allow for a large biological or inorganic sample area to be treated in one go and show how the plasma volume impacts the surface and bulk properties. A point of consideration is the homogeneity of the plasma discharge and whether or not it is uniform through the plasma volume or whether there are areas of higher population densities of reactive species or filamentary discharges throughout the volume. Inhomogeneity would cause

an imbalance within the plasma volume and would impact the outcome for applications such as etching.
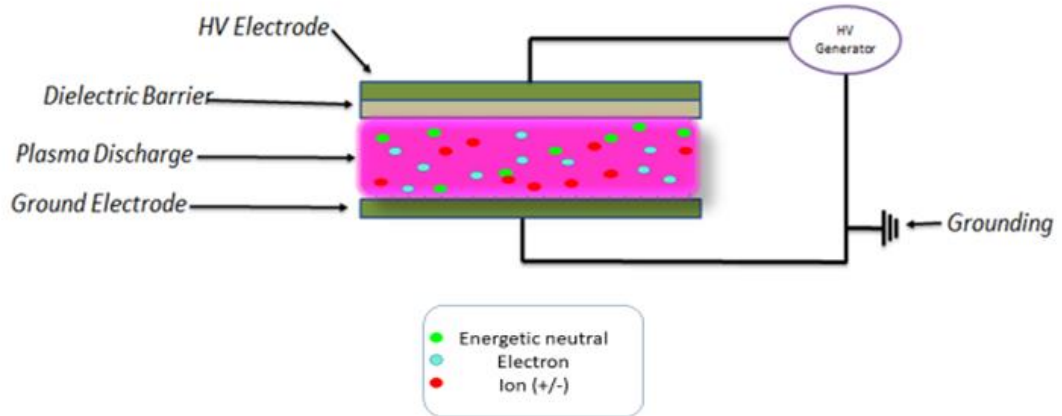
Figure 2.5: Example of an AC dielectric barrier discharge system.

Alterations to the design of DBD systems has yielded many fascinating results. One such system design is the floating electrode DBD which utilizes the sample for treatment as the grounding source and can be used for direct treatment of living tissue. In Han *et al* (2017) a DBD system was developed for the treatment of human colorectal cancer (CRC) cell lines HT29 and HCT116 and the impact ROS generation has on the formation of the CRC cells. For this work they developed a 50 kHz discharge system that used a copper electrode placed into a 100 mm diameter petri dish which was filled with biological media that the cells were immersed in. This media acted as the floating electrode for grounding. A duty cycle of 50 % was used with a pulse width of 5 μs. The setup included entry and exit points to allow for gases to be pumped through the system. The HV copper electrode was encased in an insulating material with a quartz

cover placed on the underside in contact with the electrode. Discharge occurred throughout the entirety of the petri dish volume when the media was placed under the HV electrode, whereas discharge only occurred on the edge of the electrode when the HV electrode was not yet placed into the petri dish. By using OES they were able to diagnose the discharge that occurred when using He as the inducer gas was used to prevent as much thermal damage as possible to the cell lines and a gas temperature of 340 K was measured. Emission lines from OH, O I, N_2, N_2^+, and He I were recorded with emphasis placed on ROS and RNS generation for the cell line treatment. The power used ranged from 0.6 – 7 W. Other works have included the use of floating electrodes to treat samples. Another example of these were carried out by Karki *et al* (2017). By using a HV electrode pin of 1.57 mm width with a 0.5 mm thick quartz slide adhered to the base of it and the surrounding insulating material, they were able to create a plasma streamer to interact with cell media (Karki 2017). The setup that they created was dubbed a mini dielectric barrier discharge (mDBD) plasma generator and it used the biological media that the cells were situated in as the floating electrode. In both works, a biological media was used as a floating electrode with the reactive species generated by the plasma discharge were sufficient to cause cell death, cell detachment, and interrupted the intracellular responses. By allowing the reactive species to interact with the biological media suspension, they could permeate through and interact with the cell lines present without causing thermal damage to the samples. This may be needed in future applications to reduce the amount of damage incurred from the physical and chemical interactions with the plasma discharge such as dose control and thermal damage and degradation reduction on healthy cells.

Other designs have been created to alter and optimize the plasma discharge that occurs when using DBD systems. As mentioned in the work carried out by Han

et al (2017) a floating electrode can be used as the grounding source to allow the formation of plasma between the sample surface and the HV electrode. However, the basic design of linear type DBD systems can have a drawback of losing power from floating voltage at the plasma outlet. By using a floating electrode design and altering the geometry of the DBD system, it has been shown that this loss can be brought to near 0 values. This has been shown in paper produced by Chen *et al* (2014). By making a T-shaped DBD plasma generator, a drive phase could be set to fully cancel out the floating potential and also the signal noise (Chen 2014). According to their results, this zero-potential setup would allow for fewer oxidative species to be generated and reduce the damage that may occur on mass spectroscopy samples which would lead to a better sensing performance and a less fragmented ion signal for mass spectroscopy applications. Another benefit that they found was that spectra obtained using the symmetrical T-shaped design had better data information than what was compared to a linear DBD generator.

2.5.2 APPJ and Microplasma Jet Arrays

The interest that has been gathered with regards to atmospheric plasma jets in recent times is due to their potential use in applications that were classically restricted to low pressure vacuum systems. APPJs have been investigated to determine their effiacies for surface treatments compared to previous methods. Such uses include, but are not restricted to: etching, deposition, material modification, surface sterilisation, and biological media treatment. A beneficial aspect of using APPJ systems is that, as mentioned, they do not require the use of vacuum systems and thus aid in lowering the cost of running treatment systems (Qian 2015). The various designs of APPJs can be seen in Figure 2.6.
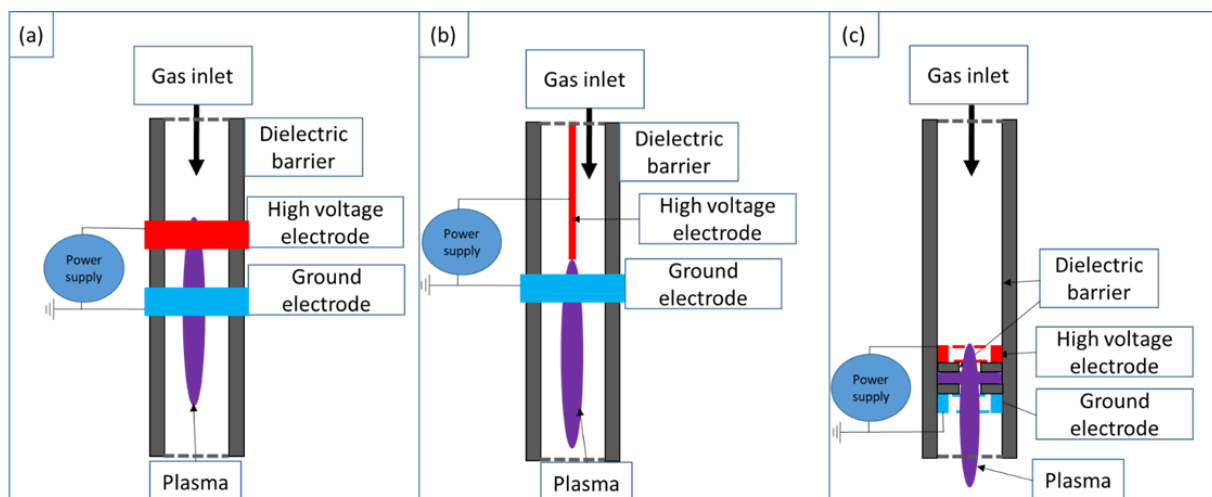
Figure 2.6: Different configurations of plasma jets **(a)** Both electrodes are set around a dielectric material with a gas flow going through the jet causing plasma to be generated inside of the dielectric tube **(b)** A high voltage pin is placed inside of the jet with the grounding set outside of the dielectric material to produce plasma as a gas flow runs through the system **(c)** Both electrode are set inside the dielectric tube with an added space placed between them.

Many works have been carried out with plasma jet systems by using either a single jet or a multijet array. The use of single jet makes for a compact treatment system that can often be very portable and versatile. By placing the jet onto a computer numerical controlled (CNC) framework, there is the possibility to move the jet over small areas to ensure that the full surface of a sample is treated. By using different gases and flow rates, one can impact the gas chemistry that is produced from the jet and tailor it according to the need of the samples being processed. However, there are drawbacks to certain plasma jet systems. Some operate at relatively high flow rates and make it difficult to carry out the treatment of liquid samples, and so require a solid or rigid sample surface in order to carry out treatments that rely only on the interactions of the reactive species of the plasma discharge. By varying the gas flow to try and not

damage a sample surface, the efficacy of the reactive species of the plasma discharge reaching and interacting with the sample surface severly drops. A way to try and overcome this can be seen in works that utilise a third electrode which acts as a second grounding space. An example of this can be seen in work of Lee *et al* (2009). By placing the sample on to a third electrode that acts as a grounding zone, the plasma discharge preferentially travels towards this zone and interacts even more with the sample being treated due to a higher density of reactive species being drawn to it (Lee 2009). This third floating electrode allowed induced a lower breakdown voltage and an increased discharge current.

Many applications seek to optimise treatment parameters and try to create an environment that can be regarded as highly efficient. To this end multijet systems are being developed in order to treat larger areas than a single jet possibly could compared to an array setup. By creating an array of plasma jets the gas chemistry, reactive species density, and gas kinetics all change and can be very beneficial for larger scale treatment procedures. Works carried out by Ichiki *et al* (2004) and Ideno *et al* (2006) show how an array of microplasma jets can be used to etch large surface areas (Ichiki 2004, Ideno 2006). The work carried out by Ideno *et al* (2006) used a single microplasma jet to intestigate the fundamental characetristics of scanning microplasma processing. In both works, however, they were able to achieve a maskless etching process and demonstrated how these jets can be used as a rapid micropabricaiton tool. However, these microjet systems operate at high temperatures and many processing protocols require NTP. Looking at other works, it can be seen that the use of plasma jet arrays with NTP discharge are very beneficial and add a lot more to the treatment of sample than using a single jet on its own. This is highlighted in works carried out by Kim *et al* (2012) and Ghasemi *et al* (2012) who show that an

array of jets overcome an inherent issue of plasma jet systems and allow for a larger treatment area of samples with increased properties of the plasma discharge (Kim 2012, Ghasemi 2012). The use of plasma jet arrays instead of increasing the size of a single jet is due to the instability and negative impact of the downstream transport of reactive species. By creating an array of jets that are close together, the electron energy and reactive species generation can be increased due to jet-to-jet coupling. This is potentially very useful for many applications that require fast treatment times and a large dosage for treatment in a shorter period of time.

2.6 Conclusion

The use of plasmas are very clearly growing at a steady rate and the possible applications of them is increasing every day. Looking at the areas that NTP can be applied shows that a large amount of innovation is being sought after and that the current technologies and processes require some form of updating. By utilising unique nature of plasma discharges, many applications will be brought to a higher level of function and will ultimately lead to new technoloigcal developments which will bring many years of theory into the real world. However, as evidenced by the works cited in this review there are still many gaps in the knowledge of plasma and their direct influence on certain samples. Therefore, it is paramount that diagnostic tools be used to investigate and characterise the exact nature of plasma discharges. Such diagnostics could include OES, OAS, LIF, and electrical characterisation. With these it can be made evident what reactive species are being generated, in what regime of the plasma volume, and what their density is like over time. To further push this, the use of plasma systems and creating plasma discharges should not be limited to the use of ambient air. Utilising different gases at varying ratios, flow rates, and pressures will provide better insights into the gas kinetics and chemistry that can be created. This will give

more knowledge on the physical interactions within the plasma volume and also what are the properties of the plasma that play a key role in certain treatment processes. In Chapters 3 – 6 of this work, investigations were carried out into the use of a commercial plasmajet system, an in-house made cylindrical DBD system, and a novel multi-pinned DBD system. The use of ambient air was beneficial in order to gain a baseline for the reactive species generated and compare them to the systems referenced and described in Chapter 2. However, other gases were then introduced into the NTP systems used for experimental research to demonstrate the importance of certain reactive species on sample surfaces and to illucidate more insights into the behavious of gas chemistries for tailoring to specific purposes. The gas chemistry was analysed using OES and OAS while various parameters, such as gas chemistry flow rates and mix ratios, were varied. The gas mixtures that were used, by chapter are:

Chapter 3 – Air, CO_2, and Ar flowing through an APPJ into an ambient air environment post-discharge.

Chapter 4 – Air as well as permeating air with a main mixture of Ar, He, Ar:He / He:Ar flowing through a cylyndircal DBD.

Chapter 5 – Air, CO_2, and Air:CO_2 flowing through an enclosed pin-to-plate DBD.

Chapter 6 – Air with no flow, but tailored chemistry through discharge frequency variance.

References

P. Attri, Maksudbek Yusupov, Ji Hoon Park, Lakshmi Prasanna Lingamdinne, Janardhan Reddy Koduru, Masaharu Shiratani, Eun Ha Choi & Annemie Bogaerts, "Mechanism and comparison of needle-type non-thermal direct and indirect atmospheric pressure plasma jets on the degradation of dyes", Scientific Reports, volume 6, 34419 (2016).

A. Bauer, Y. Ni, S. Bauer, P. Paulsen, M. Modic, J. L. Walsh, F. J. M. Smulders, "The effects of atmospheric pressure cold plasma treatment on microbiological, physical-chemical and sensory characteristics of vacuum packaged beef loin", Meat Science, volume 128, 77-87 (2017).

D. Bermúdez-Aguirre, E. Wemlinger, P. Pedrow, G. Barbosa-Cánovas, and M. Garcia-Pereza, "Effect of atmospheric pressure cold plasma (APCP) on the inactivation of Escherichia coli in fresh produce", Food Control, volume 34, 149-157 (2013).

J. Chauvin, F. Judée, M. Yousfi, P. Vicendo, and N. Merbahi, "Analysis of reactive oxygen and nitrogen species generated in three liquid media by low temperature helium plasma jet", Scientific Reports, volume 7, 4562 (2017).

C. Y. Chen, C. H. Chiang, and C. H. Lin, "Novel Atmospheric Pressure Plasma Utilizing Symmetric Dielectric Barrier Discharge for Mass Spectrometry Applications", IEEE Transactions on Plasma Science, volume 42, 3726-3731 (2014).

Z. Chen, L. Lin, X. Cheng, E. Gjika, and M. Keidar, "Treatment of gastric cancer cells with nonthermal atmospheric plasma generated in water", Biointerphases, volume 11, (2016).

P. J. Cullen, J. Lalor, L. Scally, D. Boehm, V. Milosavljević, P. Bourke, and K. Keener, "Translation of plasma technology from the lab to the food industry", Plasma Processes and Polymers, e1700085, (2017).

U. Fantz, H. Falter, P. Franzen, D. Fantz, U., Falter, H., Franzen, P., D. Wünderlich, M. Berger, A. Lorenz, W. Kraus, P. McNeedy, R. Rield, and E. Speth, "Spectroscopy—a powerful diagnostic tool in source development", Nuclear Fusion, 46(6), S297–S306, (2006).

K. Fatyeyeva, A. Dahi, D. Langevin, J. M. Valleton, F. Poncin-Epaillard, and S. Marais, "Effect of cold plasma treatment on surface properties and gas permeability of polyimide films", RSC Advances, volume 4, 31036-31046 (2014).

R. Friedl, and U. Fantz, "Spectral intensity of the N2 emission in argon low-pressure arc discharges for lighting purposes", New Journal of Physics, 14, 043016, (2012).

M. Ghasemi, J. W. Bradley, and J. L. Walsh, "Atmospheric plasma jet array for large scale surface treatment", 2012 Abstracts IEEE Int.

D. B. Graves, "The emerging role of reactive oxygen and nitrogen species in redox biology and some implications for plasma applications to medicine and biology", Journal of Physics D: Applied Physics, volume 45, 263001 (2012).

D. Han, J. H. Cho, R. H. Lee, W. Bang, K. Park, M. S. Kim, J. H. Shim, and J. I. Chae, "Antitumorigenic effect of atmospheric-pressure dielectric barrier discharge on human colorectal cancer cells via regulation of Sp1 transcription factor", Scientific Reports, volume 7. 43081 (2017).

L. Han, D. Boehm, E. Amias, V. Milosavljević, P. J. Cullen, an P. Bourke, "Atmospheric Cold Plasma Interactions with Modified Atmosphere Packaging Inducer Gases for Safe Food Preservation", Innovative Food Science & Emerging Technologies, volume 38, 384-392 (2016).

H. Hillborg, U. W. Gedde, Polymer, 1998, 39, (1991).

I. H. Hutchinson, "Principles of Plasma Diagnostics", Cambridge University Press (1987).

T. Ichiki, R. Taura, and Y. Horiike, "Localized and ultrahigh-rate etching of silicon wafers using atmospheric-pressure microplasma jets", Journal of Applied Physics, volume 95, 0021-8979 (2004).

T. Ideno, and T. Ichiki, "Maskless etching of microstructures using a scanning microplasma etcher", Thin Solid Films, volume 506-507, 235-238 (2006).

M. Ishaq, M. Evans, and K. Ostrikov, International Journal of Cancer 134, 1517 (2013).

J. Jiafeng, H. Xin, L. Ling, L. Jiangang, S. Hanliang, X. Qilai, Y. Renhong, and D. Yuanhua, "Effect of Cold Plasma treatment on Seed Germination and Growth of Wheat", Plasma Science and Technology, volume 16, 54 (2014).

S. U. Kang, J. H. Cho, J. W. Chang, Y. S. Shin, K. I. Kim, J. K. Park, S. S. Yang, J. S. Lee, E. Moon, K. Lee, C. H. Kim, "Nonthermal plasma induces head and neck cancer cell death: the potential involvement of mitogen-activated protein kinase-dependent mitochondrial reactive oxygen species", Cell Death and Diseases, volume 5, e1056 (2014).

S. B. Karki, E. Yildirim-Ayan, K. M. Eisenmann, and H. Ayan, "Miniature Dielectric Barrier Discharge Nonthermal Plasma Induces Apoptosis in Lung Cancer Cells and Inhibits Cell Migration", BioMed Research International, volume 2017, 8058307 (2017).

S. J. Kim, and T. H. Chung, "Cold atmospheric plasma jet-generated RONS and their selective effects on normal and carcinoma cells", Scientific Reports 6, 20332 (2016).

J. Y. Kim, J. Ballato, and S. Kim, "Intense and Energetic Atmospheric Pressure Plasma Jet Arrays", Plasma Processes and Polymers, volume 9, 253-260 (2012).

R. D. Knight, "Physics for Scientists and Engineers, A Strategic Approach", edited by C. Benson, Pearson (2008).

U. Kogelschatz, "Dielectric-barrier Discharges: Their History, Discharge Physics, and Industrial Applications", Plasma Chemistry and Plasma Processing, volume 23 (2003).

K. G. Kostov, L. R. Dos Santos, R. Y. Honda, P. A. P. Nascente, M. E. Kayama, M. A. Algatti, R. P. Mota, "Treatment of PET and PU polymers by atmospheric pressure

plasma generated in dielectric barrier discharge in air", Surface and Coatings Technology, volume 204, 3064-3068 (2010).

S. Kubinova, K. Zaviskova, L. Uherkova, V. Zablotskii, O. Churpita, O. Lunov, and A. Dejneka, 'on-thermal air plasma promotes the healing of acute skin wounds in rats', Scientific Reports, volume 7, 45183 (2017).

H. Lee, H. I. Yong, H. J. Kim, W. Choe, S. J. Yoo, E. J. Jang, C, and Jo, "Evaluation of the microbiological safety, quality changes, and genotoxicity of chicken breast treated with flexible thin-layer dielectric barrier discharge plasma", Food Science and Biotechnology, volume 25, 1189-1195 (2016).

H. W. Lee, S. H. Nam, A. A. H. Mohamed, G. C. Kim, and J. K. Lee, "Atmospheric Pressure Plasma Jet Composed of Three Electrodes: Application to Tooth Bleaching", Plasma Processes and Polymers, volume 7, 274-280 (2009).

J. Lee, C. W. Lee, H. I. Yong, H. J. Lee, C. Jo, and S. Jung, "Use of Atmospheric Pressure Cold Plasma for Meat Industry", Korean Journal of Food Science and Animal Resources, volume 37, 477-485 (2017).

M. A. Lieberman, A. J. Lichtenberg, Principles of Plasma Discharges and Materials Processing, publ. John Wiley & Sons, Inc. (2005).

J. Loureiro and J. Amorim, "Kinetics and Spectroscopy of Low Temperature Plasmas", series editors: K. H. Becker, J. -M. Di Meglio, S. Hassani, B. Munro, R. Needs, W. T. Rhodes, S. Scott, H. E. Stanley, M. Stutzmann, A. Wipf, Springer (2016).

P. P. Luk, S. N. Sinha, and R. Lord, "Upregulation of inducible nitric oxide synthase (iNOS) expression in faster-healing chronic leg ulcers", Journal of Wound Care, volume 14, 373–375 (2005).

N. N. Misra, L. Han, B. K. Tiwari, P. Bourke, and P. J. Cullen, editor I. S. Boziaris "Nonthermal Plasma Technology for Decontamination of Foods", Novel Food Preservation and Microbial Assessment Techniques, CRC Press, Chapter 6, pp. 155 (2014).

N. H. Nguyen, H. J. Park, S. S. Yang, K. S. Choi, and J. S. Lee, "Anti-cancer efficacy of nonthermal plasma dissolved in a liquid, liquid plasma in heterogeneous cancer cells", Scientific Reports, volume 6, 29020 (2016).

S. K. Pankaj, N. N. Misra, P. Cullen, "Kinetics of tomato peroxidase inactivation by atmosphere pressure cold plasma based on dielectric discharge" Innovative Food Science Emerging Technologies, volume 19, 153–157 (2013).

K. Panngom, S. H. Lee, D. H. Park, G. B. Sim, Y. H. Kim, H. S. Uhm, G. Park, and E. H. Choi, "Non-Thermal Plasma Treatment Diminishes Fungal Viability and Up-Regulates Resistance Genes in a Plant Host", PLoS ONE 9(6): e99300, (2014).

E. Pérez-Gómez, M. Jerkic, M. Prieto, G. Del Castillo, E. Martín-Villar, M. Letarte, C. Bernabeu, F. Pérez-Barriocanal, M. Quintanilla, and J. M. López-Novoa, "Impaired wound repair in adult endoglin heterozygous mice associated with lower NO bioavailability", Journal of Investigation Dermatology, volume 134, 247–255 (2014).

K. T. K. Phan, H. T. Phan, C. S. Brennan, and Y. Phimolsiripol, "Nonthermal plasma for pesticide and microbial elimination on fruits and vegetables: an overview", International Journal of Food Science and Technology, volume 52, 2127-2137 (2017).

F. Poncin-Epaillard, J. C. Brosse, and T. Falher, "Reactivity of surface groups formed onto a plasma treated poly(propylene) film", Macromolecular Chemistry and Physics, volume 200, 989-996 (1999).

A. E. Poor, U. K. Ercan, A. Yost, A. D. Brooks, S. G. Joshi, "Control of multi-drug-resistant pathogens with non-thermal-plasma-treated alginate wound dressing", Surgical Infections, volume 15, 233-243 (2014).

M. Qian, C. Yang, S. Liu, G. Ni, and J. Zhang, "Discharge Characteristics of an Atmospheric Dielectric-Barrier Discharge Jet", IEEE Transactions of Plasma Science, volume 43, 1780-1786 (2015).

M. R. Sanchis, V. Blanes, M. Blanes, D. Garcia-Sanoguera, and R. Balart, "Surface modification of low density polyethylene (LDPE) film by low pressure O2 plasma treatment", European Polymer Journal, volume 42, 1558-1568 (2006).

L. Scally, J. Lalor, P. J. Cullen, and V. Milosavljević, "Impact of atmospheric pressure nonequilibrium plasma discharge on polymer surface metrology"Journal of Vacuum Science and Technology A: Vacuum, Surfaces, and Films 35, 105 (2017).

E. Turrini, R. Laurita, A. Stancampiano, E. Catanzaro, C. Calcabrini, F. Maffei, M. Gherardi, V. Colombo, and C. Fimognari, "Cold Atmospheric Plasma Induces Apoptosis and Oxidative Stress Pathway Regulation in T-Lymphoblastoid Leukemia Cells", Oxidative Medicine and Cellular Longevity, volume 2017, 4271065 (2017).

N. Ulbin-Figlewicz, E. Brychcy, and A. Jarmoluk, "Effect of low-pressure cold plasma on surface microflora of meat and quality attributes", Journal of Food Science and Technology, volume 52, 1228-1232 (2013).

M. Vandamme, E. Robert, S. Lerondel, V. Sarron, D. Ries, S. Dozias, J. Sobilo, D. Gosset, C. Kieda, B. Legrain, J. M. Pouvesle, and A. Le Pape, "ROS implication in a new antitumor strategy based on non-thermal plasma", International Journal of Cancer, volume 130, 2185-2194 (2011).

C. L. Ventola, "The Antibiotic Resistance Crisis Part 1: Causes and Threats", Pharmacy and Therapeutics, volume 40, 277-283 (2015).

J. Wang, H. Zhuang, A. Hinton Jr., and J. Zhang, "Influence of in-package cold plasma treatment on microbiological shelf life and appearance of fresh chicken breast fillets", Food Microbiology, volume 60, 142-146 (2016).

A.G. Whittaker, E.M. Graham, R.L. Baxter, A.C. Jones, P.R. Richardson, G. Meek, G. A. Campbell, A. Aitken, H. C. Baxter, "Plasma cleaning of dental instruments", Journal of Hospital Infections, volume 56, 37-41 (2004).

I. Yagi, Y. Shirakawa, K. Hirakata, T. Akiyama, S. Yonemori, K. Mizuno, R. Ono, and T. Oda, "Measurement of OH, O, and NO densities and their correlation with mouse melanoma call death rate treated by a nanosecond pulsed streamer discharge", Journal of Physics D: Applied Physics, volume 48, 424006 (2015).

X. M. Zhu, Y. K. Pu, N. Balcon, and R. Boswell, "Measurement of the electron density in atmospheric-pressure low-temperature argon discharges by line-ratio method of optical emission spectroscopy", Journal of Physics D: Applied Physics, 42, (2009).

Chapter 3 - Impact of Atmospheric Pressure Nonequilibrium Plasma Discharge on Polymer Surface Metrology

Abstract

Due to the attraction of plasma technologies as a clean and efficient means of surface modification, significant research has gone into the physical and chemical aspects of polymer functionalization. In this study, it was shown that the use of an atmospheric plasma jet can efficiently modify the surface of polyethylene terephthalate samples and change their hydrophobic properties to more hydrophilic characteristics. The dependence on the changes with respect to time, distance, and atomic oxygen (O I) intensity were considered as factors. It was found that with closer proximity to the plasma source (without causing thermal degradation) and with increasing levels of O I, that the changes of water contact angle and surface free energy can be maximized. It was also observed that the electron energy distribution function, for a given chemistry, significantly differed with changes in distance from the jet nozzle. This

shows that for this type of plasma jet system, the bulk of the chemical reactions occur in the nozzle of the jet and not in the surrounding atmosphere. Therefore, this leads to more efficient energy transfer, higher gas temperatures, and better surface activation of samples when compared to systems that produce external chemical reactions due to more diffusion in the surrounding atmosphere and loss of reactive species to other atoms and molecules that are present.

3.1 Introduction

The use of polymers continues to replace traditional materials such as glass and paper for numerous processing industries. The modification and functionalisation of different polymers has been effectively achieved through the use of non-thermal plasma surface interactions. By introducing the surfaces of various materials to the reactive species, high energy electrons and ion bombardments associated with plasma discharges, a variety of interactions occur. An effect of using high energy electrons, atoms and molecules on the surface of polymer materials such as polyethylene (PE) or polyethylene terephthalate (PET), is that surfaces can be modified to become more polar and as a result they become more hydrophilic and have their surface energies increased (Pankaj 2014, Trentin 2015, Wolf 2010). This can cause surfaces to become more reactive and accepting of solutions introduced to the surface (Dowling 2012). Through the use of ion bombardment on the outer layers of a material, atomic crevices can be created which then become small binding pockets, which allows for better adhesion between plastic packaging during heat sealing of containers (Aliofkhazraei 2015, Mueller 1998). The combination of these different aspects allows for packaging films that can be sterilized, can create further reactions with the packaged samples that may increase product shelf life, create a stronger packaging seal, and impart antimicrobial properties (Ozdemir 1999).

Advantages of non-thermal plasma include reduced temperature treatment of samples, such as autoclaving; creating a more convenient method of sterilization and the ability to strengthen or functionalise materials. This allows for a wider range of samples to be treated, which is important for materials such as thin layer films for packaging as these are typically sensitive to thermal degradation. Current non-thermal plasma systems include plasma jets, dielectric barrier discharge (DBD) and corona discharge systems with applications including medical, food and material processing (von Woedtke 2013). The use of plasma treatment systems in these fields shows that there is an importance to intimately understand and predict the phenomena that take place at the surface boundaries of the treated materials. With material processing, nonthermal plasma can be used to make a plastic polymer more hydrophilic and create more binding sites for stronger adhesion for product packaging. By introducing the polymer samples to ambient atmospheric plasma discharges, the surface may undergo reactive mechanisms that create a more polar surface, allowing for better acceptance of water molecules. Various plastic polymers have been studied for the use in a large range of areas such as food packaging, electrical and biomedical industries (Trentin 2014, Yasuda 1977). Since polymers can be thermally damaged relatively easily, precautions are needed during the treatment of these materials as their integrity can be diminished quickly if exposed to the plume of a plasma jet. For the various methods that non-thermal plasmas are employed to modify different material surfaces, it is a necessity to be able to determine what and to what degree an effect occurs. Oxygen containing gases have been reported to play an important role in the modification of polymer surfaces, inducing greater effects when compared to inert gases such as argon (Ar) (Guruvenket 2004, Lehocky 2003, Morra 1990, Vesel 2012). This is due to gases having an oxygen content being able to etch and activate surfaces, modifying carbon-

oxygen bonds to create different functional groups and therefore different surface properties (Grace 2003).

In order to carry out the investigation described in this work, the use of water contact angle (WCA) and surface free energy (SFE) measurements were employed to determine how much surface modification and activation occurred after non-thermal plasma treatment. To compare the effects of treatment time, sample distance, and gases used, OES measurements were carried out to identify and analyse the intensities of atomic oxygen spectral lines generated by the plasma discharge, as well as spectral emissions of other species from the plasma. Secondly, OES was employed to identify optimum plasma treatment conditions for PET surface modification, where the EEDF was calculated for Ar gas chemistry to show shifts in the energies of electrons. Such energy shifts would indicate at which points the optimum transfer of energy and chemical reactions for functionalisation occur. These parameters were then used to create an experimental study for the determination of an online analysis of the surface metrology of plasma treated PET samples.

Air was chosen as one of the inducer gases as it is economically and environmentally friendly and is typically involved in open air reactions when other gases are employed. This provides a good baseline for determining, with a higher degree of certainty, what effects occur with changes in gas properties and how this relates to gas chemistry interactions. CO_2 was chosen due to its frequent use in the food industry. Helium (He) is a recommended gas for the PVA plasma jet system used. We also employed argon (Ar) in this study as it has similar properties to He. As both of these gases have an inert nature, they can be used to compare the gas chemistry of the other two gases and study how they would further react with the atmosphere surrounding the nozzle influencing the creation of the reactive species. This allows a comparison between

each gas to be made and identification of which species (in this case atomic oxygen) can be related back to the changes in WCA and SFE and how the chemical reactions develop over time and distance. PET is one of the most commonly used polymers for packaging. Insights into the possible secondary effects of non-thermal plasma treated samples can have on the PET film they are sealed with, and vice versa, is needed to identify what, if any, long-term benefits or problems may occur.

3.2 Experimental

3.2.1 Setup
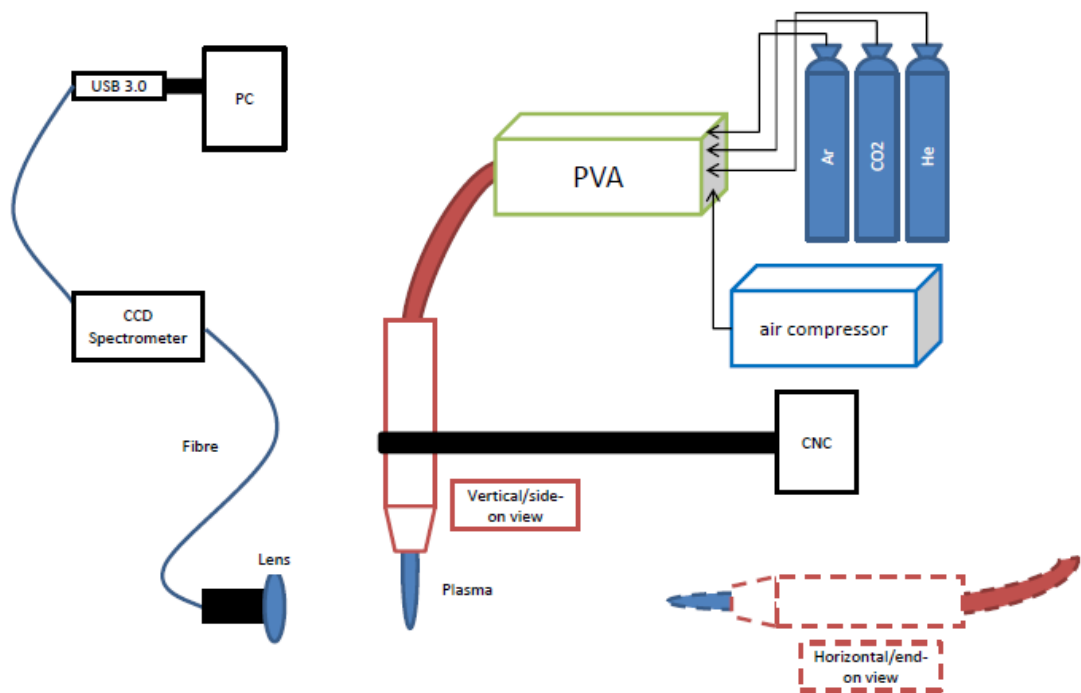
Figure 3.1: (Colour online) Schematic of plasma system set up and references of orientations used for OES acquisition.

Experimental treatments of PET were carried out using the PlasmaPen™ which is manufactured by PVA TePla and the experimental setup can be seen in Figure

3.1. The system operates at a gas pressure of 600 kPa for mixtures of gases including N_2, N_2/H_2, O_2 and CO_2. The system allows for a maximum gas flow of about 22 L/min. The frequency at which the plasma is generated is 60 Hz, creating an environment where the oscillation of electrons and heavy particles, such as ions, can occur. The diagnostics of the plasma are limited to optical spectroscopy techniques due to the plasma generator and its matching network being housed in a closed off case. An air compressor was used to generate air flow through the system so that there was a continuous gas flow out of the nozzle of the plasma jet. Apart from the compressed air, cylinders of high purity CO_2, Ar and He were used. The gas flow (from the air compressor/CO_2/Ar/He) causes the plasma to be pushed out of the plasma pen in a narrow stream and allows for greater targeting of samples. There is no control over the gas flow once the pressure has been set on the air compressor or gas cylinders used to supply the atmospheric plasma jet. The position of the jet was controlled with a robotic arm along the x-, y- and z-axes through the use of a computer numeric control (CNC) software. This allowed for high precision movement, which was a necessity to determine the minimum distance at which the treatment of PET could be operated without inducing thermal damage.

3.2.2 Polymer Treatment

The treatment of the samples was carried out in triplicate to obtain an average and to note any variances occurring during the treatment process. In total, nine batches of PET were treated. Each batch consisted of samples that were treated at four different times, this was performed three times or each sample, giving 12 samples per batch. The treatment times for these four different samples were 5, 10, 20 and 40 seconds. The same times were used throughout the different batches, but the distance from the plasma source was increased by 5 mm from batch 1 to batch 2 and from batch 2 to

batch 3. Before the plasma was ignited, each gas was allowed to run through the system to flush out any contaminants. Before taking optical emission spectroscopy measurements and prior to the treatment of any samples, the power was turned on to the system to allow for a short period of ignition to prepare the samples on the treatment stage under the jet.

3.2.3 Optical Emission Spectroscopy

In order to gather the required OES measurements, an Edmund Optics CCD spectrometer was used. This device has a spectral resolution of 1.5 nm and can record emissions between 200 – 850 nm. Due to the spectral resolution associated with this spectrometer, some emission peaks may overlap. For example, the three emission peaks of the atomic oxygen triplet at the 777 nm mark are too close for this device to separate as individual peaks and consequently display as a singular, broader emission peak (Milosavljevic 2011). The software used to record and analyse the data was BWSpec^{TM}. We have used a single fibre optic cable with a lens and a CNC machine. The optical emission spectroscopy studies were conducted by moving the jet along the z-axis (of the CNC machine) relative to the fibre optic lens. The zero point was taken as being at the jet nozzle with the jet moving farther up the z-axis and the lens then taking readings further down the plasma plume. In this study it was deemed that the common active species between all three gases was atomic oxygen (O I). This is of particular interest as it has been found to cause modifications of polymer surfaces. In other studies it has been shown that gases containing oxygen species cause a dual effect of etching and modifying bonds on polymer surfaces.

3.2.4 WCA and SFE Measurement Apparatus

Theta Lite from Biolin Scientific was used in order to carry out the WCA and SFE measurements on the PET samples. The sessile drop technique is used with this system and over the course of 10 seconds data is recorded, giving the angles on both sides of the drop on a surface and their associated standard deviations. The angles that are given from the WCA measurement can then be averaged and then chosen to calculate the average surface free energy of a sample. The software used to run these diagnostic measurements was OneAttension.

3.3 Results

Plasma diagnostics for each gas were performed using OES measurements. A comparison of the different emission spectra can be seen in Figure 3.2. In order to show the differences between the emissions for each gas, background emissions have been taken into account. Of particular interest is the ability of the approach to

differentiate between the three gases and their effects on the surface of the PET samples. In order to do this, the emissions of atomic oxygen (O I) were identified for each gas and a comparison of the different intensities was made for O I. Atomic oxygen was chosen as it has been reported that the etch rate of polymer surfaces through the use of a plasma containing oxygen has two effects: i) etching of the surface of the polymer due to reactions of the oxygen atoms with carbon atoms on the surface and ii) the creation of oxygen rich functional groups on the polymer surface due to reactions between reactive

species in the
plasma and
the surface
atoms. The
oxygen
functional
groups that the
plasma can
react with at
the polymer
surface
include C–O,
C=O, O–C=O,
C–O–O and
CP
₃ (Wang 2008). In the case of PET, the interaction of plasma with the surface leads to

the –C–O– bond breaking in ester groups, which causes a disruption in the polymer

chain, and allows for a higher level of polarity on the surface (Slepicka 2013).

However, measurements on the changes of surface roughness were not conducted

directly, but the changes of the water contact angle gave an insight into the changes

that occurred due to plasma chemistry interactions with the surface (Wenzel 1949).

Due to a decreased water contact angle it is clear that the surface roughness and

polarity increased after treatment. Table 3.1 shows the emission of O I for each gas

and their associated data.

Table 3.1: Spectroscopic data for atomic oxygen (O I) for each gas used. The

transitions, multiplets, transition probabilities (A), initial and final energy levels (E_i

and E_f) were gathered from the NIST database (NIST 2018).

Emitter	Transition	Multiplet	A	E_i	E_f
			(1/s)	(eV)	(eV)

O-615	$3p$-$4d$	$^5P_3-^5D_4^o$	5.72 x 10^6	12.7536965	10.740931
O-777	$3p$-$3s$	$^5S_2^o - {}^5P_1$	3.69 x 10^7	10.740224	9.140906
O-845	$3p$-$3s$	$^3S_1^o - {}^3 P_0$	3.22 x 10^7	10.988880	9.5213632
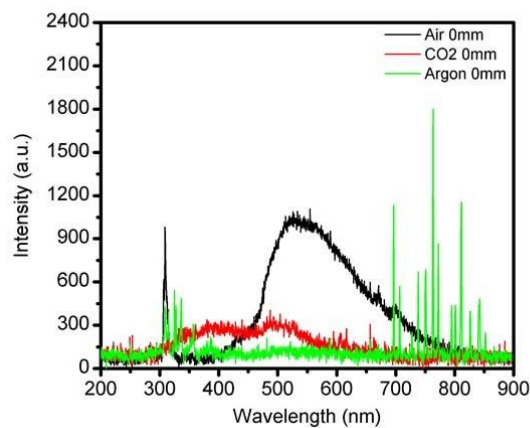
Figure 3.2: (Colour online) The typical spectral emissions of non-thermal atmospheric pressure plasma discharge for carrier gases: air, Ar and CO_2.

Figure 3.2 shows a broad continuum in the range of 400-820 nm for air and a continuum in the range of 300-700 nm for CO_2. The continuum for air represents an emission of NO_2^*. The continuum, or swan band, in CO_2 is due to the emission of CO and C_2.

3.3.1 Polymer Treatment with Air

The mechanism for the production of the NO_2^* continuum has been reported to be due to the recombination of NO + O, given by the following reaction mechanisms where M is a third body molecule, such as; O_2, O_3 or N_2 (Becker 1972, Gattinger 2009, Sjimizu 2012)

$$NO + O \rightleftharpoons [NO_2^*] \qquad\qquad (1)$$

$$N_2(v) + O \rightleftharpoons NO + N \qquad\qquad (2)$$

$$[NO_2^*] + M \rightarrow NO_2^* + M \qquad\qquad (3)$$

$$[NO_2^*] \qquad \rightarrow NO_2 + h\nu \qquad\qquad (4)$$

$$NO + HO_2 \rightarrow NO_2 + OH \qquad\qquad (5)$$
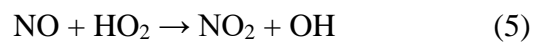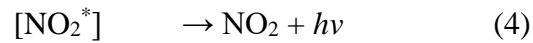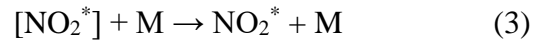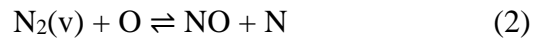
As can be seen in Figure 3.3, the emission of NO is relatively low and there are no visible emission peaks for N_2 where one would expect to see the second positive band. This lends precedence to the idea that the N_2 molecule interact with other species, in this case O, and has a vibrational transfer of energy that create NO molecules. These NO molecules can then be further oxidized and gain energy from a third body M to create NO_2^* which then emits in the wavelength range observed.
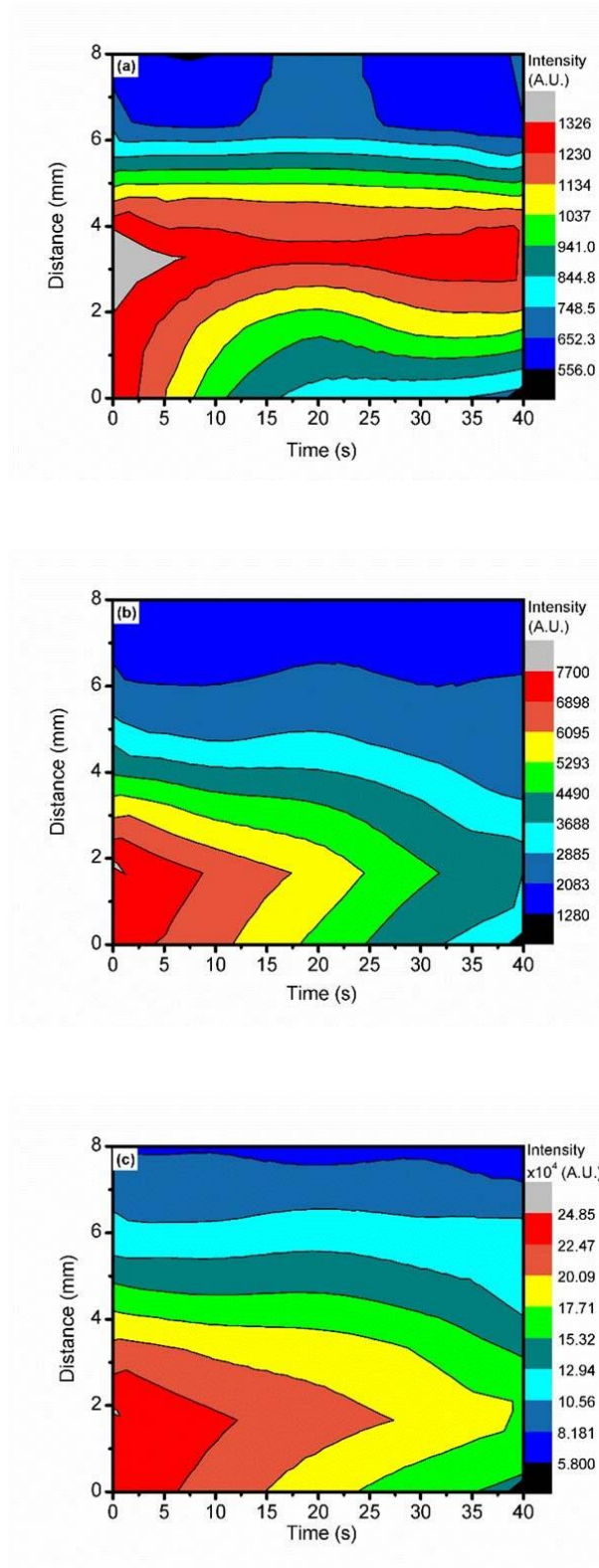
Figure 3.3: (Colour online) (a) Comparison of O I emissions in air over time and distances from the plasma jet nozzle. (b) Comparison of OH emission intensities over time and distance. (c) Comparison of the NO_2^* continuum over time and distance.

The air that is represented in Figure 3.3 was delivered to the PVA system using an air compressor. This compressor took the ambient air of the room and directed it to the plasma jet through which then generated plasma as the air flowed through at a pressure of 6 x 10^5 Pa. In Figure 3.3(a), it can be seen that the total intensities of O I emissions in air tend to be higher on average at a distance of around 2-4 mm from the nozzle. From this it can be seen that there is a dependence on the intensity and quantity of the reactive species with respect to distance.

Consequently, the closer the sample is to the source the more interaction the surface will have with the produced O I atoms. There is also a degradation over time of the O I atoms at 0 mm which indicates that there could be reactions occurring that reduce the reactive O I species over time. However, there is an increase of O I at 2 and 4 mm and then a decrease with an increase in distance, this shows that there is a recombination process occurring which is shown in reaction mechanisms (1 and 2). The high levels of OH at the beginning of the measurements when using air as the gas for plasma discharge can be associated with the high humidity present as the gas is passed through the jet from the air compressor. The intensities of OH and NO_2^* are highest at 0 mm and in the first few seconds of plasma generation. There is then a degradation over time and with respect to distance. However, as can be seen in Figure 3.3(b, c), the intensities of these do drop with an increase in distance, but also give a more consistent emission at points further away from the nozzle. This indicates that the main reactions that occur are within 0-2 mm of the nozzle and allow for a more continuous flow of reactive species further away from the nozzle due to less reactions occurring within the gas.
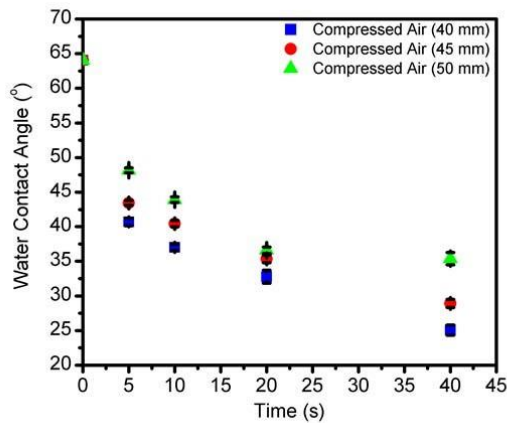
Figure 3.4: (Colour online) Changes in the WCA with different treatment times at 40, 45 and 50 mm away from the nozzle tip.

Figure 3.4 shows that distance plays a significant role in the treatment of the polymer surface. This is in line with the OES data, which shows a decrease in O I emissions with increasing distance from the plasma source. The closer the sample is to the source the more interactions it can have with the reactive oxygen species which modify the surface to become more polar and hence more hydrophilic, decreasing the WCA and increasing the SFE. The increase of the SFE can be seen in Figure 3.5.
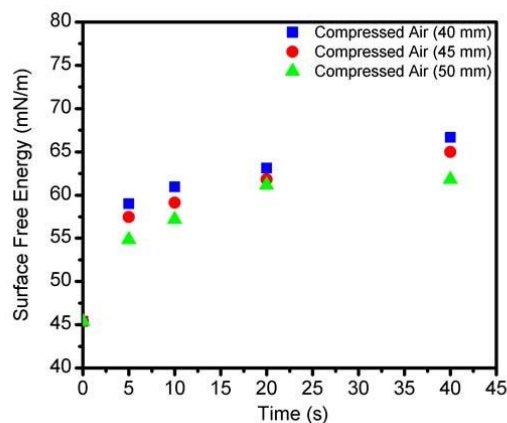
Figure 3.5: (Colour online) Changes in the SFE with treatment times at 40, 45 and 50 mm away from the nozzle tip.

3.3.2 Polymer Treatment with CO_2

The broad CO_2 emission bands were found to be swan bands which contain emissions of the CO third positive system and the Angstrom system and C_2 molecules (Mendez-Martinez 2010). As with the emission spectra of air, there does not appear to be any major emission of N_2, although it could be that the emission is too low to be detected and has blended in with the background signal. Although CO_2 gas was used, there will be interactions with the surrounding ambient air which will contribute to some of the observed emission and the reaction mechanisms. From this, the mechanism of action for the creation of these swan bands and the emission of O-615, O-777, and O-845 was found (Schmidt-Becker).

$$CO_2 \rightarrow CO + \frac{1}{2}O_2 \qquad\qquad (6)$$

$$e^- + CO_2 \rightarrow CO\ (a'^3\Sigma^+) + O \qquad (7)$$

$$e^- + CO_2 \rightarrow CO^+\ (A^2\Pi) + O \qquad (8)$$

$$N + NO_2 \rightarrow 2NO \qquad\qquad (9)$$

$$C + NO \rightarrow CO + N \qquad\qquad (10)$$
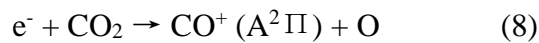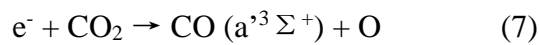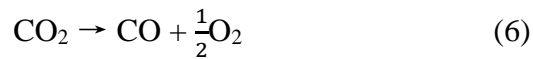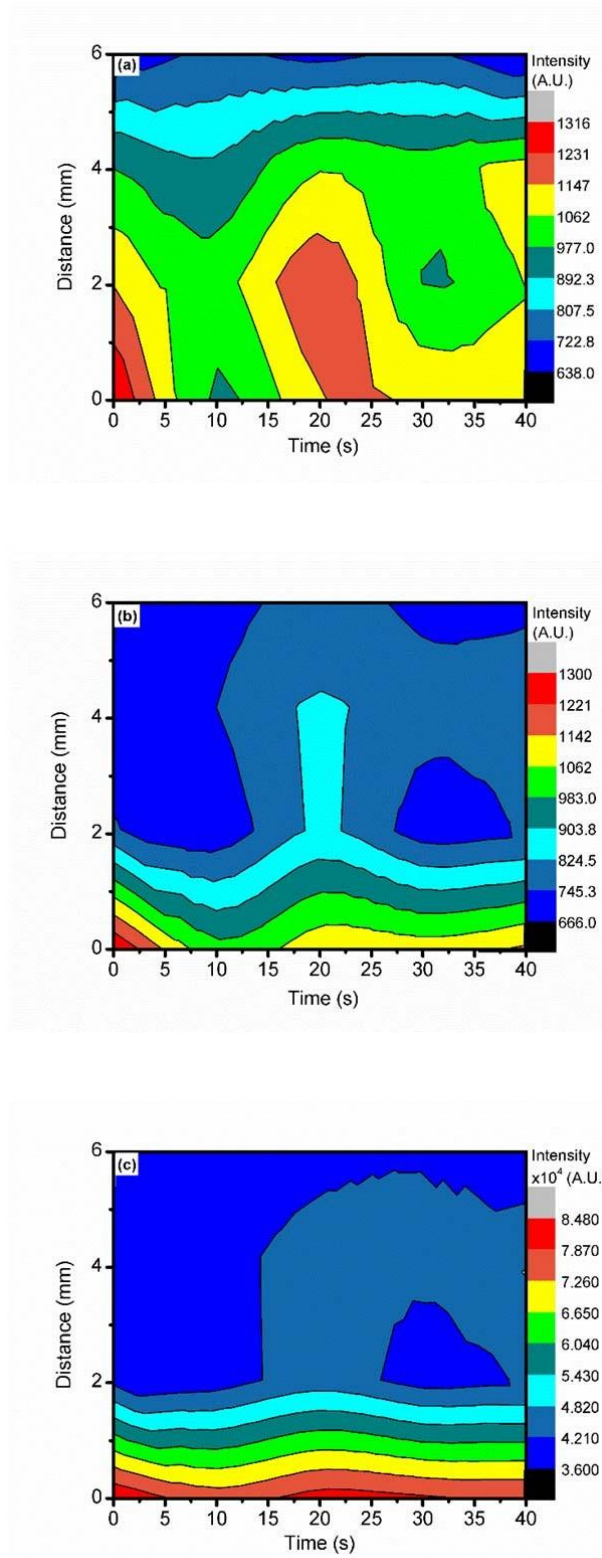
Figure 3.6: (Colour online) (a) Comparison of O I emissions in CO_2 over time and distance from the plasma jet nozzle. (b) Comparison of OH emission intensities over time and distance. (c) Comparison of the swan band continuum over time and distance.

As evident from Figure 3.6(a) there is a greater drop in the total intensities of the O I emissions for CO_2 at distances further from the nozzle. At 0 mm there is a greater change in the O I emission intensities over time, suggesting similar behaviour as observed with the air plasma discharge, with increased reaction occurring at this point and causing fluctuations in the population of the reactive oxygen species. However, at further points from the nozzle these appear to stabilize and yield more constant values for the intensities of O I. From Figure 3.6(b, c) it can be seen that the emission of OH and the overall carbon molecular spectral emissions are greatest at the nozzle and are relatively consistent over time. Moving further away from the nozzle shows that the intensities drop, meaning that most reactions have occurred at the 0 mm point and as such allow O I to continue to travel over greater distances due to saturation of reactions at the earlier position.
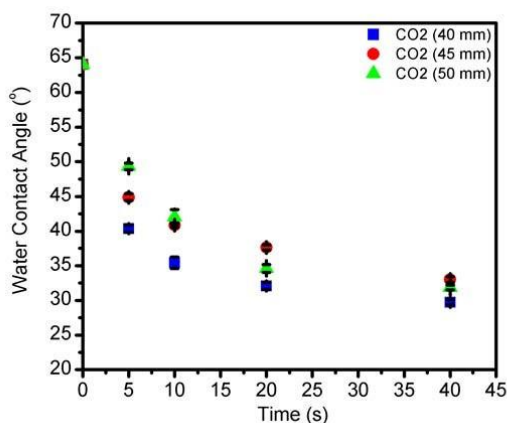
Figure 3.7: (Colour online) WCA values at varying distances and treatment times with CO_2

The WCA values in Figure 3.7 show there is a dependence on distance for the processing of the PET samples with plasma, but there is also some dependence with time. Although the different distances give varying values throughout the treatment process, the largest differences are observed between 5 and 20 s, with less differentiation at 40 s. This could be due to slight fluctuations of oxygen species over time or the introduction of more C–O bonds from other reactions hindering the process of creating a more polar surface and the maximum WCA. The SFE changes can be seen in Figure 3.8 and correspond to the changes of the WCA.
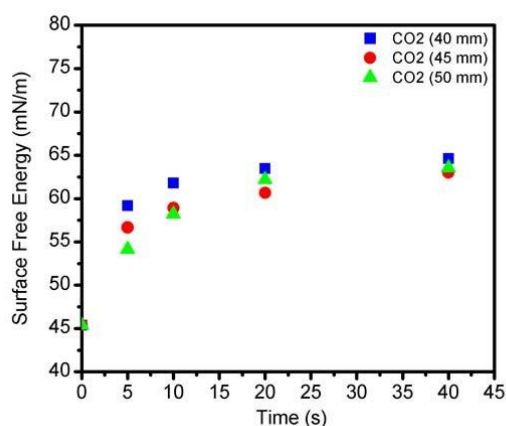
Figure 3.8: (Colour online) SFE values for PET samples treated with CO_2.

3.3.3 Polymer Treatment with Ar

Within the argon emission spectrum it can be seen that there are emissions of Ar, O, OH and the N_2 second positive system. Due to the chemically inert nature of the argon gas, it was determined that there was most likely energy transfer from the metastable atoms (spectral emission at 801 and 810 nm could be linked to metastable atom density (Grace 2003)), other atomic and molecular species in the ambient air surrounding the plasma jet, and high energy electrons (important for a spectral emission at 750 nm) all

of which were taken into consideration to aid in the reactions of different species. Reaction mechanisms (11-13) show how this could occur (Kuzuya 2004).

$$Ar + e \rightarrow Ar^* + e \qquad (11)$$

$$Ar^* + O_2 \rightarrow Ar + 2O \qquad (12)$$

$$Ar^* + N_2 \rightleftharpoons Ar + N_2{}^* \qquad (13)$$
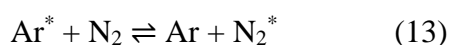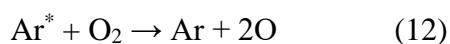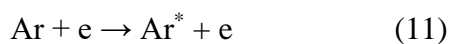
After conducting analysis on the emission spectra of all three of these gases, it was concluded that the common active species of interest between them was O I, and so the intensities of O I emissions were measured for each at the wavelengths specified in Table 3.1. The intensities were compared in order to determine if a correlation could be derived between the changes in WCA and SFE with respect to changes in O I emission as these atoms seem to have a larger impact on the modification of polymer surfaces.
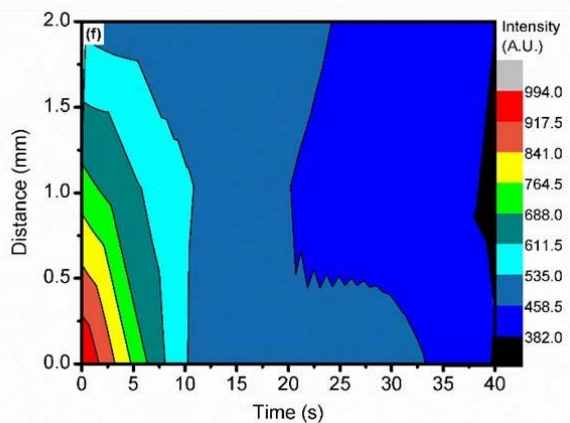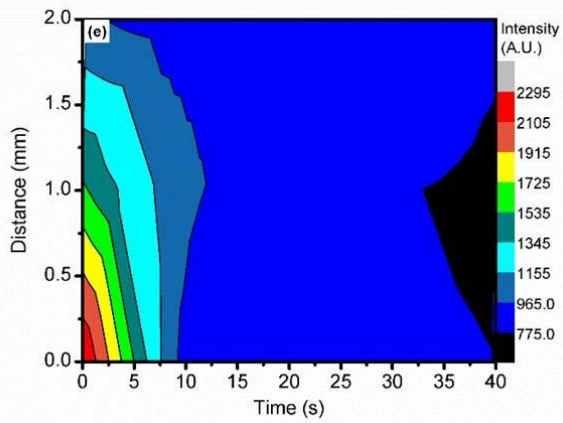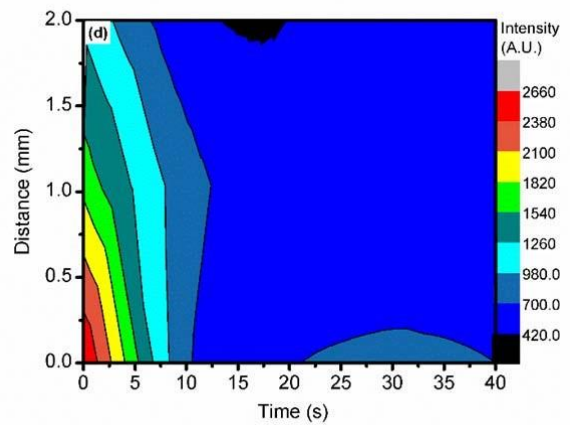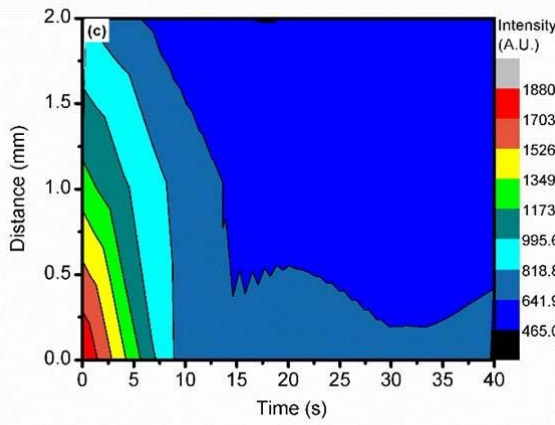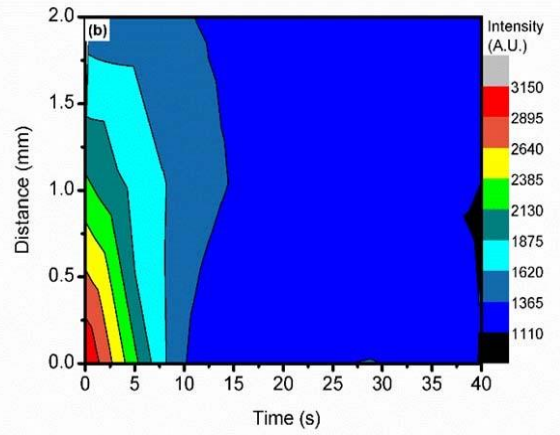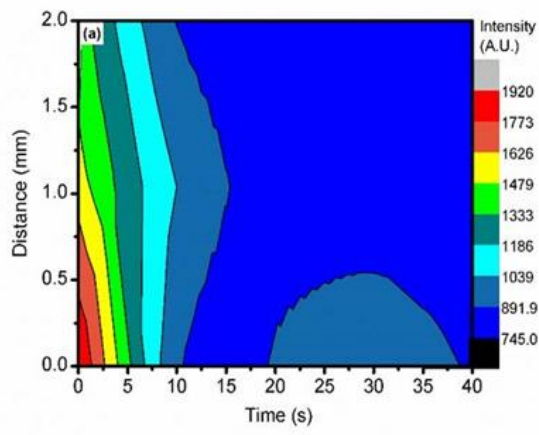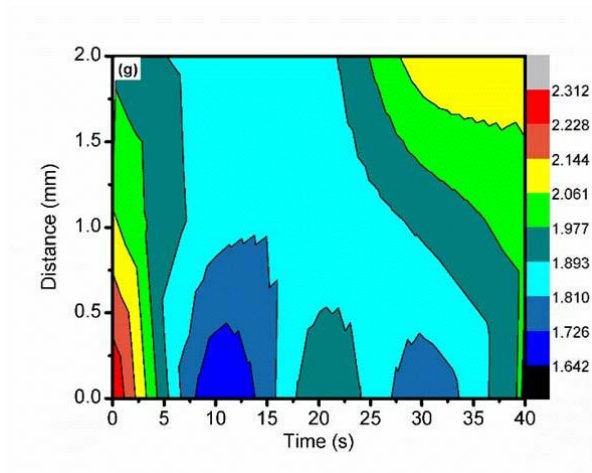
Figure 3.9: (Colour online) (a) Comparison of O I emissions in Ar over time and distance from the plasma nozzle. (b) Comparison of OH emission intensities over time and distance. (c) Graph of the emission of Ar at 750 nm (relevant for high energy electrons). (d) Graph of the spectral emissions of Ar at 811nm (could be linked with metastable atom density). (e-f) Spectral emissions of N_2 and N_2^+ molecules respectively, over time and with varying distance. (g) Ratio of N_2/N_2^+ giving a shift in the EEDF with respect to time and distance.

From the analysis of the EEDF for the experiment with Ar, it is proposed that the majority of the chemical reactions occur within the plasma jet instead of outside of the nozzle. This allows for little change to occur with regards to the efficiency of energy transfer, the degree of activation or the dissipation of reactive species when they leave the jet nozzle. As the chemical reactions occur internally rather than outside of the nozzle, more of the energized species can reach and react with the surface of the sample being treated. For chemically inert noble gases such as Ar, He or Ne, there is greater control over directional flow as there are not as many reactions with the ambient air occurring to carry away and diffuse the energetic species being created once they leave the nozzle. However, for many other atmospheric plasma jets, the chemical reactions of gases could occur outside of the jet which would result in a loss

of efficiency for sample modification. As such, noble gases would not suffice for the transfer of energy to ambient air without diffusion away from samples being rectified. The gas temperature emanating from the nozzle of the PVA system is therefore higher. This will allow for an increase in activation of surfaces as the increased temperature agitates the molecules present and the bonds on the surface of the material, allowing for easier acceptance and functionalisation at the surface boundary. From this and the addition of more directional and optimized transfer of energy due the internal chemical reactions it can be assumed that the efficiency of the surface modification will increase. Therefore, from a technological viewpoint, a system that allows for chemical reactions to occur inside the system at the point of the plasma discharge will give an increase in efficiency and better control of material modification. In this experiment, the PET samples that were treated became more hydrophilic with time with the greatest change evident at a distance of 40 mm from the jet nozzle. This can be seen in Figure 3.10 and 3.11 where WCA and SFE change respectively.
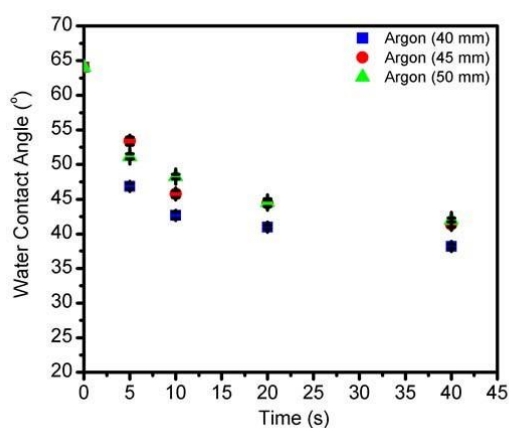
Figure 3.10: (Colour online) WCA values for PET samples treated with Ar.
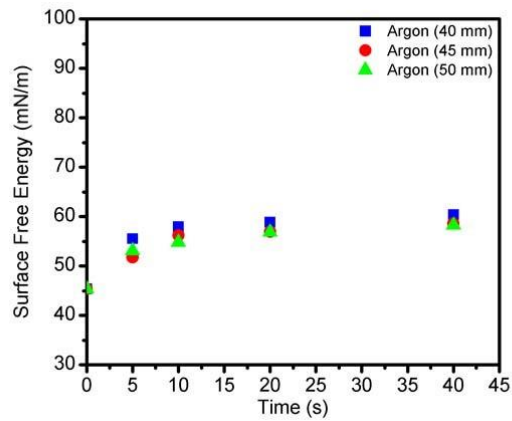
Figure 3.11: (Colour online) SFE values for PET samples treated with Ar.

As an additional measurement, further analysis with EEDF ratios was carried out by obtaining OES data for Ar-750 and Ar-811 with an end-on view perspective. The EEDF was calculated by determining the ratio of Ar-811/Ar-750. In Figure 3.12, it can be seen that the EEDF ratio tends to increase with distance but is relatively constant over time.
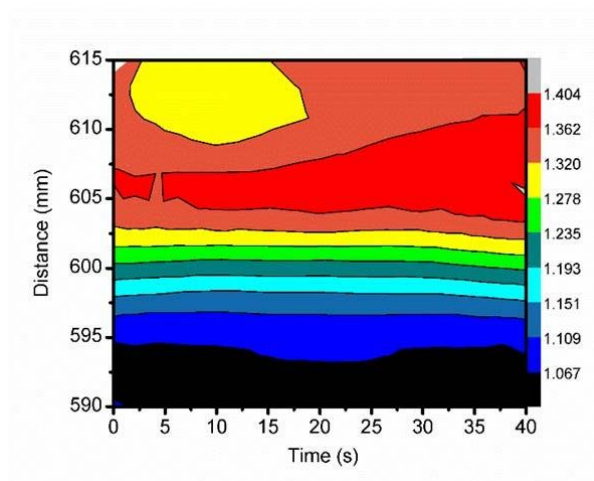
Figure 3.12: (Colour online) Ratio of Ar-811/Ar-750 giving a ratio change of the EEDF with respect to time and distance.

3.4 Discussion

Figure 3.3(b, c) shows how both OH and NO_2^* decrease in intensity over time and distance. However, from 0 to 4 mm there is a dependence on time and from 6 mm onwards a steady state appears for OH and NO_2^*. From this it can be deduced that OH and NO_2^* are dependent on each other throughout the course of the reactions, as proposed in mechanism (3) where M is OH. As both of these decrease, O I is able to remain at a steady state from 2-6 mm from the jet nozzle, as shown in Figure 3.3(a). This data shows that although there are many reactive species created by the plasma discharge, in the case of air, the majority of the chemical reactions take place within the nozzle of the plasma jet and just at the exit. Further points from the nozzle have a more equalized and homogenous state and can therefore create a more controllable activation and modification process for material surfaces. Looking at the intensity graphs of atomic oxygen (O I) emission for air and CO_2 plasma discharge, it can be seen that the emission of O I for air is a lot more consistent than CO_2. The emission of CO_2 undergoes a lot of fluctuation and can be reduced by up to 40% at times. From this it is seen that for closer distances, the amount of O I generated by air will cause it to have more of an effect on the polymer surface over time.

For CO_2, the emission of O I is greatest in the region of the nozzle exit to 2 mm along the plasma plume. This can be seen in Figure 3.6(a), which also shows that there are fluctuations which seem to repeat over a certain interval of time (i.e. 0, 20 and 40 s) which gives evidence of the chemical reactions that arise within the gas over time. These fluctuations coincide with the changes seen in the OH and swan band emissions in Figure 3.6(b, c). This shows that OH and the swan band emissions have a "relationship" with each other during the chemical reaction that then give rise to the observed emission spectra. The emission intensities seen in the swan band spectra are

higher than those of the OH emissions, but changes of intensity with respect to time and distance show a strong correlation between the changes in OH intensities over time and distance. This shows that there is a stoichiometric relationship between the OH species and the emitters of the swan band in CO_2. However, as these two decrease in intensity so does O I, which gains a more continuous emission over time. From these results it can be deduced that due to the decreased interaction with OH and the swan band emitters, O I emission become more predictable. Therefore, the reactions for CO_2 occur mainly within the nozzle or at the opening of the jet. Since the energy levels of CO_2 (and its dissociation products) are in the range of up to 11eV, they have similar energy levels to the chemistry of ambient air. In other words C_2, CO, and CO^+ have similar energy levels to N_2 and O. This allows for a more efficient transfer of energy through radiative processes. So at further distances from the polymer surface, CO_2 could create more O I closer to the surface in comparison to that of air. This is due to a greater penetration through the ambient air due to a longer chain of radiative energy transfer between the CO_2 discharge and the ambient air surrounding it.

All emissions from the spectra obtained from the plasma discharge of Ar decrease in intensity with increasing distances along the plasma plume. Over the space of 10 s, the intensities drastically drop for each species and then stay relatively constant for the remainder of the 40 s. When comparing the emission of O I with Ar-750, it can be seen that these two have some form of interaction which is proposed by reaction (12). This allows us to see how much dependence the O I species have on Ar metastables as the requirement for energy transfer is essential. Another possibility of these reactions is the dependence of the Ar metastables on energized N_2 through the mechanism shown previously (13). As N_2 and N_2^+ emission decrease, the level of Ar metastable emissions also decrease and consequently the amount of O I emissions.

The EEDF ratios from N_2/N_2^+ appear to increase slightly after a drop between 10 and 20 seconds. This is due to the N_2^+ species decreasing more over time as the N_2 species stay relatively constant after the initial drop after 10 s at the nozzle and then remain consistent at 2mm, due to the excited states energy difference.

The dependence of surface modification on the amount of O I available to react with and functionalise the surface has been shown. The treatment of the polymer surfaces at distances further away from the plasma source caused the surfaces to be less functionalised, which coincides with a decrease in the amount of O I. The use of air and CO_2 gave similar results with respect to changes of WCA and SFE for the treated samples. This was expected as the total intensities of the atomic oxygen in air are close to CO_2. Ar caused the least amount of change for the samples as the amount of atomic oxygen present was less than the other two, however it did provide a more consistent change in WCA and SFE. From all of these results, it can be shown that the majority of reactions caused by the plasma discharge of the plasma jet system occur mostly within the nozzle of the jet or just outside the exit. For the majority of the reactive species, their intensities reduced quickly after 2 mm from the source and after which point the emitted light intensities were consistent over time

3.5 Conclusion

After obtaining values for the emission intensities of O I and comparing them to the induced changes in WCA and SFE values of PET samples, this study found that there is proportionality between the modification of the polymer surface and the amount of reactive oxygen species produced. Other studies have shown that gases containing oxygen species cause a dual effect of etching and modification of bonds on polymer surfaces and that gases that contain active species of oxygen cause more of an affect

through etching and forming polar groups. The results obtained from this study show an agreement with this (Wang 2008, Slepicka 2013, Wenzel 1949, Donegan 2013, Nwankire 2010). The levels of O I in CO_2 and air were roughly the same with only slight variances over time. It was also found that the changes in WCA and SFE of samples treated with air and CO_2 were close to each other. A dependence on the distance that the sample is from the plasma source was also observed. With the balance between thermal degradation and plasma interactions taken into consideration, the closer the sample is, the more changes its surface will undergo.

With Ar it can be seen that there is not as much of a change compared to CO_2 and air for the induced changes in WCA and SFE with less fluctuations in O I over time. After calculating the EEDF for Ar, it was noted that the ratio increases with distance from the nozzle exit. From this observation it can be concluded that the majority of the chemical reactions occur within the jet rather than externally in the surrounding ambient air. This is also confirmed by the end-on OES measurements of Ar. Consequently, the studied plasma jet creates a more efficient means to transfer energy to ambient air from the carrying gas. This can be seen in the shift of the EEDF further away from the nozzle point, showing that the bulk reactions happen internally. One of the reasons that could give rise to a difference between the proposed efficiency of this system compared to other systems that are used is their frequency of operation. Other factors that would also need to be considered include the power of the system, electrode geometry, and the system design. Examples would be the SurFX AtomFlo 400 system, which operates at 10-25 kHz, and the PlasmaStreamTM system, which operates at 27.12 MHz (Donegan 2013, Nwankire 2010). This can also be obtained from analysing the data showing that the emissions of OH, NO_2^* and the swan bands in CO_2 degrade and fluctuate with an increase in distance from the nozzle opening.

However, the distance of the jet to the substrate surface is not the only factor that is important for polymer activation. The type of polymer used, gas chemistry, and treatment time are also factors governing the induced effects.

References

M. Aliofkhazraei, Surface Energy, 1st ed. (InTech, 2015), pp. 123-152.

K. H. Becker, W. Groth, and D. Thran, Chem. Phys. Lett. 15, 215 (1972).

M. Donegan, V. Milosavljević and D. P. Dowling, Plasma Chem. and Plasma Proc. 33, 941 (2013).

D. P. Dowling, J. Tynan, P. Ward, A. M. Hynes, P. J. Cullen, and G. Byrne, Int. J. of Adhesion & Adhesives. 35, (2012).

R. L. Gattinger, W. F. J. Evans, I. McDade, D. A. Degenstein, and E. J. Llewellyn, Can. J. Phys. 87, 925 (2009).

J. M. Grace and L. J. Gerenser, J. of Disper. Sci. and Technol. 24, 305 (2003).

S. Guruvenket, G. M. Rao, M. Komath, and A. M. Raichur, App. Surf. Sci. 236, 278 (2004).

M. Kuzuya, T. Izumi, Y. Sasai, and S. Kondo, Thin Solid Films 457, 12 (2004).

M. Lehocky, H. Drnovská, B. Lapciková, A. M. Barros-Timmons, T. Trindade, M. Zembala, and L. Lapcik, Jr., Colloids and Surf. A 222, 125 (2003).

E. H. Lock, T. B. Petrova, G. M. Petrov, and S. G. Walton, Phys. Plasmas 23, 043518 (2016).

E. F. Mendez-Martinez, P. G. Reyes, D. Osorio-Gonzalez, F. Castillo, and H. Martinez, Plasma Sci. and Technol. 12, 314 (2010).

V. Milosavljevic, A.R. Ellingboe, and S. Daniels, The Euro. Phys. J. D 64, 437 (2011)

M. Morra, E. Occhiello, and F.Garbassi, Surf. Interf. Anal. 16, 412 (1990)

C. Mueller, G. NTPaccio, A. Hiltner, and E. Baer, J. of A. Polym. Sci. 70, 2021 (1998)

NIST, "Atomic Spectra Database Lines (wavelength order)," http://physics.nist.gov, (2016).

C. E. Nwankire, V. J. Law, A. Nindrayog, B. Twomey, K. Niemi, V. Milosavljević,
W. G. Graham, D. P. Dowling, Plasma Chem. and Plasma Proc. 30, 537 (2010).

M. Ozdemir, C. Yurteri, and H. Sadikoglu, Crit. Rev. Food Sci. Nutr. 39, 457
(1999).

Chapter 4: Spectroscopic Study of Excited Molecular Nitrogen Generation Due to Interactions of Metastable Noble Gas Atoms

This chapter has been published in its entirety as:

L.S. carried out all experimental work. J.L., M.G., P.C., and V.M. were co-authors of this work.

Abstract

This work provides an insight into the generation of excited nitrogen species by allowing noble gases to interact both with one another and ambient air. He and Ar were utilized to generate the optimum selectivity process to create reactive nitrogen species. An optimum setting for the generation of excited molecular nitrogen species, based on their excited energy levels, was obtained when using a mixture of Ar‑He at a ratio of 10:1. At that point, when a voltage of 27 kV is applied to the system, it reached the maximum efficiency for selectivity processes to occur which allowed for a greater non‑radiative transfer of energy through the mixture of noble gas atoms and into the molecular nitrogen present in ambient air.

Keywords

4.1 Introduction

Non-thermal plasma discharge in open air results in charged species, energetic photons, active radicals, and also a low degree of ionization gas (Kunhardt (2000), Napartovich (2001)). Measurements and analysis of the physical and chemical interactions of NTPs has been a subject of intense study for many decades. Optical spectroscopy may, however, provide better insights into the reactive species being generated, the electron energy range within the plasma for atomic and molecular excitation, and the mechanisms and kinetics of energy transfer with respect to radiative and collisional processes (Ono (2007), Crintea (2009), Wang (2011), Thiyagarajan (2013), Xiao (2014),). Through this, the possible chemical reactions that could interact with surfaces can be ascertained. With this in mind, NTPs have gained a lot of attention for potential applications ranging from agriculture to medicine (Fridman (2008), Heslin (2014), Jo (2014), Weltmann (2016)).Plasma interaction with sample surfaces can cause surface modification, functionalization, sputtering and etching. Examples include atomic etching of circuits or deposition of oxygen species onto polymers (Øiseth (2002) Cristaudo (2016), Scally (2017)). Furthermore, when used on organic samples, the introduction of oxygen or nitrogen containing radicals can sterilize surfaces due to an increase of reactive oxygen and nitrogen species that cause stresses within organic matter, which leads to degeneration. These processes can inactivate the likes of *Escherichia coli* (Daeschlein (2009), Yu (2012)).

Many treatments utilize molecular nitrogen (N_2) as a working gas (Penetrante (1999), Silva (2004), Lloyd (2009), Liu (2014), Marasca (2016), Morgan (2017)). Ambient air introduces the N_2 species into the system used in this work to interact with the other gases used. As well as introducing N_2, the ambient air present in the system

brings with it a certain amount of humidity and thus adsorbed moisture content, which can give rise to the formation of hydroxyl radicals (OH) and atomic hydrogen (H) when plasma is ignited in the system. There are, however, other species that are produced from sources such as factories and vehicles which include nitrous oxides (NO_x) and other greenhouse gases which are considered to be hazardous emissions. By utilizing NTP systems, it has been shown that hazardous pollutants such as NO_x can be broken down into much more acceptable species that are not as harmful as the hazardous waste and volatile organic compounds that are the byproduct of many industrial and mechanical processes (Penetrante (1997), Durme (2008)). The implementation of NTP systems is not restricted to industrial processes. They have seen a growing use in material processing, nanotechnology, and medical applications (Ishaq (2013), Lu (2016)). An added benefit to atmospheric plasma chemistry is that they can be used to destroy bacterial cells and other organic materials growing on surfaces which one would want to sterilize (Traylor (2001), Liu (2009), Boekema (2015), Janda (2016). In order to understand the formation of the many reactive nitrogen species (RNS) and reactive oxygen species (ROS) that can be produced, the gas chemistry and kinetics of a system must be analyzed thoroughly.

The second positive system (SPS) of the excited N_2 emission bands are seen in the near-UV region. The emission wavelengths range from 315 – 450 nm and the specific peaks of interest in this work are at 315, 337, 357, 380, 405, and 425 nm with an emission of ionic nitrogen (N_2^+) from the first positive system (FNS) at 391 nm. The emission from the SPS are due to transitions from $C^3\Pi_u \rightarrow B^3\Pi_g$ and the emissions of the FNS system are due to transitions from $B^2\Sigma_u^+ \rightarrow X^2\Sigma_g^+$. Argon (Ar) and helium (He) were chosen as a means of increasing nitrogen production under optimum control parameters (e.g. lower voltages compared to ambient air alone) as they are known to

aid in the production of the excited N_2 species. By determining a correlation between the emissions of these species, it can be shown that absolute emission intensities can be used as an indicator to benchmark the most efficient conditions for generation of the excited nitrogen species. In this work an atmospheric plasma system, which operates with noble gas and ambient air chemistry, was employed. The system operates at a frequency of 50 kHz and makes use of a cylindrical dielectric barrier discharge geometry with a helically inclined dielectric barrier. He and Ar were used individually with permeating ambient air as a background gas to develop a baseline of nitrogen emissions. After determining the interactions that occur between Ar and He with ambient air present within the system, they were then mixed at different ratios as a means to show a selectivity process to optimize the generation of excited nitrogen species. The resonant and metastable atoms of Ar and He are taken into consideration when determining the possible pathways and mechanisms of energy transfer for excited nitrogen generation. Studying the impact of He and Ar on N_2 generation of the SPS and FNS and how to optimize it was the main goal of this experiment. The experiment aims to provide a better understanding of (1) the chemistry and physics of noble gases with ambient air (2) how to create an environment which can either increase excited N_2 species or reduce the possible interactions of energetic Ar and He with samples sensitive to etching or atomic bombardment (i.e. utilizing a method that optimizes nitrogen excitation through selectivity processes) (3) and how to do so without generating NO_x and other greenhouse gases.

4.2 Experimental

4.2.1 Experimental Setup and Electrical Diagnostics

The device used to carry out the OES measurements in this work was an Edmund Optics CCD spectrometer. Due to the resolution of this device being in a range of 0.6 – 1.8 nm (wavelength dependent), some emission peaks overlapped and could not be fully analyzed with confidence. Spectral emissions could be recorded between 200 nm and 850 nm. The spectra were recorded through BWSpec^{TM} software and analyzed by integrating the area under each peak. By implementing OES, it could be found how certain parameters change the interactions within the plasma and ascertain which parameter had the highest impact on the plasma kinetics and characteristics. The flow rates of the gases were varied from 1 L min^{-1} to 5 L min^{-1} when using each gas individually. When mixing the gases, ratios from 10/1 to 2/1 were used. This was achieved by keeping one gas at a constant flow rate of 1 L min^{-1} and varying the other from 0.1 L min^{-1} to 0.5 L min^{-1}. Prior to inducing the plasma discharge, the gases were allowed to flow through the system to flush the reactor so as to equalize the emissions obtained and minimize any fluctuations over time. The frequency used was 50 kHz. This was found to be the resonant frequency that gave the optimum plasma discharge within the system. Going above or below this resulted in a reduction of the emission intensities and changing the frequency by +/- 1.5 kHz resulted in the cessation of the plasma discharge. The optimum frequency was chosen through the use of OES monitoring and obtaining the maximum values from the voltage and discharge current waveforms for 17, 22, and 27 kV. These can be seen in Figure 4.1.
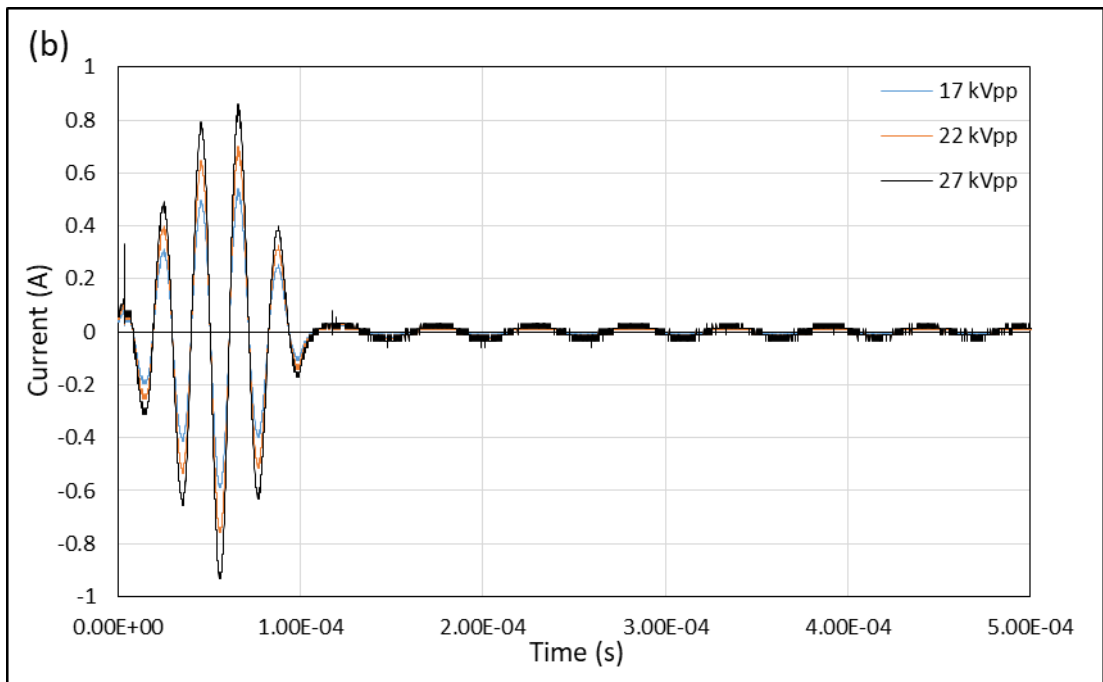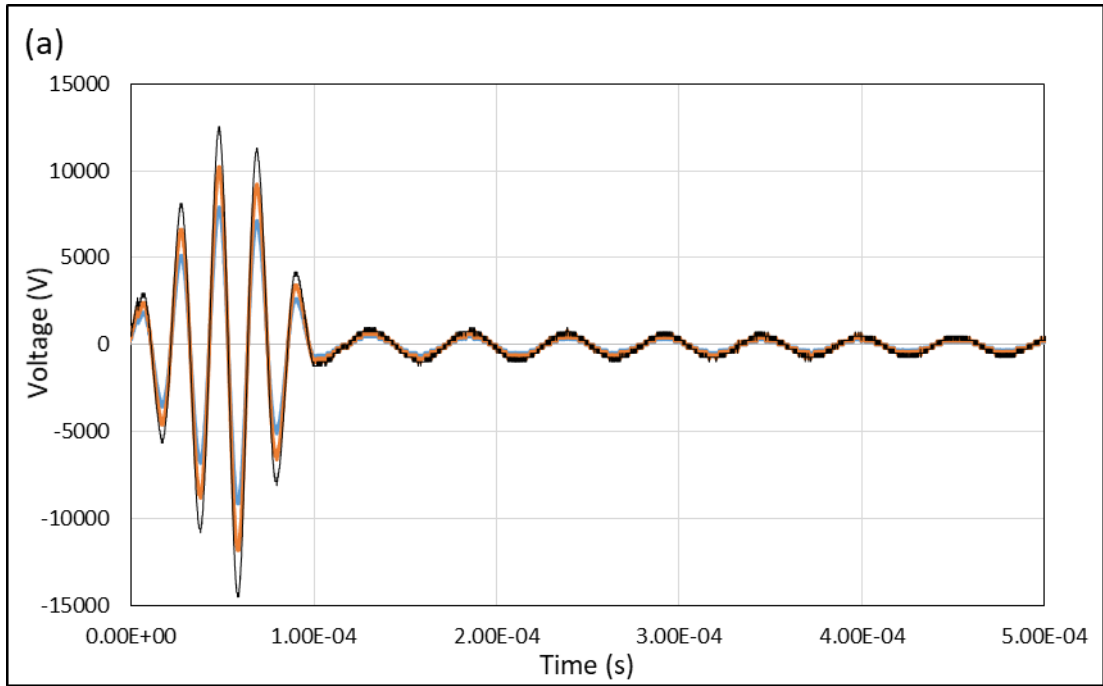
Figure 4.1: a) Reading of maximum voltage waveforms when frequency was set to kHz and the voltage applied was 17, 22, and 27 kV **b)** Discharge current waveform recorded when using the three listed voltages.

Overall there were fifteen points of measurement; five positions along the length of the system with three different sides (top, left, and right). The length of the aluminium ground electrode was 190 mm long and the outer radius of polycarbonate tube was 16 mm. The discharge gap between the dielectric surface and the inner radius of the polycarbonate tube was 8 mm. The HV steel axle had a radius of 5 mm, the inner radius of the polycarbonate tube was 14 mm and the dielectric thickness is 1 mm. The material used to make up the helical dielectric barrier was acetal. The setup of the system is shown in Figure 4.2.
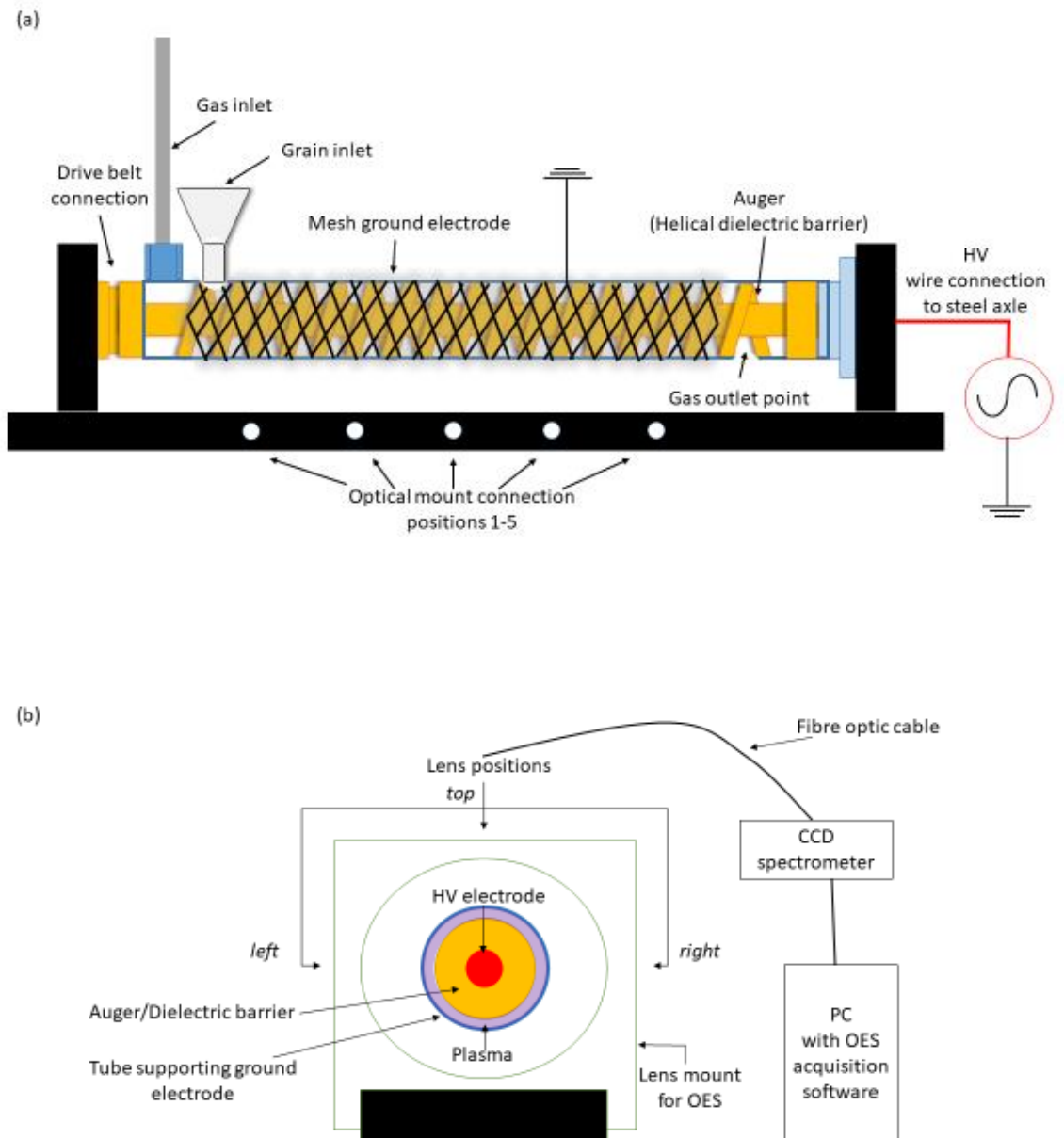
Figure 4.2: a) Diagram of plasma system setup which can treat samples internally between the auger flights where plasma discharge is created **b)** Optical mount setup for OES measurements.

4.2.2 Analysis of Spectral Lines

The OES data that was recorded during the experimental procedure described in this work was analyzed using an integration process. The peak associated with the wavelength of each species was documented and the absolute value was found by setting a minimum and maximum for each emission. This was then integrated to give the total counts for each species to give a singular value, which was divided by a factor of 1×10^3 in order to create an easier comparison between results. When obtaining the data for the emission spectra of the plasma discharge, a temporal evolution analysis of the discharge was carried out by acquiring 21 spectra for each measurement. This was done by measuring the emission intensities every 5 s with an integration time of 750 ms for a total of 100 s, with the first spectra being recorded at the zeroth moment. These spectra were then analyzed through integration of the peaks as described above. However, in order to calculate the error of the averaged values, the standard deviation was calculated by using each intensity that was measured during the 100 s measurement timeframe as the comparison value against the mean value plotted. After obtaining the standard deviation the standard error was calculated for each mean value.

4.2.3 Spectral Information for Species Generated with Ambient Air

Plasma systems that are exposed to ambient air, whether it is an unsealed dielectric barrier discharge system or a plasma jet that injects plasma into open air, there are certain factors to take into consideration. These include the changes in humidity, ventilation speed, and impurities introduced by the air. Humidity aids in the creation of emission lines of hydroxyl radicals (OH), hydrogen (H), nitrous oxides (NO_x), atomic oxygen (O), and excited molecular nitrogen of the SPS and FNS (N_2 and N_2^+). Measurements using OES show that, for this study, there seems be no emission lines

for NO or O. Importantly, there was a clear detection of the SPS and FNS of N_2 from 315-425 nm. These emission bands were of highest interest in order to compare the dynamic relationship between Ar metastables and high energy atomic He.

The spectral emissions of the SPS have an excited energy range of 11-11.2 eV and the N_2^+ emission of the FNS at 391 nm has a threshold energy of 18.8 eV. High energy electrons and/or He metastable species can contribute sufficient energy to ionize molecular nitrogen and generate the emission seen at 391 nm. However, the SPS emissions seen can be created through the direct excitation of neutrals from low energy electrons. The SPS emission lines have similar excitation energies, but their emissions occur at different wavelengths due to their energy levels after emission being different. For example, those at $\lambda = 337$, 357, 380, and 405 nm all have an excited vibrational quantum number of $v' = 0$ (in the $C^3\Pi_u$ state), but their quantum vibrational numbers after emission are $v'' = 0$, 1, 2, 3,…12 (in the $B^3\Pi_g$ state). This gives rise to the spread of emission throughout the band and a main peak ($v' = 0 - v'' = 0$) amongst the band heads (namely $\lambda = 337$ nm for the SPS and $\lambda = 391$ nm for the FNS). Species that are also observed in this work are the emissions of OH and H. The dissociation of H_2O is the main cause of OH and H. The details of all the species related to the presence of atmospheric air seen in the OES measurements are shown in Table 4.1.

Table 4.1: Spectroscopic data used for species generated with the presence of ambient air (Hegemann (2003), Milosavljevic (2014), Kramida (2017)).

Excitation energy (eV)	Emission wavelength (nm)
4.17	OH – 310
11.20	N_2 – 315
11.01	N_2 – 337
11.01	N_2 – 357
11.01	N_2 – 380
18.8	N_2^+ – 391
11.01	N_2 – 405
11.20	N_2 – 425
12.09	H_α – 656

4.2.4 Spectral Information for Ar

Many plasma systems use Ar as an operating gas due to its inert nature and steady state discharge (Richter (2001)). The applications that utilize Ar the most are those that require some form of etching, bombardment, or other physical interaction which will not oxidize surfaces (Youngblood (1999)). Examples of such uses and processes include the cleaning of metallic surfaces, etching of circuit boards, and ablation of solid/powder samples (Cobum (1979), Herman (1995)). However, these processes are usually performed within a vacuum chamber so as to eliminate any cross contamination. Therefore, when used in open air there are some extra considerations to keep in mind. Although Ar itself is chemically inert, it has sufficient energy to aid in the generation of reactive species through interaction with atoms and molecules present in the ambient air. An example of this is the dual effect of etching and functionalization that can be induced on polymer surfaces through the use of Ar-air

plasmas. As Ar bombards the surface and creates atomic crevices, atomic oxygen or OH can bind to free bonds on the surface to create a more hydrophilic environment. This work focuses on those interactions by allowing the Ar to flow through a system that has ambient atmospheric air residing inside of it and accessing it throughout the experiment from various opening points.

By using Ar as the main working gas, the breakdown voltage of the system drops to less than half of what is necessary when using solely ambient air i.e. ambient air required at least 40 kV peak to peak (PP) to observe any plasma discharge and Ar began at 13-14 kV (PP). Creating a lower threshold for plasma discharge is because Ar allows for a build-up of excited species and energetic particles, such as electrons, whereas air quenches this affect due to the strong electronegativity of oxygen. The main point of interest for this study is how this introduction allows for the generation of selected excited nitrogen species. By utilizing the metastables created when generating a plasma discharge with Ar, N_2 can be excited through non-radiative energy transfer. The atomic species used in this study can be seen in Table 4.2, with the emissions arising from the de-excitation branching of Ar metastables denoted by $1s_5$ and $1s_3$ in Paschen notation (Friedl (2012)). The other emission wavelengths are associated with excited Ar atoms that have their promoted electron situated in a resonant state.

Table 4.2: Spectroscopic data of Ar used for this study (Traylor (2001)).

Excitation energy (eV)	Wavelength (nm)	Paschen notation
13.33	Ar-696	$2p_2 \rightarrow 1s_5$
13.33	Ar-727	$2p_2 \rightarrow 1s_4$
13.48	Ar-750	$2p_1 \rightarrow 1s_2$
13.17	Ar-763	$2p_6 \rightarrow 1s_5$
13.15	Ar-772	$2p_7 \rightarrow 1s_5$
13.28	Ar-794	$2p_4 \rightarrow 1s_3$
13.09	Ar-801	$2p_8 \rightarrow 1s_5$
13.08	Ar-811	$2p_9 \rightarrow 1s_5$
13.33	Ar-826	$2p_2 \rightarrow 1s_2$

The Ar-750 atomic emission line is sensitive to the high-energy electron region of the electron energy distribution function (EEDF) and is created through direct excitation from high-energy electrons. Conversely, the Ar-811 atomic emission line is sensitive to low-energy electrons. By using a line ratio method, the distribution of high and low energy electrons can be ascertained, providing insights into how the reaction mechanisms and gas kinetics occur. The EEDF for plasma that use Ar can be obtained by using the line ratio of Ar-811/Ar-750 (Milosavljevic (2015)). The main transitions of interest for calculating the EEDF are the radiative decays of Ar-750 ($2p_1 \rightarrow 1s_5$) and Ar-811 ($2p_9 \rightarrow 1s_5$). The $2p_1$ line is dominated by direct excitation from the ground state by high energy electrons, whereas the $2p_9$ is reported to be dominated by excitations from low energy electron interactions. The possible pathways that the Ar

2p levels may be populated through include direct excitation from the ground state, excitation of 1s metastables from low energy electrons, and cascade excitation from upper levels such as ($3p^5 5s$ and $\rightarrow 3p^5 5d$ levels). The metastable levels accessible to create the 2p levels are $1s_3$ and $1s_5$ since the resonant states ($1s_2$ and $1s_4$ rapidly decay to the ground state) $1s_5$ has been found to have a much larger direct excitation cross-section between the two (Donnelly (2004), Biloiu (2010), Boffard (2010)). The peak cross-section has consistently been found to be much larger for the $1s_5$ excitation to the $2p_9$ level than for the excitation cross-section for the ground state, with values being 15 to 700 times higher for the $1s_5$ level (Donnelly (2004)). Due to the forbidden and allowed states and the dipole/parity rules, the dominant transitions that allow for the population of $2p_9$ is from the metastable $1s_5$ state from low energy electron interactions, while the population of $2s_1$ is generated by direct excitation from the ground state due to high energy electrons (Boffard (1999)). From this, it can be ascertained that a ratio of ($2p_9 \rightarrow 1s_5 / 2p_1 \rightarrow 1s_2$) (Ar-811/Ar-750) gives a ratio of low energy electron to high energy electron excitations.

4.2.5 Spectral Information for He

The emission spectra recorded during this study revealed four emission lines of He. These emission lines can be sub-divided into two different categories of energy sets: singlet and triplet. Transitions of electrons between singlet and triplet states are forbidden due to dipole-dipole interactions and the breaking of symmetry of electron configurations and spin reversals. Electrons may only pass from a singlet state to a triplet state, or vice versa, through non-radiative processes known as intercombination crossing. However, these crossings have very low transition probabilities for neutral He. Due to this, only emissions from these energy sets are analyzed in this work rather

than their interactions with one another. The singlet states of atomic He analyzed are He-667 and He-728 with the triplet states being He-587 and He-706.

The metastables that He can produce have high energy levels and allow for non-radiative transfer of energy to N_2 with sufficient energy to create excited N_2 of the SPS and FNS. The atomic He emissions at He-471, He-587, He-667, He-706, and He-728 have energy levels that are the same as the resonate levels of their respective energy sets. To further determine the kinetics within the plasma discharge the EEDF was calculated for the He discharge using the line ratio method as for Ar. However, the lines used when carrying out the calculation for He were: N_2-337 and N_2^+-391. N_2-337 is sensitive to changes caused by low energy electron, and N_2^+-391 is sensitive to changes from high energy electrons. Given the high energies of excited He and the long-lived metastable species that can be generated, it is often put forward that these species are responsible for the formation of N_2^+-391. However, in some studies it has been argued that electron collisions are the most dominant and influential particles in the formation of N_2^+-391. Works have been carried out that bring forward the point that the difference in excitation cross-sections between He atoms and N_2. The smaller cross-section of He compared to N_2 allows free electrons to have more time to be accelerated by the applied electric field and are thus able to reach higher energy levels that can ionize N_2 and generate N_2^+ (Naveed (2006)). Another work that uses a He gas flow in a plasma jet that shows the interactions and kinetics with ambient air, a steady state reaction process is considered along with the dominance of electron impact excitation of N_2 to N_2^+-391 (Begum (2013)). The work carried out by Begum et al. (2013) used the ratio of the excited N_2 species from the SPS and FNS to show how the electric field changes and how the electron kinetics vary with different percentages of air to He. So from this, we assume, much like the work they carried out, that the

dominant process for N_2^+-391 generation is due to high energy electron collision with N_2 due to the lower cross-section value of He allowing the free electrons to be accelerated by the applied electric field. Getting a ratio of N_2-337/N_2^+-391 gives the ratio of low energy electrons to that of high energy electrons with values >1 meaning a larger population of slow electrons and <1 equating to a larger population of fast electrons (Milosavljevic (2017)). Information used for the identification and analysis of the emission species of He that were used in this work are seen in Table 4.3.

Table 4.3: Spectroscopic data of He used for this study (Traylor (2001)).

Excitation energy (eV)	Wavelength (nm)
23.59	He-471
23.07	He-587
23.07	He-667
22.72	He-706
22.92	He-728

4.3 Results

Due to the cylindrical geometry of the system used in this experiment, it was assumed that the plasma generated would be radially homogenous. Analyzing the data from the OES measurements showed that this is the case. When comparing the results from point to point, the same ratios and emission patterns were observed, thus highlighting the strength of the method of analysis when comparing the emission intensities relative to one another. Changes in the flow rate of the gases did affect the emission of certain species. However, the emissions changed linearly with increasing flow rates and

remained stable over time. The greatest changes occurred due to increases in the applied voltage. In order to summarize the results into concise graphs, the emissions from the plasma that were recorded when using the lowest and highest flow rates at each of the three voltages (17 kV, 22 kV, and 27 kV PP) for each gas were analyzed. Due to the homogeneity of the plasma, the results shown were taken from the top of the first position as a representation of the whole geometry.

4.3.1 Discharge of Ar in Ambient Air

The plasma generated when using Ar showed strong emissions of Ar, OH, and N_2 (SPS). There were also small, but distinguishable emissions of H_α at 656 nm. As seen in Figure 4.3 the intensities of N_2 increases with the use of higher voltages, but they also decrease with an increase in flow rate. However, the intensities of the excited Ar species increase with both voltage and flow rate. When the flow rate of Ar is increased, the ambient air within the system is flushed out even more so and the quantity Ar being introduced increases. In this case the percentage of Ar is higher and more excited atomic Ar emissions can be measured, whereas in the case of ambient air there is a decrease of N_2 and OH with an increase of the Ar flow rate. From the analysis of the emission intensities as shown in Figure 4.3(a) and (b), it can be observed that the atomic Ar species and excited N_2 species of the SPS have interactions with one another. The kinetic mechanisms (1-3) show the interactions that are most probable to generate excited Ar and N_2 species (Biloiu (210)). Mechanisms (4-7) show how O and NO are destroyed and are not detected within this plasma discharge (Biloiu (210)). The intensity of the emissions that occur due to the relaxation of the Ar metastable species increase with voltage and gas flow rate, but not as much when compared to that of Ar-727 and Ar-826. As the metastables of Ar are known to transfer energy to N_2 to generate the SPS system, it is expected that these excited Ar species would not

increase as much compared to their resonant state due to their greater ease of being quenched.

$$Ar + e \rightarrow Ar(2p) + e \qquad\qquad (1)$$

$$N_2 + e \rightarrow N_2(C^3\Pi_u) + e \qquad\qquad (2)$$

$$Ar(2p) + N_2 \rightarrow Ar + N_2(C^3\Pi_u) \qquad\qquad (3)$$
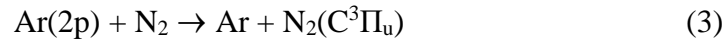
As can be seen from the data presented, there is no detection of NO or O in the emission spectra obtained. The lack of these species can be explained by the assertion of mechanisms (4-7) below where M is a third body atom or molecule (Schmidt-Bleker (2016)). In this experiment M is considered to be Ar or He.

$$O + O_2 + M^* \rightarrow O_3 + M \qquad\qquad (4)$$

$$M^* + NO \rightarrow M + N + O \qquad\qquad (5)$$

$$O + H_2O \rightarrow 2OH \qquad\qquad (6)$$

$$2N + M \rightarrow N_2 + M \qquad\qquad (7)$$

The intensity of Ar-750 does change noticeably with a change in voltage, but does vary with a change in flow rate. The excitation of Ar-750 is due to the impact of high energy electrons so it is an indicator of how the distribution of electron energies change with the parameters used. This is shown in Figure 4.4 which were obtained by using the line ratio method Ar-811/Ar-750 giving the EEDF. The increases of EEDF can be caused by a larger concentration of Ar being present at higher flow rates, which allows for more kinetic interactions in the form of electron-Ar collisions which are not quenched as much through energy transfers processes with N_2.
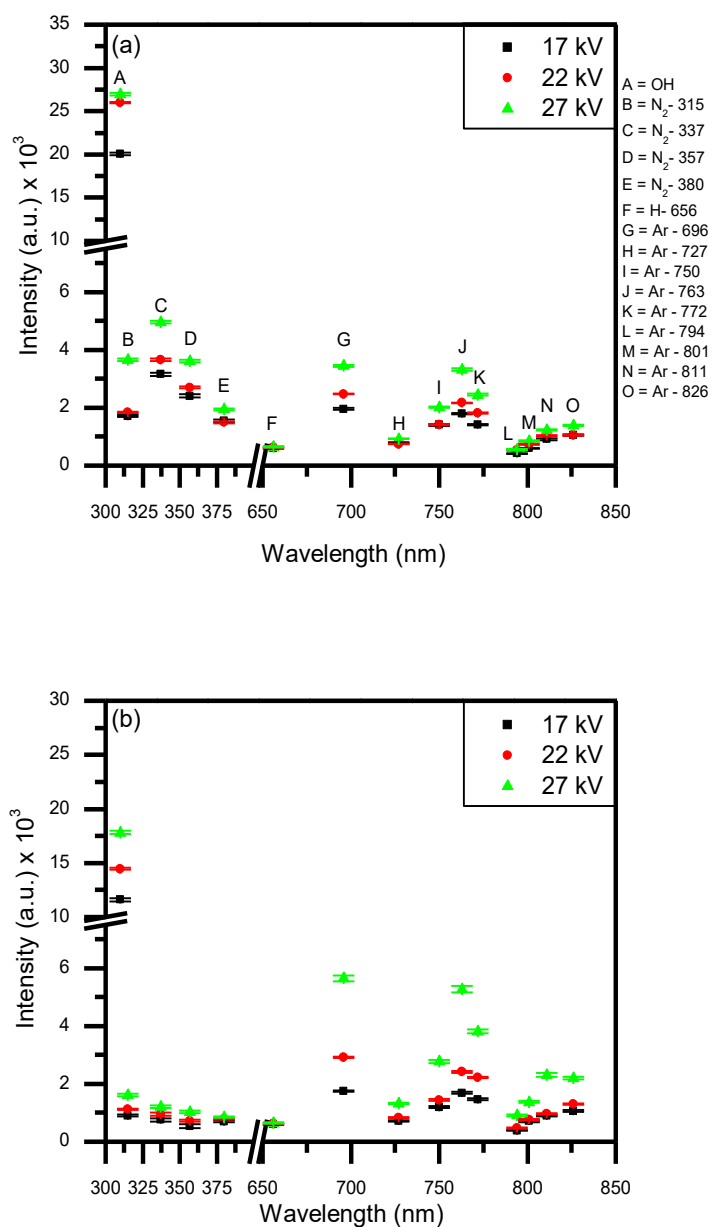
Figure 4.3: The changes in the intensities for the N_2 SPS, OH, Ar and H_α are shown with the species being represented by their wavelength on the x-axis. The legend in 3(a) labels the species (A-O) for each wavelength displayed. **a)** shows the intensities when the flow rate of Ar is kept at 1 L min^{-1} and **b)** represents intensities when the Ar flow rate is 5 L min^{-1}.
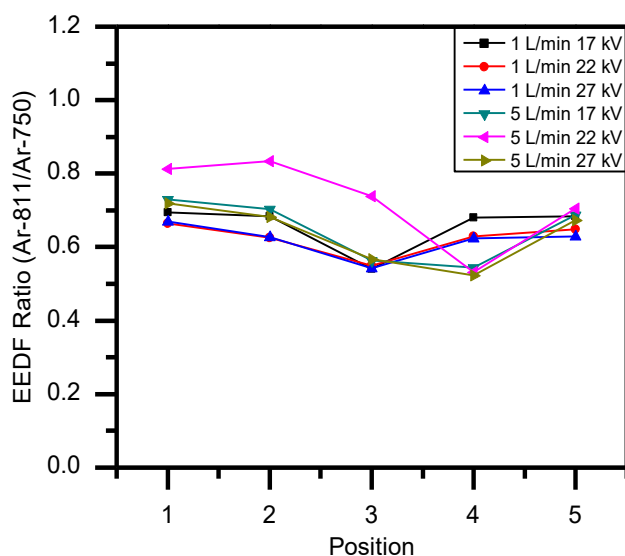
Figure 4.4: The changes in the averaged EEDF across 5 positions along the plasma discharge system, obtained from the line ratio of Ar-811/Ar-750 when using Ar at a flow rate of Ar = 1 L min^{-1} and Ar = 5 L min^{-1}.

4.3.2 Discharge of He in Ambient Air

Figures 4.5a and 4.5b show the dependence of the emissions of N_2 from the SPS and FNS with respect to changes in voltage and gas flow rate. They also show the dependence of He emissions on voltage and gas flow rate. The trends seen for N_2 are the same as when Ar was the operating gas. However, there is an increase in the number of excited N_2 species generated in the SPS and there is also N_2^+ generated from the FNS at 391 nm. The intensity of He undergoes noticeable changes with changes in voltage and flow rate. An increase in voltage increases the excited population density of He, but an increase in gas flow causes a decrease in two of the atomic He species (He-471 and He-587) at 23.0736 and 23.59 eV and increase in one atomic He species (He-706) at 22.72 eV. Compared to the use of Ar as the main feed gas, the increase of the He flow rate through the system shows an increase in the

emission of OH. The changes in emissions of N_2^+ and He when comparing the flow rate of 1 L min^{-1} to 5 L min^{-1} suggest that the increased flow rate introduces more He and reduces the amount of ambient air in the system and does not quench the excited He species as much. This in turn allows for the energetic He species to interact with the H_2O adsorbed within the system more so and generated more OH. The kinetic mechanisms (8-9) as well as mechanisms (1-7) highlight the most probable routes for energy transfer and generation of the species seen in the emission spectra (Jansky (2014)).

$$He + e \rightarrow He(2S_3) + e \qquad\qquad (8)$$

$$He + e \rightarrow He^+ + 2e \qquad\qquad (9)$$

$$N_2 + e \rightarrow N_2^+ + 2e \qquad\qquad (10)$$

The EEDF for He plasma was calculated from the line ratio method with the emission lines of N_2-337 and N_2^+-391 and is shown in Figure 4.6. The shown EEDF values were found when the flow rate was set to 1 L min^{-1} and 5 L min^{-1} and for all three voltages used (17 kV, 22 kV, and 27 kV PP). The somewhat more spontaneous changes in the EEDF compared to the other gases and gas mixes is that excited N_2 densities would be higher at the beginning of the system and become saturated until they reach another point further down the system, but with higher flow rates, they become more dispersed throughout the system. The generation of He* and He^+ within the plasma would give rise to high energy species and electrons. Consequently, an increase of these species would not impact the generation of N_2^+ at 391 nm as much as N_2 in the SPS.
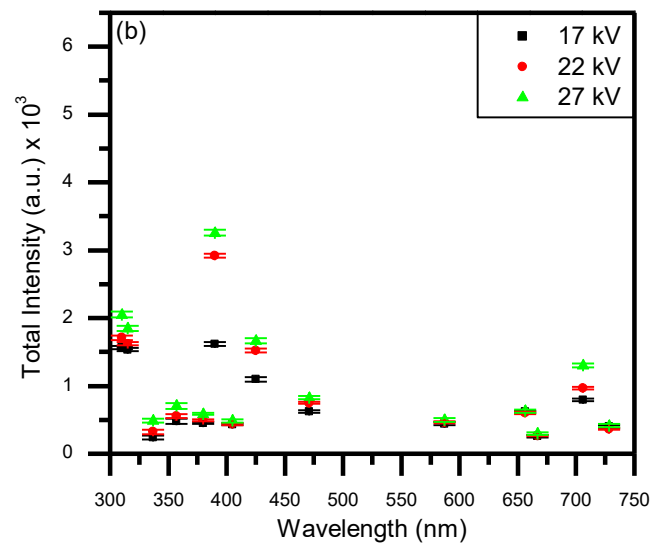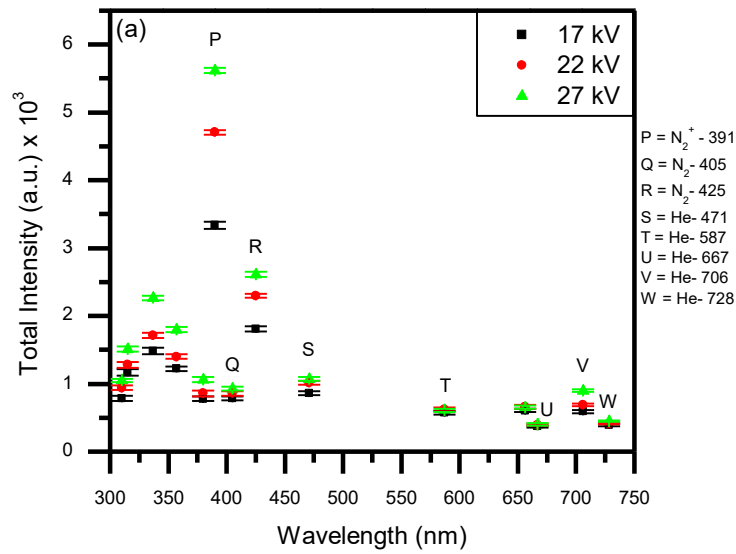
Figure 4.5: The changes in the intensities for OH, N_2, N_2^+, H_α, and He are shown with the species being represented by their wavelength on the x-axis. The legends in 3(a) label species (A-E) and 5(a) labels the species for every other wavelength displayed on figures 4.5(a) and (b). **a)** shows the intensities when the flow rate of He is kept at 1 L min⁻¹ and **b)** represents intensities when the He flow rate is 5 L min⁻¹.
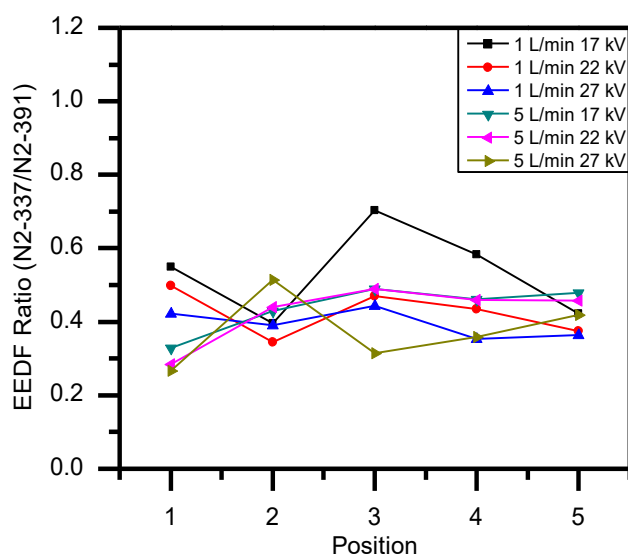
Figure 4.6: The changes in the average EEDF with respect to the positions along the plasma system, obtained from the line ratio of N_2-337/ N_2^+-391 when using He in air when the flow rate was set to He = 1 L min^{-1} and He = 5 L min^{-1}.

4.3.3 Discharge of an Ar-He Gas Mixture in Ambient Air

The use of Ar as the main carrier gas with the addition of He sees an increase in the generation of the N_2 SPS. Even though He is introduced into the system from 0.1 L min^{-1} up to 0.5 L min^{-1} in intervals of 0.1 L min^{-1}, there are no noticeable emissions of the atomic He species or N_2^+ seen compared to when He was the only gas used to interact with the ambient air. With increases of voltage, all species other than H_α increase in intensity and this can be clearly observed from the trends shown for their respective intensities in Figure 4.7. However, it can also be seen in Figure 4.7 how the intensity of Ar is decreased with an increased addition of He into the gas mixture. By prescribing mechanisms (1-3 and 8-10) to the results found, the most probable kinetic mechanisms can be ascertained and show how the formation of N_2 is increased so

much while He or N_2^+ are not detected (Olthoff (1994), Hoskinson (2016)). The quenching of He is most probable through Penning excitation or through lack of excitation due to its lower excitation cross-section compared to N_2 (Naveed (2006), Begum (2013), Jansky (2014), Hoskinson (2016), Schmidt-Bleker (2016), Milosavljevic (2017)). Given that Ar emissions are at a maximum when He is set to 0.1 L min^{-1} and most of the Ar peaks drop when He is set to 0.5 L min^{-1}, there must be some shift in the energy distribution as the Ar 750 line increases while the generation of N_2 SPS species stays relatively constant. Given that the Ar-750 line is associated with high energy electrons and that Ar acts as a quencher through Penning ionization, the increase of He takes away some of the population of excited Ar(2p) species through kinetic processes and creates an environment that allows for a higher generation of Ar-750. Given that N_2-337 is associated with low energy electrons and the SPS can be created by collisional processes with excited Ar species, the increase of the generation of Ar(2p) species compared to the plasma discharge when using only Ar with air gives rise to a higher population of excited species in the SPS.

$$He^* + Ar \rightarrow He + Ar(2p) + e \qquad\qquad (11)$$
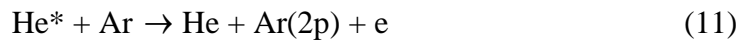
Since there is no detectable emission of N_2^+-391 when using a gas mixture of Ar-He, the EEDF must be calculated by using the same line ratio as was used for Ar. This shows that the quenching of He atoms through Penning excitation plays a significant role in the kinetics of Ar, and as a consequence, the generation of excited N_2 SPS and FNS species.
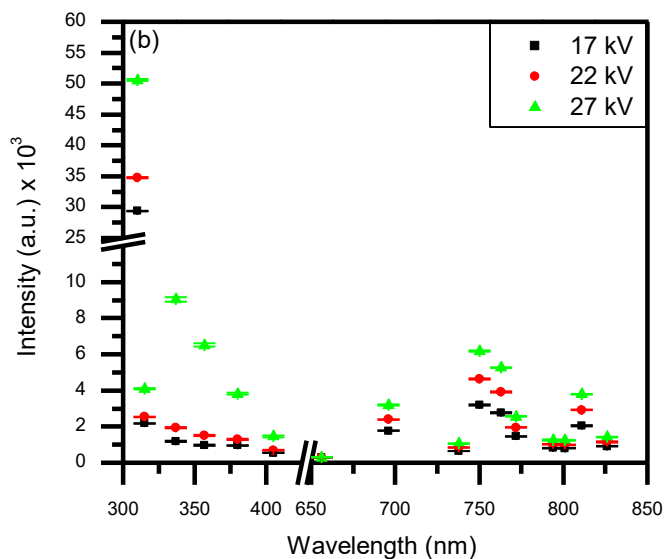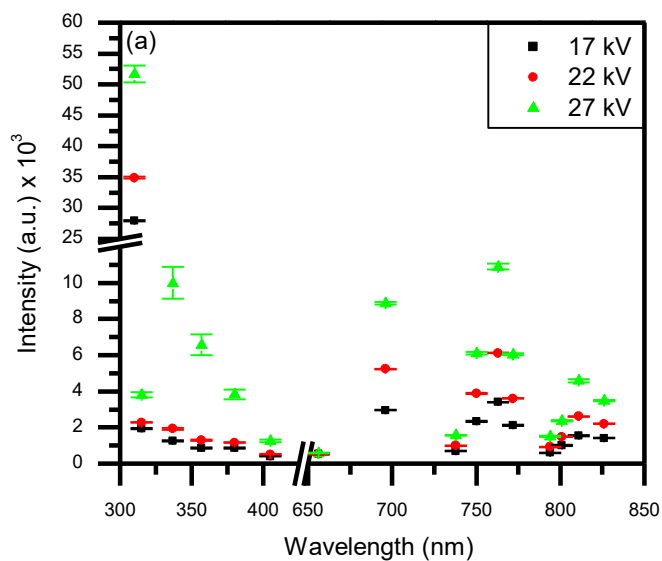
Figure 4.7: The changes in the intensities for OH, N_2, Ar, and H_α are shown with the species being represented by their wavelength on the x-axis. The legend in 3(a) labels species (A-O) and the legend in Figure 4.5(a) labels species (P) that can be seen here. Ar is kept at 1 L min^{-1} **a)** shows the intensities when the flow rate of He is set to 0.1 L min^{-1} and **b)** represents intensities when the He is set to 0.5 L min^{-1}.
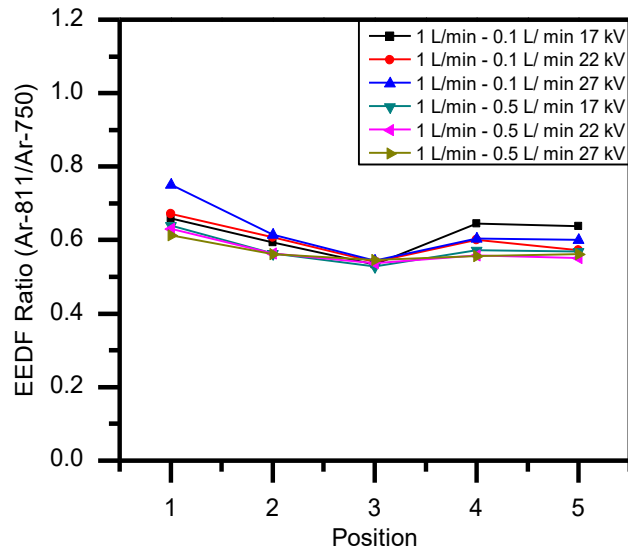
Figure 4.8: The changes in the average EEDF obtained from the line ratio of Ar-811/Ar-750 when using Ar-He in air are shown for 5 positions along the plasma system. Ar is kept at 1 L min^{-1} and the EEDF is shown for a flow rate of He = 0.1 L min^{-1} and He = 0.5 L min^{-1}.

4.3.4 Discharge of a He-Ar Gas Mixture in Ambient Air

The introduction of Ar into the system when using He as the dominant gas creates a similar mix of species to the Ar-He mixture. However, there are slight differences in the values of the intensity. Interestingly, N_2^+ was not detected in the emission spectra even though the flow rate of He in this instance is at 1 L min^{-1}, which has been shown to be sufficient to generate N_2^+ when only introducing He into the system. This means that the introduction of Ar, even at the lowest flow rate of 0.1 L min^{-1}, is sufficient to quench the excited He species through Penning excitation and, therefore, impedes the generation of N_2^+ species. The intensity of N_2 species increases when the voltage is raised and is seen to decreases with an increase of Ar in the gas mixture. OH, however,

has a higher intensity maximum when the amount of Ar in the gas mixture is greatest. This is clearly seen in Figure 4.9(a) and 4.9(b). The use of He with additives of Ar creates an environment in which the Ar-750 species have an increased intensity compared to a mix of Ar-He and even when Ar is used on its own. The EEDF calculated from the line ratio method when using He-Ar was carried out using the ratio of Ar-811/Ar-750. There was a minimum EEDF value found when the Ar flow rate was set to 0.1 L min^{-1}. From Figure 4.10, it is observed that the maximum value can be seen when the Ar flow rate is set to 0.5 L min^{-1} has minimal variance with changes in the applied voltage.
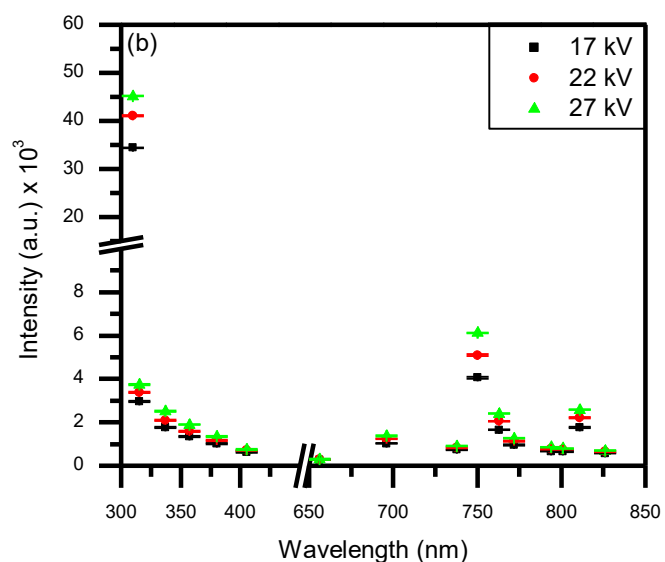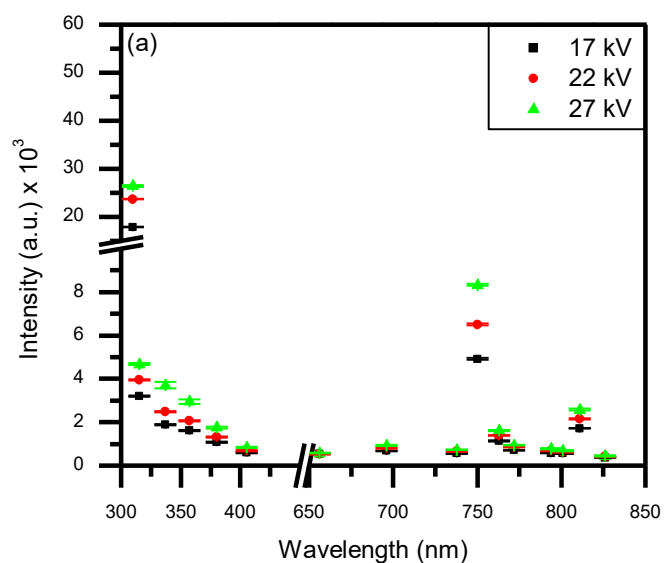
Figure 4.9: The changes in the intensities for the N_2 SPS, OH, Ar, and Hα are shown with the species being represented by their wavelength on the x-axis. The legend in 3(a) labels species (A-O) and the legend in Figure 4.5(a) labels species (P) that can be seen here. **a)** shows the intensities when the flow rate of He-Ar is kept at 1 L min^{-1} – 0.1 L min^{-1} and **b)** represents intensities when He-Ar is kept at 1 L min^{-1} – 0.5 L min^{-1}.
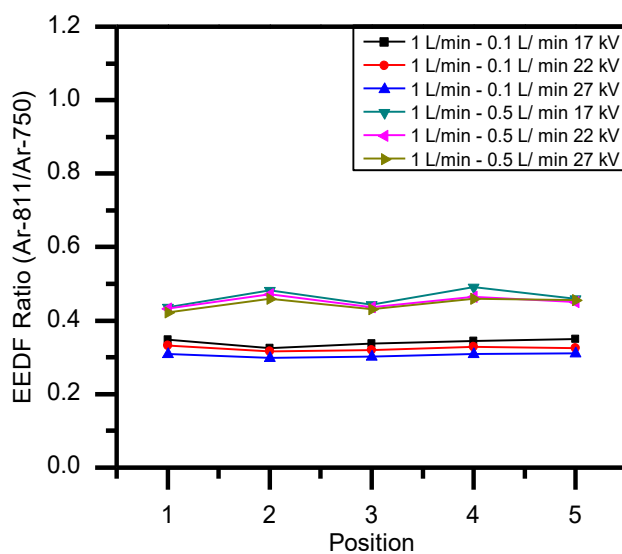
Figure 4.10: The changes in the average EEDF obtained from the line ratio of Ar-811/Ar-750 when using He-Ar in air are shown. He is kept at 1 L min^{-1} the average EEDF is shown with respect to the positions along the plasma system when the flow rate of Ar $= 0.1$ L min^{-1} and Ar $= 0.5$ L min^{-1}.

4.4 Discussion

As previously mentioned, the changes observed with respect to time were minimal and from which we can conclude that the plasma discharge was relatively stable and homogeneous throughout the system. Although there is a larger deviation in the emission of the N_2 SPS and OH, as seen in Figure 4.7, this is suspected to be due to variations in the populations of excited species as the suggested kinetic mechanisms take place. In order to determine the roots and mechanisms of excited N_2 generation and how Ar and He play roles, the emissions of atomic Ar and He need to be thoroughly analyzed. Before this can be done, however, an explanation must be found with regards to the interactions between the excited Ar and He species. This will provide a better understanding as to what steps and processes are most important for

the generation of excited and reactive N_2 species. Looking through the results for each gas mixture, it can be seen that the highest intensity achieved is when a mixture of Ar-He with Ar being kept at a flow rate of 1 L min^{-1} and He of 0.1 L min^{-1} is used. This is even higher than just using Ar or He on its own at 1 L min^{-1}. However, as He is increased to 0.5 L min^{-1} the intensity values of Ar in this gas mixture is comparable to when Ar is the only gas used and kept at 1 L min^{-1}. It has been determined that the Ar species quench the energetic He atoms through Penning ionization. This means that there is a multi-step mechanism, similar to He-Ne discharge tubes, when using a mixture of Ar and He for plasma.

With this in mind, and noting how the resonant states of Ar are increased more so than the associated metastable emissions, there are two possible reasons for this apparent preferential pathway for energy transfer between He atoms and Ar atoms. For this we look at N_2, as the intensity of these excited species should also be affected by increases in metastable populations. The intensity of the excited N_2 species does in fact increase compared to when Ar is the sole gas, but is still less than for pure He, giving it the second highest values of intensity when using the Ar-He mix. The second, and most probable route for non-radiative energy transfer, is the interaction of He atoms with non-metastable resonant Ar species, such as the spectral emission at 696 nm. The reason that this is the likely route is that due to the much shorter lifetime of these species, the less likely the population will be saturated and a faster reaction time between these particles and He can occur. Going further than this, and basing other points on the experimental results obtained, the use of gas mixtures where Ar is the dominant gas (Ar-He) and where He is the dominant gas (He-Ar) show no detectable He emission lines or N_2^+ -391. This would suggest that the He atoms are being quenched or are not excited to high enough states as when only He was used. Given

that the Ar and N_2 SPS systems have increased intensities compared to when solely Ar was used, it would be suggested that the introduction of He creates a denser electron population to interact with N_2 and Ar. The lack of N_2^+-391 emission would suggest that the energies are not high enough to cause ionization. Looking at the N_2, Ar-811, and Ar-750 emission lines with changes of gas mixtures, credence can be given to the idea that He adds a larger amount of energetic electrons to the system and allows for a higher generation of N_2 SPS and Ar species. If the energy was high enough to ionize Ar, we would expect to also see some amount of N_2^+ as this can be created through Penning ionization with Ar^+, but given that none is detected, it is put forward that the main excitation kinetics for the Ar-750 and Ar-811 are due to electron interactions and allows us to use the line ratio method as was carried out for Ar alone. Taking into consideration both points, it is likely that both play a role in the energy transfer process, but the percentage of interactions would be higher for those Ar species that are not metastables, and thus Penning excitation plays a major role in the kinetics of this work. As the gases were mixed, it was found that the intensity of the SPS was highest when the mixture of Ar-He was set to a ratio of 10:1 with a voltage of 27 kV PP. This can be seen in Figure 4.11(a) and 4.11(b).
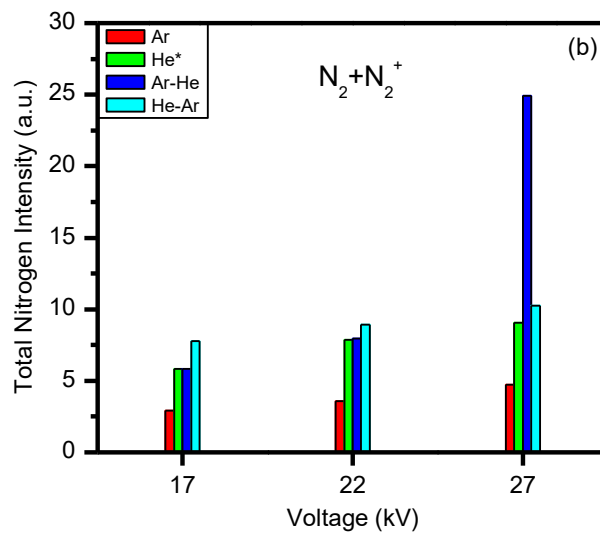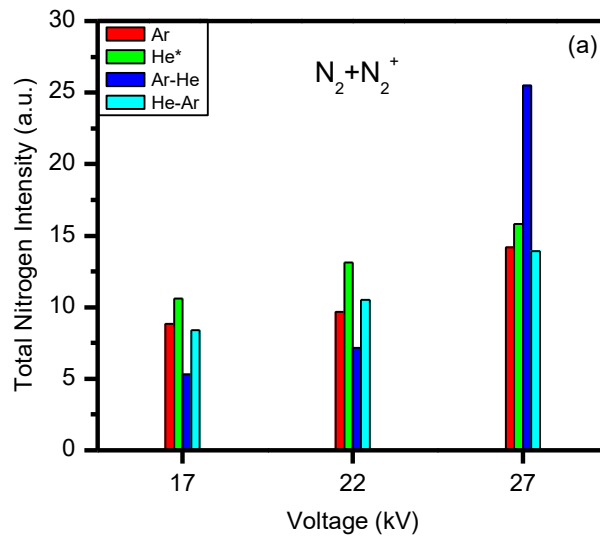
Figure 4.11: The total intensities for all nitrogen species generated during plasma discharge for each gas used during this study. **a)** shows the intensities when the flow rate of Ar and He are at 1 L min^{-1} when used on their own and the mixtures of Ar-He and He-Ar were kept at 0.1 L min^{-1} and **b)** shows the intensities when the flow rate of Ar and He are at 5 L min^{-1} when used on their own and the mixtures of Ar-He and He-Ar were kept at 0.5 L min^{-1}. (*N$_2^+$ was only recorded when He was used as the sole working gas for interactions with ambient air.*)

Table 4.4: Factor differences between the total nitrogen emissions when comparing the intensities of the Ar-He mixture to the other gases used to highlight the effect of optimizing the selectivity process (i.e. [Ar-He intensity/compared gas intensity]).

| | Flow Rate | | | Flow Rate | | |
| | 1 L min^{-1} | | 0.1 L min^{-1} | 5 L min^{-1} | | 0.5 L min^{-1} |
Voltage/Gas	Ar	He	He-Ar	Ar	He	He-Ar
17 kV	0.6027	0.5026	0.6342	2.0121	0.9961	0.7503
22 kV	0.7389	0.5464	0.6826	2.2198	1.0126	0.8912
27 kV	1.8007	1.6143	1.8306	5.2833	2.7596	2.4290

However, it was found that there was no apparent emission of He when using the Ar-He mix, but He would obviously still be a contributing factor in the dynamics of the plasma kinetics and chemistry. As mentioned previously, the quenching of He due to the presence of Ar reduces the amount of He available to interact with N_2 and consequently when the quantity of Ar is larger than that of He, as seen with Ar-He, the emission lines are completely quenched and the energy is transferred from Ar to N_2. This can be supported by the fact that there was also no N_2^+ generated other than when using just He, thus showing that the high-energy atoms of He interact with Ar before having any chance of directly exciting N_2. This intermediary step of energy transfer to Ar and then to N_2 would decrease the efficiency of excited N_2 species as there would be energy loss when going from one species to another. Further, as the gas mixture of He-Ar is implemented, the intensity of excited N_2 species decreases due to the low amount of He available to interact with the entirety of the N_2 SPS due to quenching with Ar atoms, which also limits the maximum potential for energy

transfer and again stops the generation of N_2^+. Finally, by using Ar on its own, there is a limit to the maximum intensity as the excitation comes directly from the power supplied to the system which, by extension, limits the amount of excited N_2 species generated as there is less possibility of energy transfer through collisions with higher energy particles such as He atoms. From this, there is a benefit to utilize an addition of He to generate a potential non-radiative collisional transfer of energy with Ar when a ratio is maintained with He being roughly 10 times less than Ar.

4.5 Conclusion

It has been found that the use of Ar, He, and mixes of these gases is a viable method for enhanced selectivity of excited N_2 species generation at lower voltages, current, and temperatures compared to using solely ambient air. By using Ar, there were strong signals of the N_2 SPS and when using He the highest values for the intensity of the N_2 SPS and FNS were recorded. It was also found that by mixing the gases together that interactions occur between the Ar and He atoms present causing the He species to be quenched. Similar findings can be found in the electrical discharges of helium and neon mixes. Although there was no atomic oxygen detected in the plasmas generated in this work, ozone is likely generated. This could possibly be the reason why there was no detection of NO emissions during the plasma discharge, with any atomic oxygen sufficiently excited to bond to O_2 and create O_3, thus eliminating interactions with atomic nitrogen. Biological studies using this reactor (not a part of this work) showed a reduction in bacteria activities due to the O_3 molecule. Overall, it was found that the optimum parameter used to generate the most amount of N_2 excited species for interaction with samples was when He was used, but the gas mixture of Ar-He with

Ar at 1 L min^{-1} and He at 0.5 L min^{-1} was capable of creating a relatively high intensity of N_2 while minimizing the amount of He and Ar present for interactions.

Acknowledgments

References

A. Begum, M. Laroussi, and M. R. Pervez, *AIP Advances*, **2013**, *3*, 062117.

I.A. Biloiu, and E. E. Scime, *Phys. of Plasmas*, **2010**, *17*, 113508.

B. K. H. L. Boekema, M. Vlig, D. Guijt, K. Hijnen, S. Hofmann, P. Smits, A. Sobota, E. M. van Veldhuizen, P. Bruggeman, and E. Middelkoop, . *Phys. D: Appl. Phys.*, **2015**, *49*, 044001.

J. B. Boffard, G. A. Piech, M. F. Gehrke, L. W. Anderson, and C. C. Lin, *Physical Review A*, **1999**, *59*, 1050-2947.

J. B. Boffard, R. O. Jung, C. C. Lin, and A. E. Wendt, *Plasma Sources Sci. Technol.*, **2010**, *19*, 065001.

J. W. Coburn and H.F. Winters, *J Appl. Phys.*, **1979**, *50*, 3189.

D. L. Crintea, U. Czarnetzki, S. Iordanova, I Koleva, and D. Luggenhölscher, *J. Phys. D: Appl. Phys.,* **2009**, *42*, 045208.

V. Cristaudo, S. Collette, N. Tuccitto, C. Poleunis, L. C. Melchiorre, A. Licciardello, F. Reniers, and A. Delcorte, *Plasma Process. Polym*, **2016**, *13*, 11.

G. Daeschlein, T. von Woedtke, E. Kindel, R. Brandenburg, K.-D. Weltmann, and M. Jünger, *Plasma Process Polym.*, **2009**, *7*, 3-4.

V. M. Donnelly, *J. Phys. D: Appl. Phys.*, **2004**, *37*, R207-R236.

J. V. Durme, J. Dewulf, C. Leys, and H. V. Langenhove, *Appl. Catal. B: Environ.*, **2008**, *78*, 324.

G. Fridman, G. Friedman, A. Gutsol, A. B. Shekhter, V. N. Vasilets, and A. Fridman, *Plasma Process. Poly.*, **2008**, *5*, 6.

D. Hegemann, H. Brunner, and C. Oehr, *Nuc. Instr. Meth. Phys. Res. Sec. B*, **2003**, *208*, 281.

I. P. Herman, "*Optical Diagnostics for Thin Film Processing*", Academic Press 1st edition, **1995**.

C. Heslin, D. Boehm, V. Milosavljević, M. Laycock, P. J. Cullen, and P. Bourke, *Plasma Med.*, **2014**, *4*, 153.

A. R. Hoskinson, J. Gregorío, J. Hopwood, K. Galbally-Kinney, S. J. Davis, an W. T. Rawlins, *J Appl. Phys.*, **2016**, *119*, 233301.

M. Ishaq, M. Evans, and K. Ostrikov, *Inte. J. Can*, **2013**, *134*, 1517.

M. Janda, V. Martišovitš, K. Hensel, and Z. Machala, *Plasma Chem. and Plasma Process.*, **2016**, *36*, 767.

J. Jánsky, and A. Bourdon, *Plasma Sources Sci. and Technol.,* **2014**, *23*, 025001.

Y. K. Jo, J. Cho, T. C. Tsai, D. Staack, M. H. Kang, J. H. Roh, D. B. Shin, W. Cromwell, and D. Gross, *Crop Sci.*, **2014**, *54*, 796.

A. Kramida, Y. Ralchenko, J. Reader, and NIST ASD Team (2015). NIST Atomic Spectra Database (ver. 5.3), [Online]. Available: http://physics.nist.gov/asd [2017, September 29]. National Institute of Standards and Technology, Gaithersburg, MD.

E. E. Kunhardt, *IEEE Trans. Plasma Sci.*, **2000**, *28*, 189.

Liu, P. Sun, N. Bai, Y. Tian, H. Zhou, S. Wei, Y. Zhou, J. Zhang, W. Zhu, K. Becker and J. Fang, *Plasma Process. Polym.,* **2009**, *7*, 3-4.

C. W. Liu, Y. Sung, B. C. Chen, and H. Y. Lai, *Intern. J. Environ. Res. Pub. Health*, **2014**, *11*, 4427.

M. A. Lloyd, S. J. Hess, and M. A. Drake, *J. Dairy Sci.*, **2009**, *92*, 2409.

X. Lu, G. V. Naidis, M. Laroussi, S. Reuter, D. B. Graves, and K. Ostrikov, *Phys. Rep.*, **2016**, *630*, 1.

E. Marasca, D. Greetham, S. D. Herring, and I. D. Fisk, *Food Chem.*, **2016**, *199*, 81.

V. Milosavljević and P. J. Cullen, *Euro. Lett.*, **2015**, *110*, 43001.

V. Milosavljević and P. J. Cullen, *Euro. Phys. J. Appl. Phys.*, **2017**, *80*, 20801.

V. Milosavljević, M. Donegan, P. J. Cullen, and D. P. Dowling, *J. Phys. Soc. Jap.*, **2014**, *83*, 014501.

N. Morgan, D. Ibrahim, and A. Samir, *J. Ener. Environ. Chem. Engin.*, **2017**, *2*, 25.

A. P. Napartovich, *Plasmas Polym.,* **2001**, *6*, 1.

M. A. Naveed, A. Qayyum, S. Ali, and M. Zakaullah, *Physical Lett. A*, **2006**, *359*, 499-503.

S. K. Øiseth, A. Krozer, B, Kasemo, and J. Lausmaa, *Appl. Surf. Sci.*, **2002**, *202*, 92.

J. K. Olthoff, R. J. Van Brunt, S. B. Radovanov, and J. A. Rees, *IEE Proc.-Sci. Meas. Technol.*, **1994**, *141*, 1350-2344.

R. Ono and T. Oda, *Int. J. of Plasma Environ. Sci. Technol.*, **2007**, *1*, 123.

B. M. Penetrante, M. C. Hsiao, J. N. Bardsley, B. T. Merritt, G. E. Vogtlin, A. Kuthi, C. P. Burkhart, and J. R. Bayless, *Plasma Sources Sci. Technol.*, **1997**, *6*, 251.

B. M. Penetrante, R. M. Brusasco, B. T. Merritt and G. E. Vogtlin, *Plasmas Pure App Chem.*, **1999**, *71*, 1829.

H. H. Richter, A. Wolff, R. Hippler, S. Pfau, M. Schmidt, K.H. Schoenbach (Eds.), *Low Temperature Plasma Physics*, Wiley-VCH, Berlin **2001.**

L. Scally, J. Lalor, P. J. Cullen, and V. Milosavljević, *J. Vac. Sci. Tech. A: Vac., Surf., and Films*, **2017**, *35*, 105.

A. Schmidt-Bleker, J. Winter, A. Bösel, S. Reuter, and K.-D. Weltman, *Plasma Sources Sci. and Technol.,* **2016**, *25*, 015005.

A. S. Silva, J. L. Hernández, and P. P. Losada, *Analy. Chem. Acta*, **2004**, *524*, 185.

M. Thiyagarajan, A. Sarani, and C. Nicula, *J. Appl. Phys.,* 2013, *113*, 233302.

M. J. Traylor, M. J. Pavlovich, S. Karmin, P. Hait, Y. Sakiyama, D. S. Clark, and D. B. Graves, *J. Phys. D: Appl. Phys.*, **2001**, *44*, 472001.

Z. B. Wang, G. X. Chen, Z. Wang, N. Ge, and H. P. Li, *J. Appl. Phys.,* **2011**, *110*, 033308.

K. D. Weltmann and T. von Woedtke, *Plasma Phys. Control. Fusion*, **2016**, *59*, 014031.

D. Xiao, C. Cheng, J. Shen, Y. Lan, H. Xie, X. Shu, Y. Meng, J. Li, and P. K. Chu*, J. Appl. Phys.,* 2014, *115*, 033303.

J. P. Youngblood, and T. J. McCarthy, *Macromolecules*, **1999**, *32*, 6800.

Q. S. Yu, H. Li, A. C. Ritts, B. Yang, M. Chen, L. Hong, C. Xu, X. Yao, and Y. Wang, *Plasma for Bio-Decontamination, Medicine and Food Security*, NATO Science, Springer, Dordrecht, **2012**

Chapter 5 - Significance of a Non-Thermal Plasma Treatment on LDPE Biodegradation with *Pseudomonas Aeruginosa*

L.S. and L.W. carried out all experimental work. M.G., P.J., and V.M. were co-authors of this work.

Abstract

The use of plastics has spanned across almost all aspects of day to day life. Although their uses are invaluable, they contribute to the generation of a lot of waste products that end up in the environment and end up polluting natural habitats such as forests and the ocean. By treating low-density polyethylene (LDPE) samples with non-thermal plasma in ambient air and with an addition of $\approx 4\%$ CO_2, the biodegradation of the samples can be increased due to an increase in oxidative species causing better cell adhesion and acceptance on the polymer sample surface. It was, however, found that the use of this slight addition of CO_2 aided in the biodegradation of the LDPE samples more than with solely ambient air as the carbon bonds measured from Raman spectroscopy were seen to decrease even more with this change in gas composition and chemistry. The results show that the largest increase of polymer degradation occurs when a voltage of 32 kV is applied over 300 s and with a mixture of ambient air and CO_2 in the ratio 25:1.

5.1 Introduction

Fossil fuels have been extensively used to fabricate various polymers that span uses from the medical to food industry and permeate multiple facets of day-to-day life. The current infrastructure of material creation allows different polymers to be fabricated through processes that give fine control of material properties and gives rise to versatile approaches to tailor these materials for multiple needs (Prausnitz (2004), Andrady ((2009), North (2019)). However, although they are invaluable due to their durability and ease of application to multiple areas, plastics made from fossil fuels are highly resistant to many natural processes of degradation (Campo (2008)). Due to this, certain problems arise from the improper disposal of plastic waste, litter, and their long lifetime. Such issues include: (i) pollution of oceans (ii) ingestion of plastics by animals causing contamination in the food cycle (iii) endangerment of different species due to environmental impacts (iv) soil contamination and (v) introduction into water systems that feed into lines for human consumption (Rillig (2012), Jambock (2015), Rochman (2015), Geyer (2017), Haward (2018), Lebreton (2018)). The areas impacted by plastic waste and pollution will continue to suffer as populations increase and puts more demand on their generation, which ultimately puts more stress on the environment. Some of the most widely used polymers to date include low density polyethylene (LDPE), high density polyethylene (HDPE), polyethylene terephthalate (PET), polypropylene (PP), and polyvinyl chloride (PVC). These, and more, can be seen in Table 5.1. The percentages seen in Table 5.1 define how much each listed plastic contributes to the total amount of plastic pollution that currently exists. The five polymers listed (PET, LDPE, HDPE, PP, and PVC) in Table 5.1 contribute to a combined total of 81.5% of known plastic pollution with the remaining 18.5% coming from other plastics. Currently, the methods of plastic disposal and recycling are not

able to facilitate the amount of plastic waste being created, most of which comes from plastics that have short use times (less than a year). It is reported that around 79% of plastic waste ends up in landfills or the natural environment and by 2050, there will be an estimated 12 billion tons of plastic waste existing between landfills and the natural environment (Geyer (2017)). From this, it is easy to see that, although plastics are well established in our daily lives and their manufacturing infrastructure is well imbedded in the industrial sector, there needs to be a serious change for a more sustainable method or alternative of plastic generation and disposal.

With the large quantity of plastics being introduced into the environment, new developments have been made to stem the quantity that remains in it by utilising materials that have much shorter lifetimes and can still function in the place of classic plastic materials. This has led to the development and implementation of plastics and polymers that can degrade through the introduction of biological media and different environmental conditions. These are known as biodegradable polymers (Ochi (2011), Tsutsumi (2008)). Interest in biodegradable polymers has increased in recent times to replace other synthetic polymers. Some biodegradable polymers that have come to the forefront include polylactic acid (PLA), polyglycolic acid (PGA), polyvinyl acetate (PVA), polycaprolactone (PCL), and polymers with fibrous blends that consist of biomaterials such as starch (Shah (2008)). Methods that can be used to fabricate biodegradable polymers include the use of microorganism growths and plant matter extracts (Shah (2008)). As of late, more methods have been developed in order to create biopolymers and polymers blends in order to achieve better results for applications such as medical implantation, tissue growth, replacements for other plastic fibre resins, and food packaging (Li-Na (2013), Bhatia (2014)). Although the use of biodegradable polymers will help to eliminate many negative aftereffects of

fossil fuel-based polymer waste, research is still needed to fully understand and optimise their generation for specific uses to better advance various applications.

Table 5.1: Information to compare plastic polymers that are resistant to biodegradation and those that are more readily able to degrade through natural means ((Cacciari (1993), McNeill (1995), Middleton (2000), Bodros (2007), Hiraishi (2007), Cappitelli (2008), Shah (2008), Tokiwa (2009), Sivan (2011), Esmaeili (2013), Li-Na (2013) Restrepo- Flórez (2014), Dobslaw (2017), Fatimah (2017), Seggiani (2018)).

Polymer.	Uses	Structure	Contribution to Plastic Pollution %	Means of Degradation
Low/no biodegradability				
PET	Clothing fibres, food and liquid containers, engineering resins.	$[C_{10}H_9O_4]_n$	12.8	UV exposure, thermal oxidation, *Ideonella sakaiensis*.
LDPE	Lab equipment, plastic bags, food packaging.	$[C_2H_4]_n$	23.9	UV exposure, oxidising solvents, *Lysinibacillus xylanilyticus, Pseudomonas,* and *Aspergillus niger*
HDPE	Plastic bottles, food containers, corrosion protectors, 3D printing filament.	$[C_2H_4]_n$	17.6	UV exposure, oxidative solvents, hydrolysis.
PP	Dielectric sheets, medical implantations, piping systems, hinges.	$[C_3H_6]_n$	24.3	UV exposure, microbial communities mixed with starch.
PVC	Electrical cables, flooring, window insulation.	$[C_2H_3Cl]_n$	2.9	UV exposure, *Phanerochaete chrysosporium, Lentinus tigrinus, Aspergillus niger, Aspergillus sydowi*
Biodegradable				
PLA	Medical implants, packaging material, injection moulding.	$[C_3H_4O_2]_n$		*Amycolatopsis* and *Saccharotrix*.
PGA	Medical suture, food packaging, tissue engineering.	$[C_2H_2O_2]_n$		Hydrolysis.
PVA	Wood glue, nonwoven binder, primer, adhesive.	$[C_4H_6O_2]_n$		Filamentous fungi, bacterial, fungal species, algae.
PCL	Tissue repair scaffold, targeted drug delivery, dentistry, herbicide containers.	$[C_6H_{10}O_2]_n$		*Penicillium* and *Aspergillus*.

Published works have shown that the current-state-of-art plasma systems can be used to aid in the abatement and destruction of volatile organic compounds (VOCs) as well as aiding in the degradation of polymeric materials. The use of packed bed NTP reactors, as well as pre-treatment of VOCs before introduction to a biotrickling filtration (BTF) stage, has shown that the removal of 95%+ of VOCs can be achieved (Desmet (2009), Yoshida (2016), Veerapandian (2017)). The use of packed bed NTP reactors has been shown to be of use to increase the efficiency of plasma discharge as the introduction of ferroelectric materials (BaTIO3, NaNO2, TiO4) aids in the generation of a stronger electric field by polarisation. Furthermore, this gives rise to the formation of higher energy electrons within the NTP discharge region. From this, a higher rate of energy transfer can arise and form more reaction pathways for VOC breakdown (Desmet (2009)). From these reaction mechanisms, the VOCs may dissociate into smaller constituent parts that are less harmful. These smaller constituent parts of VOCs can then be filtered through zeolite screening or BTF in order to further increase the systems VOC degradation efficiency (Desmet (2009),)). The use of BTF post NTP treatment allows biodegradation to occur. This helps in further breakdown of VOCs and also helps to trap and degrade harmful compounds formed from the breakdown of the VOCs after NTP treatment (Desmet (2009), Wei (2011), Dobslaw (2017), Veerapandian (2017)). Some of the VOCs that these systems have been shown to help degrade include styrene, toluene, benzene, PLA, and polyolefins (Desmet (2009), Wei (2013), Runye (2015), Zeng (2015), Yoshida (2016), Dobslaw (2017), Veerapandian (2017)).

Being able to modify and functionalise biodegradable polymers to tailor specific properties and characteristics is a very important step in the research of alternative material selections to increase and improve the quality of more natural and

greener products. This also extends to knowing how to best tackle the existing pollution to try and decrease it and to potentially create a modification process to functionalise polymers such as PET, PP, and LDPE to reduce their lifetimes in landfills and oceans. Current processes that are already installed to produce classically non-biodegradable polymers may be difficult to change quickly, and so an alternative may be needed that can be implemented into these industrial manufacturing processes to achieve a reduction in waste production while maintaining high quality of the produced materials for their intended uses. One such method to do this may be to implement installations of non-thermal plasma (NTP) systems. It has been shown that the colonisation of polymer surfaces by microorganisms depends on the functional groups present on the polymer surface, but it is also generally accepted that samples with higher hydrophilicity may give rise to an easier colonisation process for these microorganisms (Restrepo-Flórez (2014)). For LDPE and HDPE, it has been found that oxidised groups on the sample surface are easier for microorganisms to degrade and that the adhesion of microorganisms can be increased by creating a more oxidised and hydrophilic surface (Esmaeili (2013), Wei (2013), Restrepo-Flórez (2014), Zeng (2015), Dobslaw (2017)).

5.2 Experimental

5.3.1. Non-Thermal Plasma Treatment

The use of a novel dielectric barrier discharge (DBD) NTP system was employed to treat the samples of LDPE. This DBD system utilises a newly developed pin design that allows for the generation of NTP with an AC power supply without the use of any insulating material placed between the electrodes as a dielectric material. Although no solid material was used (plastic sheet, insulating cover etc.), the gases used would act as a dielectric to an extent to hinder electrical arcing from one plate to another before

plasma discharge could occur. The system itself uses two steel plates as electrodes, the ground electrode being flat and the high voltage electrode having an array of optimally placed pins. The pins on the high voltage electrode were initially tested with them all being placed so their points would sit on the same plane, but this produced a non-homogenous discharge and generally created plasma along the edge of the system rather than the full way through. To optimise this, the pins were then arranged in a convex pattern that had the central pins down closer to the ground electrode with the distance from pin to ground plate decreasing slightly as they were placed further from the centre. This caused plasma discharge to occur throughout the entire system as the applied electric field was not focused along the edge points of the high voltage electrode and was spread out more homogeneously between the electrodes. For this experiment, the distance from one plate to another was 10 cm, but from the central pin tip to the ground electrode, it was 7 cm. The system can be seen in Figure 5.1. The power supply was able to generate plasma discharge with a resonant frequency of 52 kHz and voltages of 27, 29.6, and 32 kV. The duty cycle was kept at 118 μs with a discharge frequency of 1 kHz. The power at these parameter settings were 3.74, 5.66, and 7.67 W for 27, 29.6, and 32 kV respectively.

Covering the system was a plastic container that had holes bored into it to allow for optical studies, gas input, contain reactive species and reduce loss through diffusion, to allow ambient air to pervade through the system, and to allow excess build-up of gas during the introduction of the ambient air:CO_2 mixture to escape so as not to cause any unequal distribution of the gases. The LDPE samples were placed on the ground electrode of the system after it was cleaned with ethanol and allowed to dry in order to sterilise the surface and decrease the risk of contamination of the samples. The samples were treated on both sides, so for the treatment of 30 s, the

sample was treated on both sides for 30 s to try and modify the total surface area of the LDPE strips. When using the gas mixture of ambient air and CO_2, the gas was given time to fill up the container so as to make sure there was an equal gas distribution throughout the system. After plasma treatment on both sides, the samples were left inside the container to allow any post-discharge species to interact with and modify them (i.e. O_3).
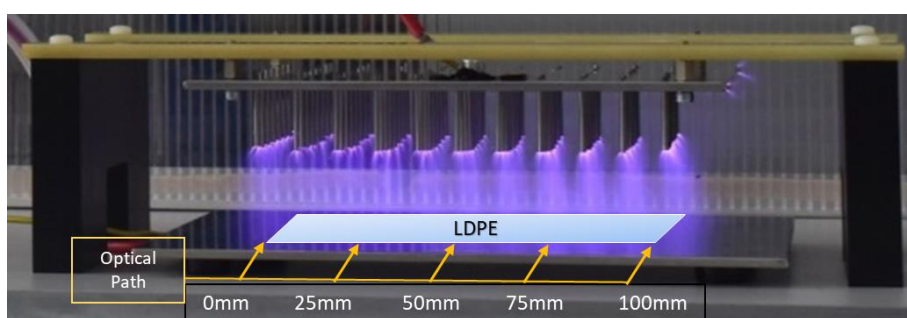
Figure 5.1: The NTP pin system that was used. Not seen is the plastic box that was used to cover the system during treatments and optical measurements. LDPE samples were placed within the plasma discharge for the duration of their treatment. Shown is plasma discharge in ambient air.

5.2.2. LDPE Sterilisation and Bacterial Broth

The use of LDPE for this experiment was to try and determine the impact that NTP treatment has on the biodegradation of classically non-biodegradable polymers. However it has been found that some bacteria may degrade certain polymers by using the polymer as a carbon source for consumption to gain energy for cell growth. However, even before treating the LDPE samples, they needed to be prepped. Sheets of LDPE were washed with a mix of 30% deionised water and 70% ethanol (Albertsson (1980), Tribedi (2013)). After this wash, they were oven dried at 50°C. After they were successfully dried, they were then brought to the NTP system for

treatment. They were placed into the system after the ground electrode was cleaned with 100% ethanol and air dried. The sterilised sheets were then treated for 30, 120, and 300 s at voltages of 27. 29.6, and 32 kV in ambient air and a 25:1 mix of ambient air to CO_2. The treatments consisted of treating the sterilised samples on both sides to ensure total surface area interaction with the plasma discharge. After being treated, the samples were cut into 1 x 5 cm strips and placed into a broth media which contained the bacteria *Ps. aeruginosa* for incubation for periods of 10, 20, 20, and 40 days to investigate the effect of biodegradation. After incubation, the plastic strips were placed in a 10 ml solution of 0.9% NaCl for 2 hours and then vortexed for 10 minutes. This was to remove the biofilm layer and measure the density of it, which was found to be between 1.1×10^6 and 1.5×10^6 CFU. Slight fluctuations were found to occur, but this was assumed to be due to remnants of the cell growth remaining on the samples even after washing, as shown in Figure 5.10. The growth medium, a nutrient basal media, was also tested to ascertain the concentration of cells within it. The growth medium concentration was found to be consistently 2.7×10^7.

Cultivating the bacteria *Ps. aeruginosa* was done according to work carried out by Kyaw *et al* 2012. The broth media that was made to incubate the bacteria and samples was made from the following: 12.5g/L K_2HPO_4, 43.8g/L KH_2PO_4, 1.0g/L $(NH_4)SO_4$, 0.1g/L $MgSO_4*7H_2O$ with 5ml of trace elements solution: 0.232g/L H_3BO_3, 0.174g/L $ZnSO_4*7H_2O$, 0.116g/L $FeSO_4(NH_4)2SO_4*6H_2O$, 0.096g/L $CoSO_4*7H_2O$, 0.022g/L $((NH_4)_6Mo_7)_{24}*4H_2O$, 0.008g/L $CuSO_4*5H_2O$, and 0.008g/L $MnSO_4*4H_2O$. Inoculation and incubation was carried out under sterile conditions. 30 mL of nutrient basal media was added to a falcon tube. After this, 10 strips of LDPE were added to the tube. 0.6ml of bacterium in 0.85% saline solution were added to tube; initial concentration for each incubation was kept at 0.5 McFarland Standard.

Incubation maintained at 37°C and tubes were placed in rotary shaker at 120 rpm. The tests were performed in triplicate and the tubes were regularly tested for cell growth and to make sure that there was no contamination present. When the incubation of the LDPE strip in the media was over, they were removed and washed with a 2% SDS solution for 4 hours and dried. After this, they were placed back into tubes containing deionised water and washed in a sonic bath for 30 minutes to remove any excess residue that may be present. When this was finished, the strips were then dried in an oven at 50°C and dried overnight. Once dried, the samples were placed on a weighing scales to determine if there was any measurable loss after degradation in the bacterial broth. This gravimetric method did not give the results that were expected as there was no consistent pattern or trend in the values obtained for the weights of each batch of samples. The results that were obtained showed very small loss values and also showed higher weights compared to the values they gave before introduction to the bacterial broth. This was found out to be due to fluctuations in organic matter being adhered to the sample surface as is shown in Figure 5.11.

5.2.3. Optical Emission and Absorption Spectroscopy

The OES and OAS both used an Edmund Optics CCD spectrometer that has a wavelength dependent resolution of 0.6-1.8 nm. Because of this, some of the peaks that were measured were in fact an amalgamation of multiple species. An example of this is can be seen at 777 nm, which is in fact an overlapping of 3 peaks that cannot be fully resolved with the spectrometer used. These three emission peaks would be from O I with λ = 777.194, 777.417, and 777.539 nm and transitions of $3s^5S_2^o - 3p^5P_{1,2,3}$ respectively and an upper energy level of 10.47 eV (Scally (2017)). For this experiment, however, the total intensity measured at 777 nm was sufficient as this included all O I emission lines of interest. When taking the OES measurements of the

plasma discharge, the acquisition time was 1.2 s with a delay of 3.8 s and a total of 61 acquisitions. This was to cover the fill 300 s of plasma discharge that was used for the maximum treatment time of the LDPE samples. These measurements were carried out over 3 voltages (27 kV, 29.6 kV, and 32 kV) for ambient air and ambient air:CO_2 at a 25:1 mixture ratio at 5 different points along the treatment area of the sample. The points of measurement were at 0, 25, 50, 75, and 100 mm from the left most section of the plasma discharge to the right most side.

OAS measurements were taken along the same positions as the OES measurements and also used the same acquisition time and delay settings, but were measured for a period of 415 s to gain information on the changes in O_3 post-discharge. Overall there were 84 spectra recorded for the OAS measurement of each parameter setting. Although the same spectrometer as was used in the OES measurements, a UV/Vis/NIR light source was used as a reference to detect changes in light intensity and thus determine the average spatial density of O_3. The light source used was a BDS130 deuterium/tungsten lamp with a spectral output of 190 - 2500 nm. The optical path used when recording the OAS data was 29 cm. After recording the data from the OAS experiment, equation 1 was used to determine the average spatial density of O_3, where D(t) is the density (cm^{-3}), L is the optical path (cm), I(0) is the reference intensity with no plasma discharge, I(t) is the measured intensity during and after plasma discharge, and $\sigma(\lambda)$ is the wavelength dependent absorption cross-section for the species of interest. For O_3 at 253.7 nm, the absorption cross-section is 1.154×10^{-17} cm^2. For OAS, the power supply timer was set to 300 s so it would automatically shut off while the measurements were still being taken in order to show the changes in O_3 over time during post-discharge.

5.2.4 Raman

In order to determine the changes in carbon bonds to detect signs of biodegradation, Raman spectroscopy was implemented. In order to carry out these measurements, the DXR SmartRaman Spectrometer from ThermoFisher Scientific Ltd. was used. The chemical structure of LDPE consists of C-C, CH_2, CH-CH_2, and CH_2-CH_2 bonds. Throughout the structure, there are no polar groups, and since the change in carbon bonds is of interest, Raman spectroscopy is suitable as the bonds that are sought after tend to have strong signals compared to infrared measurement. A 780 nm diode laser at 120 mW was used to carry out the measurements and detect the chemical groups within the polymer. The setup utilises a CCD and a universal sampling accessory with a 50 μm slit aperture. The measurements that each sample underwent consisted of 10 exposures with each exposure lasting 15 s. This was done at 3 random sampling points for each sample to obtain a better averaging of the measured spectra for analysis. Once the spectra were obtained, it was necessary to process the data using a polynomial fit baseline as there was a high amount of fluorescence that distorted the peaks of the spectra. This baseline procedure was carried out in Origin Pro 8^{TM}. After this baseline procedure was carried out, an averaging of the data from the 3 random sampling points was carried out for each sample and then plotted.
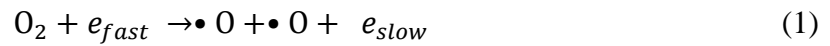
5.3 Results and Discussion

Characterising the NTP treatment system was carried out by implementing optical diagnostics. By utilising the non-intrusive nature of optical measurements, the gas chemistry along the profile of the sample treatment area was determined for the use of ambient air and ambient air with a CO_2 admixture at a ratio of 25:1 (ambient air: CO_2). By using the OES and OAS results from the optical measurement and comparing them with the changes seen in the Raman spectra, the optimum parameter setting to induce the greatest amount of biodegradation of LDPE can be ascertained.

5.3.1. Optical Diagnostics

From the measurements of the plasma discharge at each power setting and with the use of solely ambient air, as well as with the introduction of CO_2, there were many common emission species and ozone was clearly detected. However, the use of just ambient air led to the formation of excited atomic nitrogen (N I) and with CO_2 as an admixture with ambient air the generation of C_2 was detected. The formation of these reactive species, and the others detected in this work, can be inferred to through the use of the electron energy distribution function (EEDF) obtained from the line ratio of (N_2-337/N_2^+-391) (Wang (2009)). From this, the most likely paths for reactions mechanisms can be highlighted and the energetics that occur at the samples surface during treatment give rise to a better understanding of possible surface modifications.

The first set of results to be compared are the average spatial densities of O_3 that were measured throughout the treatment area as well as temporally to show the evolution of this powerful oxidant. Figure 5.1(a-c) shows the spatial and temporal evolution of ozone for the three applied voltages and demonstrates the potential to have an amount of it remain to interact with the sample surface even after plasma

generation has been stopped. From each graph of Figure 5.2, it can be seen that at the very beginning the average density of O_3 increases relatively the same for each setting. However, when a higher voltage is applied, there is a larger difference between each set of values and the values from measurements that were more central in the system have higher maximum values compared to the edge areas. This is due to species such as O_2, OH, and H_2O having longer residence times within the applied electrical field which allows them to aid in more reaction mechanisms that create O_3 as the energetics would be larger here due to their residence time in the direct electrical field. The possible reactions mechanisms can be seen below in reactions (1-3), where M is a third body atom or molecule such as O, N_2^* or OH (Wang (2009), Tribedi (2013), Scally (2018)).

$$O_2 + e_{fast} \rightarrow \bullet O + \bullet O + e_{slow} \tag{1}$$

$$\bullet O + H_2O + \leftrightarrow 2OH \tag{2}$$

$$\bullet O + O_2 + M^* \rightarrow \bullet O_3 + M \tag{3}$$
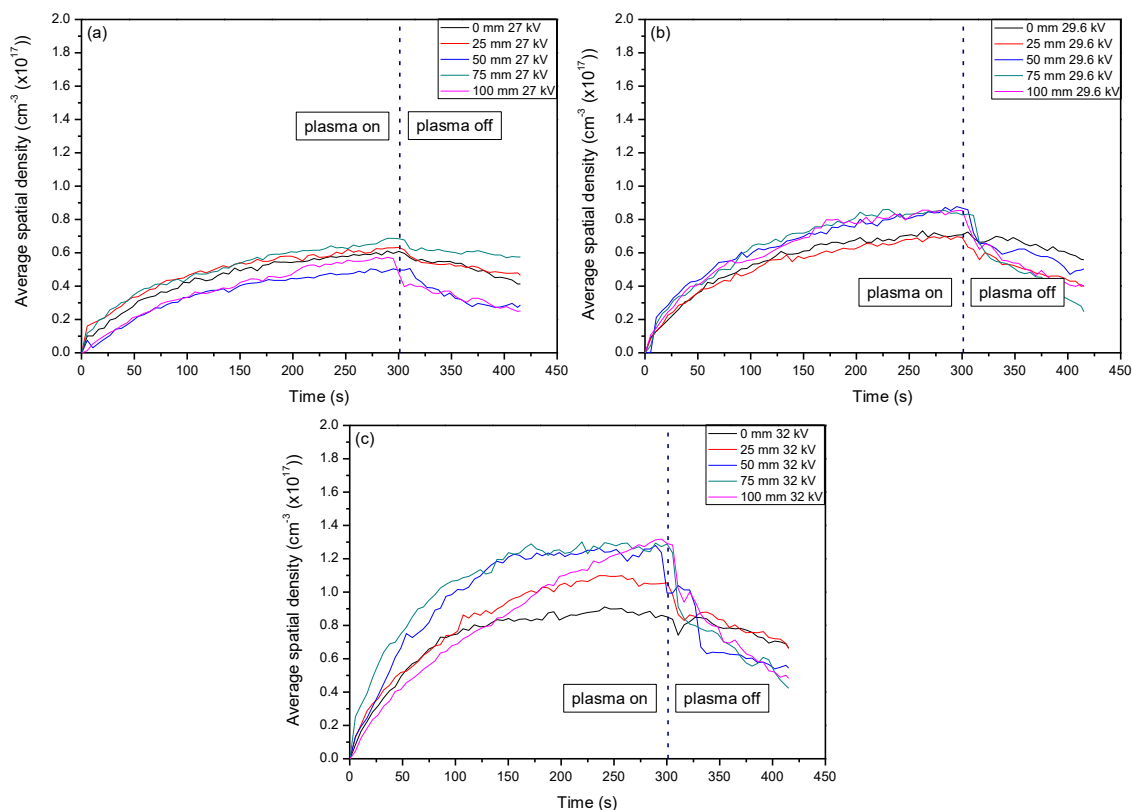
Figure 5.2: Average spatial density profile of O_3 at 253.7 nm when ambient air was the only gas present for plasma discharge. The line divides values at the point when the plasma system was set to stop generating plasma. (a-c) show the changes of O_3 average spatial density with respect to voltage.

Figure 5.3(a-c) shows the average spatial density of O_3 when CO_2 was introduced as a slight admixture into the ambient air being used. By having a CO_2 additive in the plasma discharge, the formation of O_3 is higher than when solely ambient air is used. Setting the flow rate of ambient air to 1 L min^{-1} with the introduction of CO_2 being set at 0.04 L min^{-1} impacts the creation of O_3 through reaction mechanisms 4 and 5 that can then go on to aid in mechanism 3 and the formation of O_3 (Albertsson (1980)). From these results, it can already be seen that the

159

tailoring of the plasma system to generate more of certain reactive species is possible. From the optical absorption spectroscopy (OAS) results, it can be seen that the formation of a highly oxidative species has been maximised by simply introducing a slight amount of an additive gas, CO_2 in this case. The formation of O_3 is important for this study as it can help to form a more polar sample surface during plasma treatment, and as previously stated, it is generally taken that the more polar a sample surface, the better cell adhesion will be. For this study, and indeed for many other applications, this is an important note to take into consideration when forming new technologies and methods for sample processing. Optical diagnostics are also of great importance to form a better understanding of the gas chemistry that is induced. From here, the optical emission spectroscopy (OES), optical absorption spectroscopy (OAS), and Raman Spectroscopy must be looked at to form a more concrete conclusion as to what gas chemistry is most desirable for polymer degradation in this study.

$$CO_2 + e_{fast} \rightarrow CO(a'^3\Sigma) + \bullet O + e_{slow} \qquad (4)$$

$$CO_2 + e_{fast} \rightarrow CO(A^2\Pi) + \bullet O + e_{slow} \qquad (5)$$
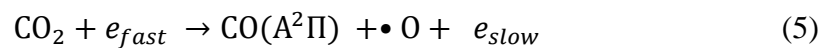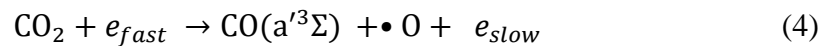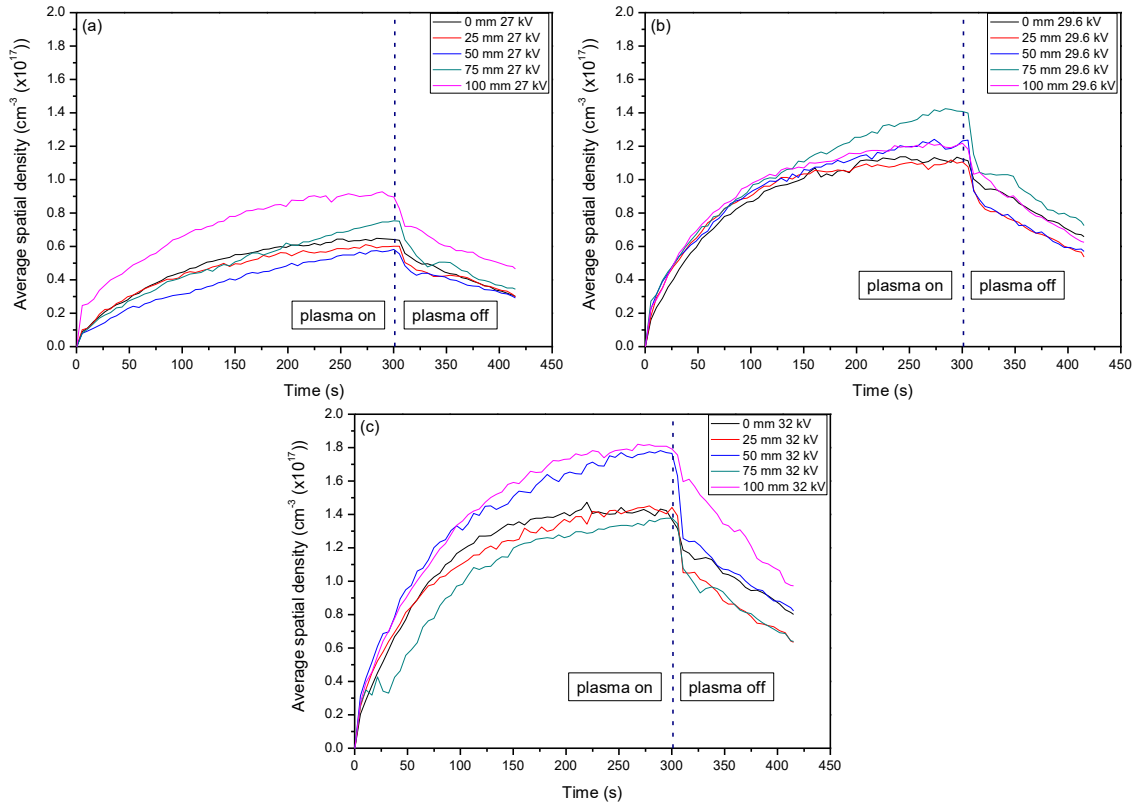
Figure 5.3: Average spatial density profile of O_3 when CO_2 was introduced to the plasma discharge. The line divides values at the point when the plasma system was set to stop generating plasma. (a-c) show the changes of O_3 average spatial density with respect to the change of voltage settings.

The EEDF results from the use of ambient air in the central regions (25 – 75 mm) show that, over time, the electron energies begin to dissipate while the edges of the system (0 mm and 100 mm) maintain their values. This can be described as the same reasoning for the formation of O_3 over time. Due to the increased residence time within the system, the excited nitrogen species become saturated and undergoes a temporal evolution of excitation and deexcitation processes, while the edges of the system have more consistent populations of ground state N_2 to interact with that do

not alter the spatial evolution as much. From Figure 5.4, it can then be seen that the electron energies are distributed more towards the low energy with increases in voltage. These changes in electron energetics are very important to understand the formation of other species within the plasma and how they alter the sample for degradation purposes.
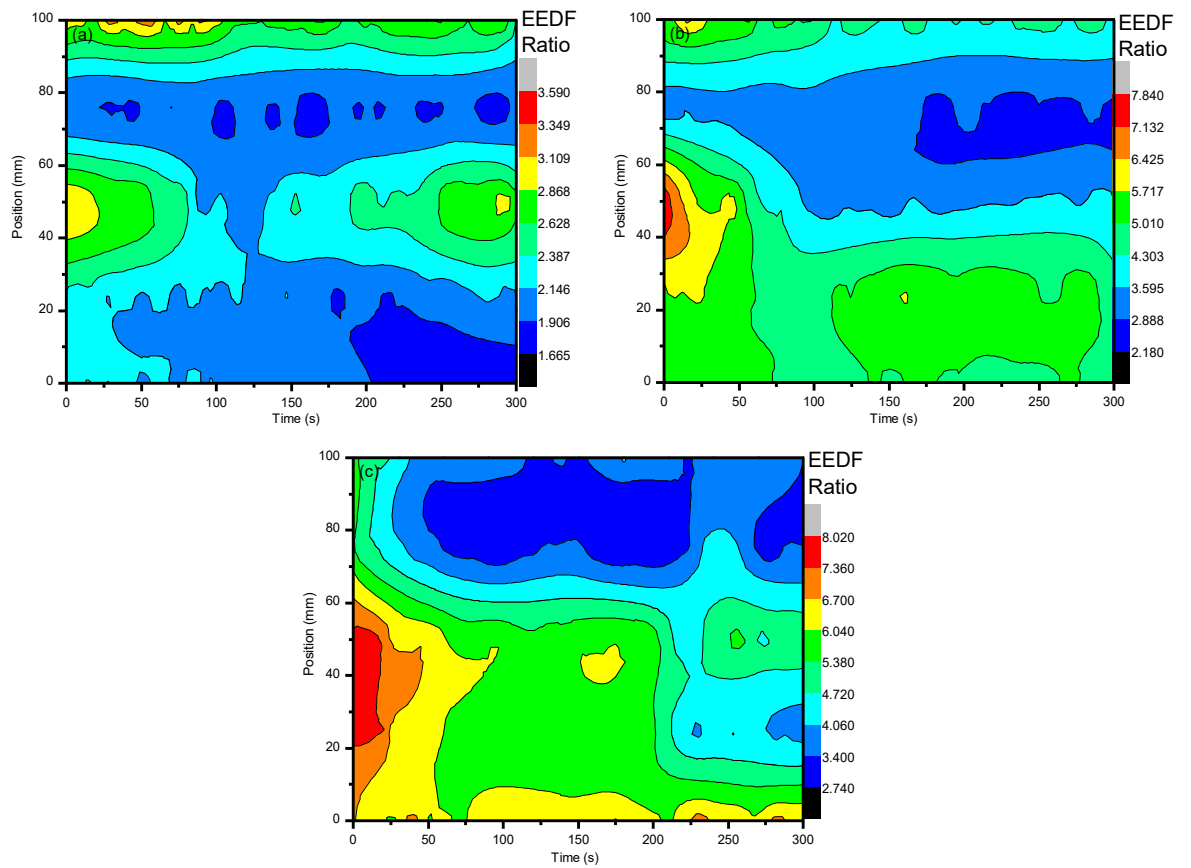
Figure 5.4: Shows the line ratio of (N_2-337/N_2^+-391) to give the EEDF when using ambient air. This portrays how the electron energies are altered with the different parameter settings, most importantly the variation of working gas composition. (a), (b), and (c) represent discharge at 27, 29.6, and 32 kV respectively.

With an addition of CO_2 at ~3.8% to the system, a drastic change in the electron energies is incurred. By using the same line ratio method and spectral line profiles (N_2-337/N_2^+-391) that were used for the EEDF of ambient air, a comparison can be easily drawn between the two experimental setups and easily diagnose the energetics of the use of the different gases. When CO_2 is introduced to the system, the EEDF is much more inclined to be sensitive to the impact of low energy electrons. As can be seen, the values for the EEDF are much higher when CO_2 is introduced, even as a small percentage of the total working gas used. However, there is a greater spread of energetics for the air: CO_2 mixture compared to that of just ambient air. As can be seen, the spread of values for ambient air when 27 kV, 29.6 kV, and 32 kV are applied is 1.93, 5.66, and 5.28 respectively. As CO_2 is introduced, the spread becomes 4.48, 9.90, and 6.50 for 27 kV, 29.6 kV, and 32 kV respectively. This fluctuation can be seen in Figure 5.5(a-c) below and occurs with a distribution of higher values from the centre of the system out to the edges, showing that lower energetics are detected at this point. This is due the quenching mechanisms of N_2^* by CO_2. From mechanisms (3-5), it can be seen that energetic electrons dissociate CO_2 into CO and O, which aid in the formation of O_3. Since we see a much higher generation of O_3 with the introduction of CO_2, it is good to assume that CO_2 is dissociated through electron impact. Given that the excitation cross section and electronegativity of CO_2 is higher than that of N_2, any energetic electrons that are generated are more likely to interact with CO_2 over N_2, causing an indirect quenching of N_2^+. From this it can be understood how the electron energetics are kept at a relatively low level as they do not have necessary time to undergo more interactions with the applied electric field as they impart their energies for dissociative mechanisms.
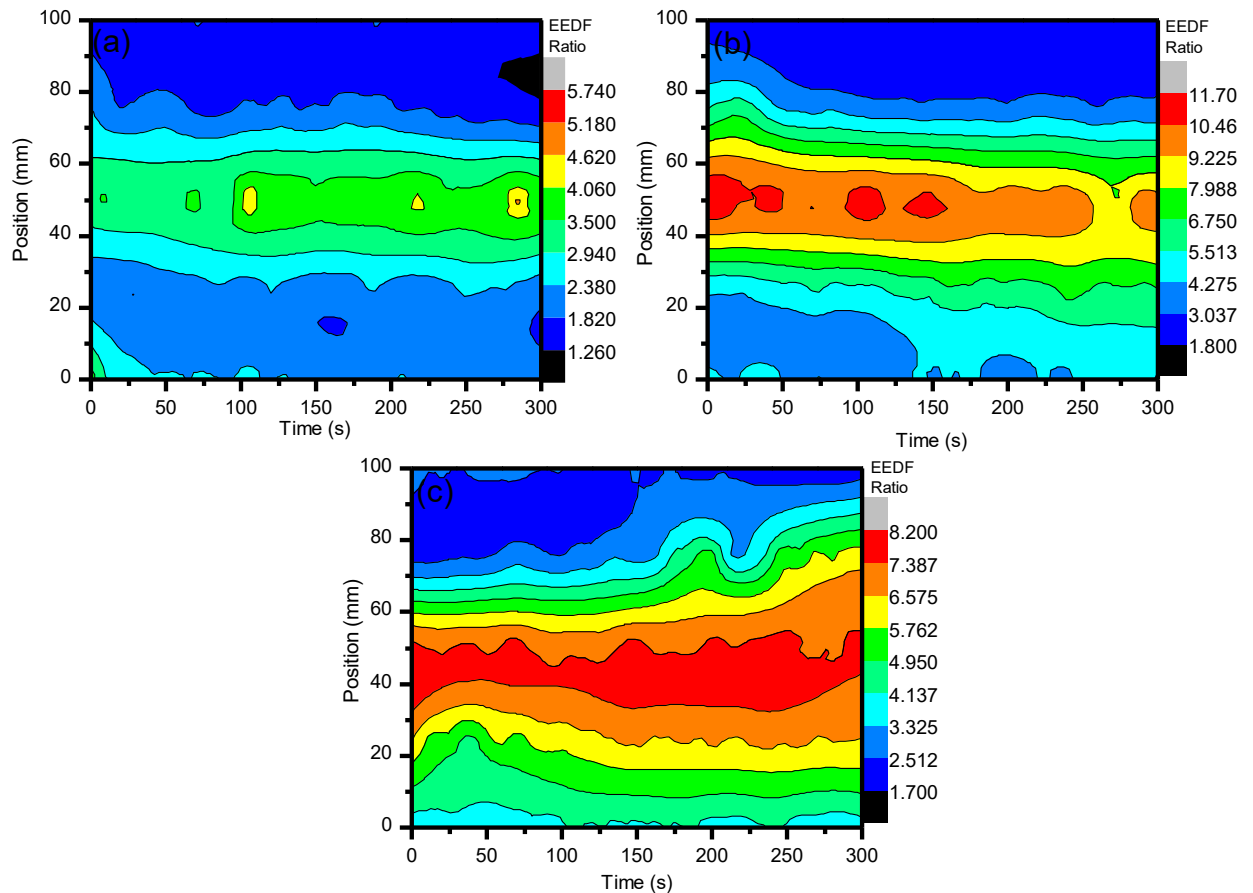
Figure 5.5: Shows the line ratio of (N_2-337/N_2^+-391) when using ambient air with ~3.8% CO_2. This portrays how the electron energies are altered with the different parameter settings, most importantly the variation of working gas composition. (a), (b), and (c) represent discharge at 27, 29.6, and 32 kV respectively.

Knowing that there are oxidative species being generated within the system is important, as it was suspected that these may aid in the adhesion and biodegradation of the LDPE samples being treated. For this, there was a focus on reactive species containing oxygen and through the use of OES, atomic oxygen (O I) was found at 777 nm and OH was found at 309 nm. Figure 5.6(a-c) shows the generation of OH with the use of ambient air for the different applied voltages. It can be seen that an

appreciable amount of OH is generated throughout the system, but there are points that show higher generation over others. As the voltage increases, the generation of OH becomes more prevalent throughout the entirety of the system, but there is still a decrease in OH emissions over time which indicates that there is a saturation event that blocks the formation of any new OH. From what we found with the generation of O_3 and from what can be seen of O I in Figure 5.7 (a-c), there may be a reduction in the production of OH due to recombination effects of OH back to H_2O and allowing more O I to become available over time, as described in reaction (2). This can be seen as the fluctuation of O I seen in Figure 5.7(a-c) would represent changes in available pathways and over time, this would be influenced by O_3 dissociation and the recombination of 2OH back into H_2O + O.
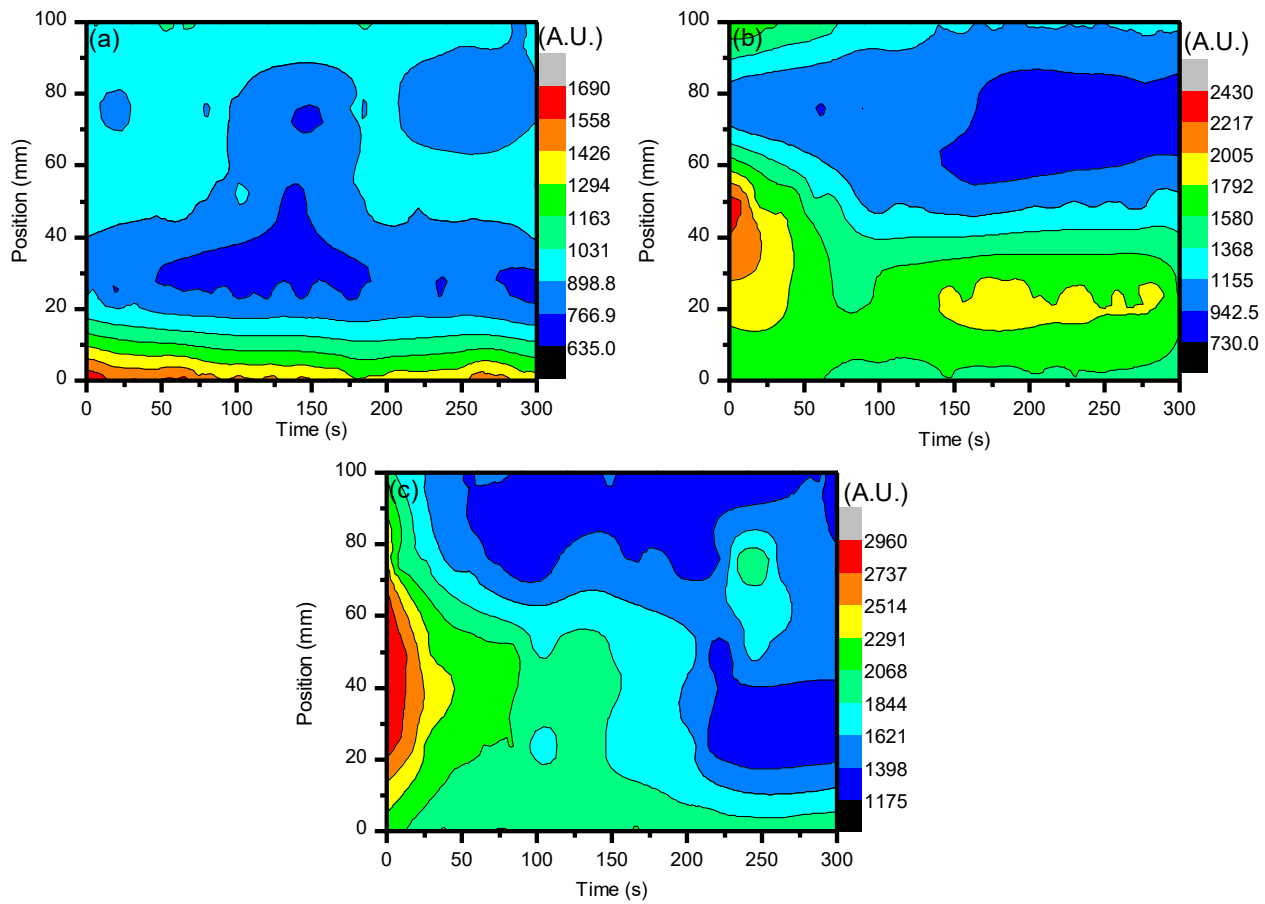
Figure 5.6: The above shows the spatial and temporal evolution of OH when using ambient air as the sole working gas in the plasma system. (a-c) represent 27 kV, 29.6 kV, and 32 kV respectively.
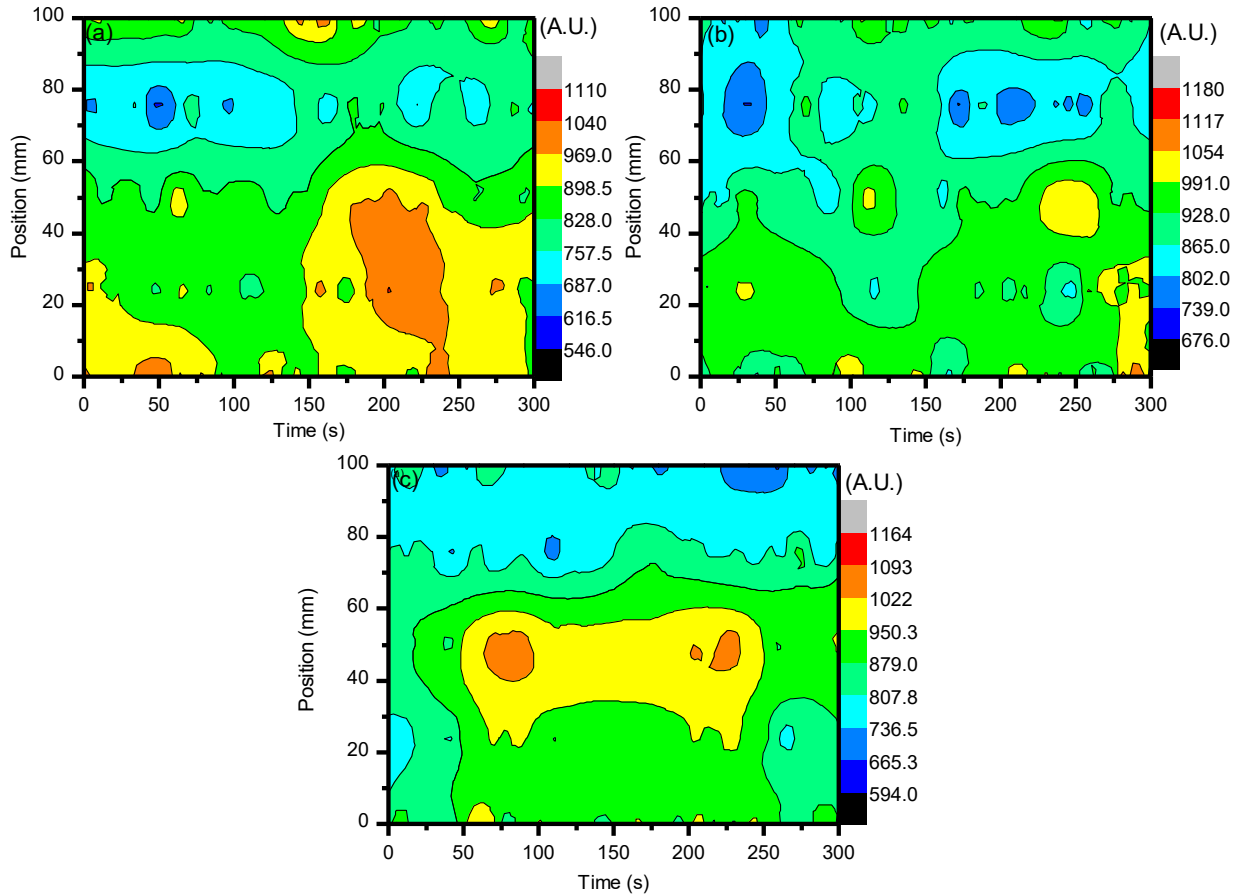
Figure 5.7: The evolution of O I with respect to the spatial and temporal profile of the ambient air plasma discharge is shown here with an applied voltage of 27 kV, 29.6 kV, and 32 kV shown in (a), (b), and (c) respectively.

The generation of OH and O I when CO_2 is introduced to the system during plasma discharge both increase appreciably. This can be seen in Figure 5.8(a-c) and Figure 5.9(a-c) below. From the previous results of the EEDF line ratio in Figure 4(a-c), it can be seen that the electron energies are more distributed throughout the lower energy portion for the plasma being generated when CO_2 is introduced, and as previously stated, this is due to the dissociation of CO_2 into CO + O from more appropriately energised electrons through collisional processes that decreases the potential energy that the electrons can reach. This aids in a higher formation of O I

167

species, which in turn takes part in the formation of OH and O_3. However, there is a much larger increase of OH compared to the increase of O I due to recombination mechanisms that form CO back into CO_2 as well as the continuous increase of O_3 that is present at much higher levels compared to those measured with solely ambient air.
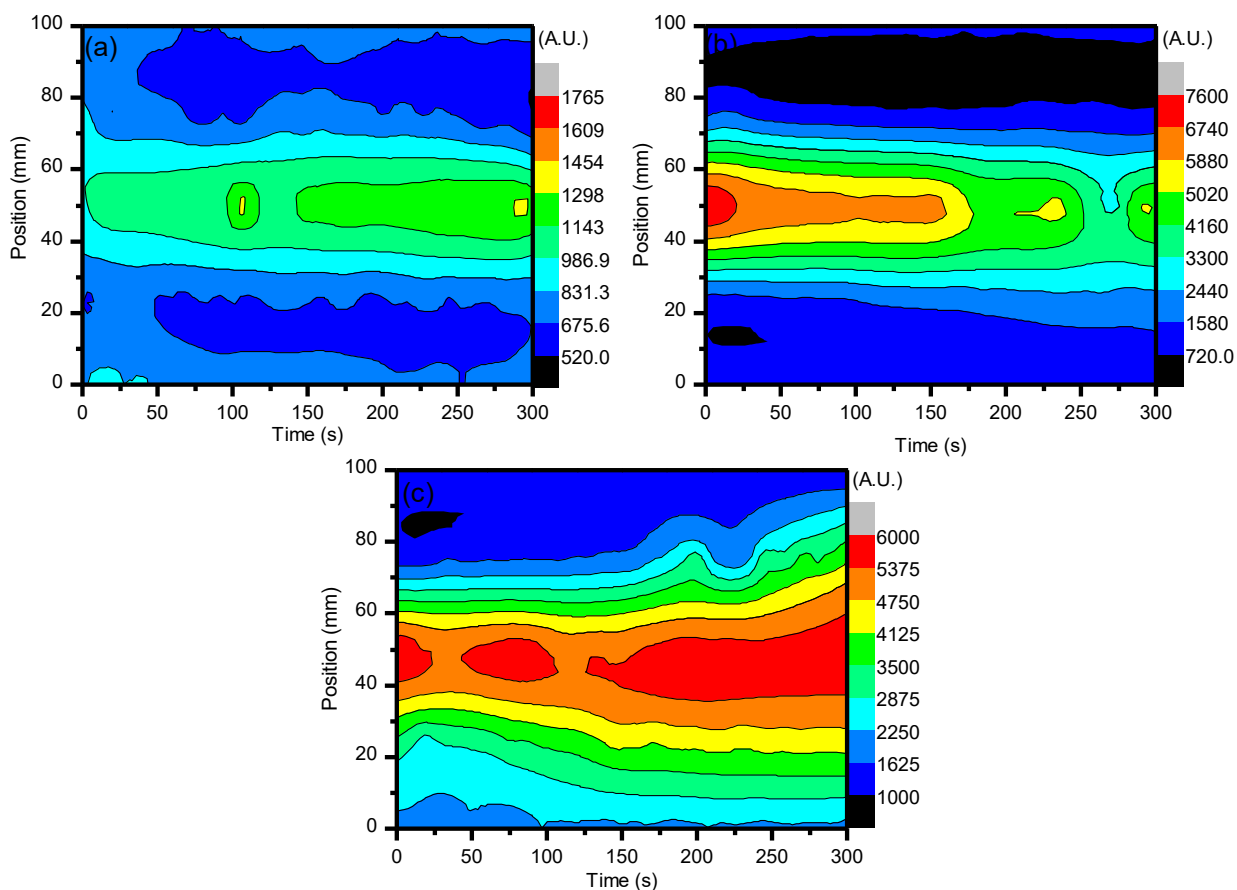
Figure 5.8: The formation of OH as detected by OES when the ambient air introduced to the system contained ~3.8% CO_2. (a-c) represent voltages 27 kV, 29.6 kV, and 32 kV respectively.
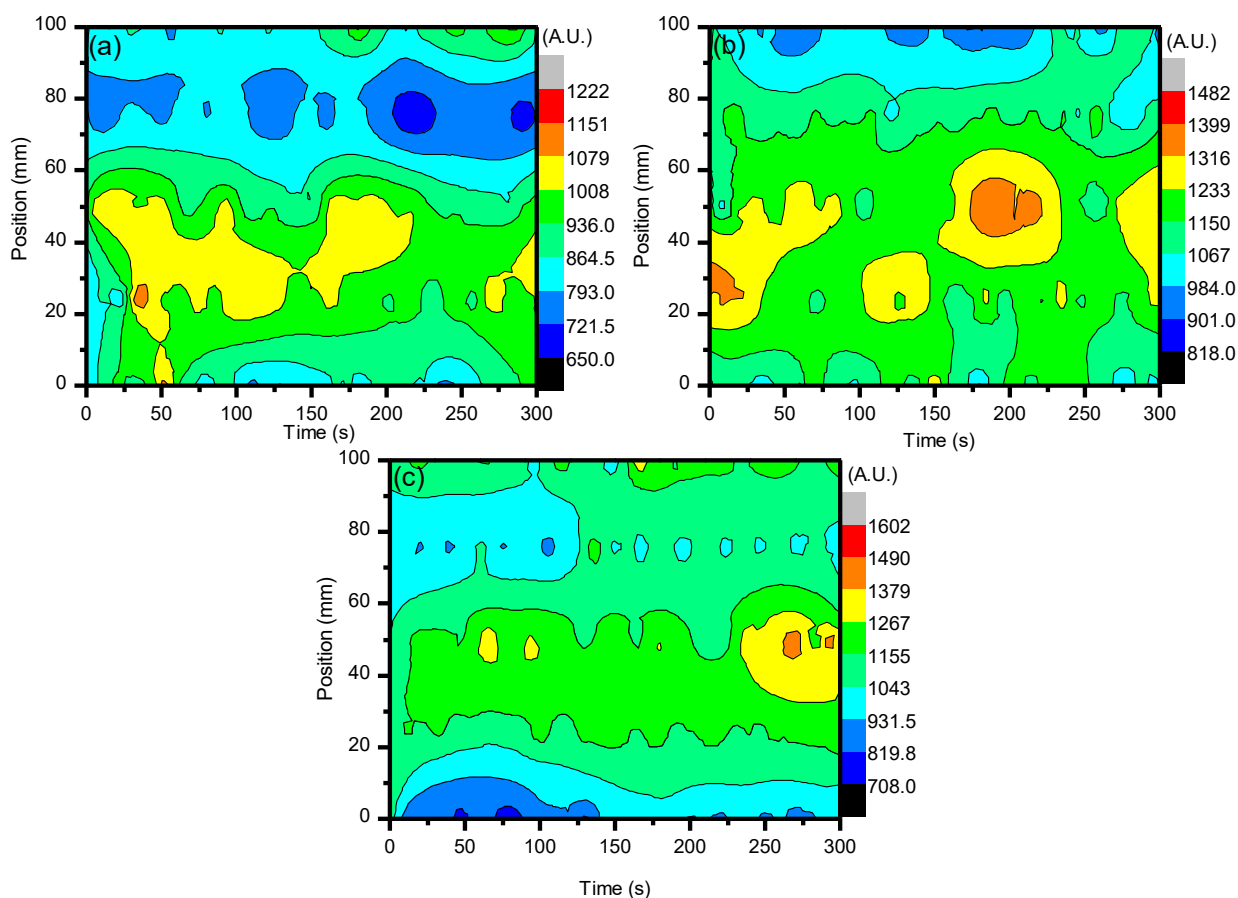
Figure 5.9: The formation of O I when the ambient air introduced to the system contained ~3.8% CO_2. (a-c) represent the applied voltages of 27 kV, 29.6 kV, and 32 kV respectively.

5.3.2 Weight Loss and Raman Spectroscopy

From the results obtained from the OES and OAS measurements, it can be seen that the introduction of CO_2, even at small quantities, aids in the formation of reactive species. These oxidative species were specifically targeted as they can help to functionalise a samples surface to become more polar, and therefore more accepting of cell adhesion for various cultures. This was thought to support the biodegradation of the treated samples as the cells should more readily bind to the sample surface and

begin decomposition of the carbon bonds that make up the polymer. In order to determine the amount of degradation that the treated samples undergo, the samples were weighed after plasma treatment and after introduction to the bacteria *Ps. aeruginosa.* The results of the weight loss method for degradation detection can be seen in Figure 5.10(a-c) and Figure 5.11(a-c). As can be seen from these results, the only sample that consistently lost weight was the reference sample, which was sterilised and untreated LDPE. The other samples showed sporadic losses and gains in weight with no discernible pattern or trend. There is a possibility that the samples that were treated could gain more weight over the degradation time, but this is difficult to ascertain without more data on this. From this, it cannot be discerned whether there was any degradation present or not. So, in order to determine what is occurring and whether or not the introduction of the bacteria after plasma treatment has any significant impact, Raman spectroscopy measurements were carried out to monitor any changes in the bonds of the samples. Most importantly, it was of great interest to measure any changes in the carbon bonds of the sample to show that the samples were being degraded from the bacteria using carbon as an energy source for growth and proliferation.
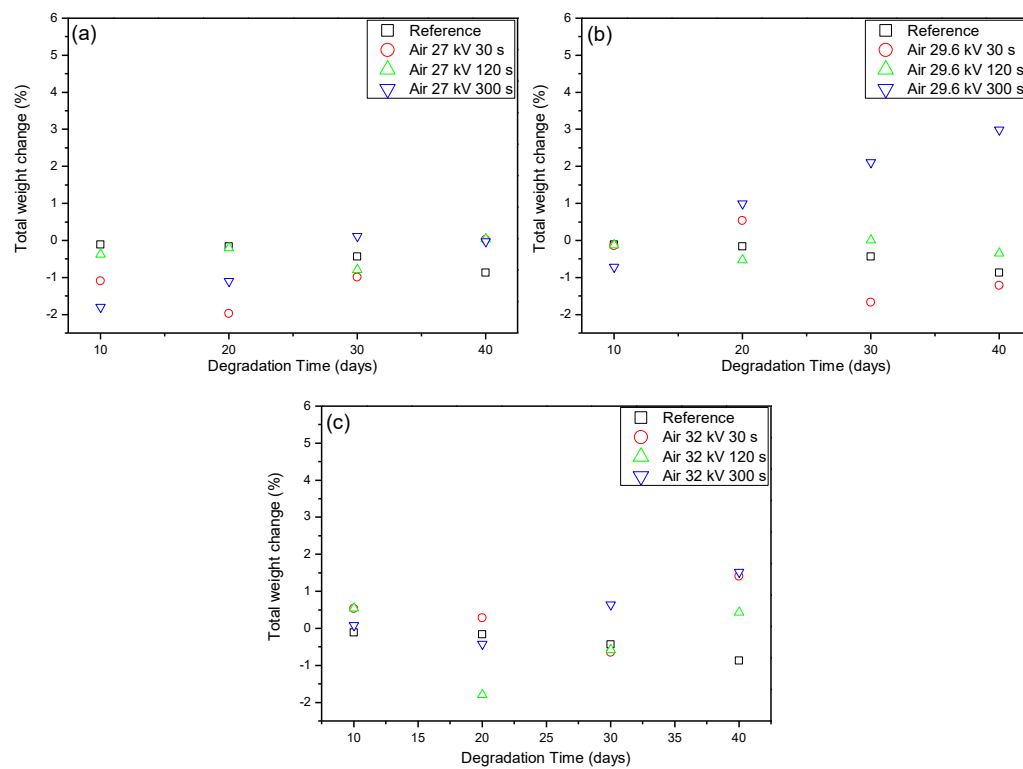
Figure 5.10: Percentage weight change of LDPE when introduced to the bacterial broth of *Ps. aeruginosa* for 10, 20, 30, and 40 days.
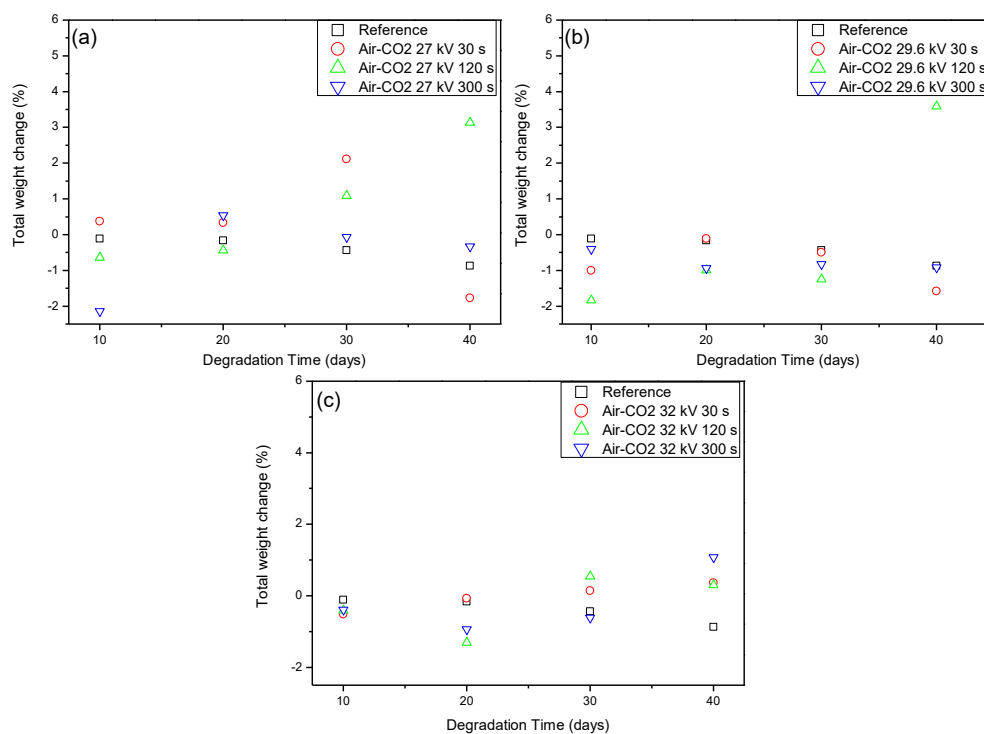
Figure 5.11: Percentage weight change of LDPE when introduced to the bacterial broth of *Ps. aeruginosa* for 10, 20, 30, and 40 days after being treated with plasma discharge containing ~3.8% CO_2 in ambient air.

Shown in Figure 5.12 is a reference sample of LDPE which was sterilised, but not introduced to the bacterial broth for degradation, as well as degraded reference samples that were introduced to the bacterial broth medium without any plasma treatment. This shows the bonds that are of interest for our study and how they are important to measure in order to determine the changes in the carbon groups of the polymer as a function of degradation time. If there are decreases seen from these measurements, then this can be taken as a better sign of biodegradation compared to the weighing of the samples. Figure 5.12 sets the baseline of how much degradation

may occur without any extra treatments and sets the standard for degradation after plasma treatment and whether or not it can be increased.
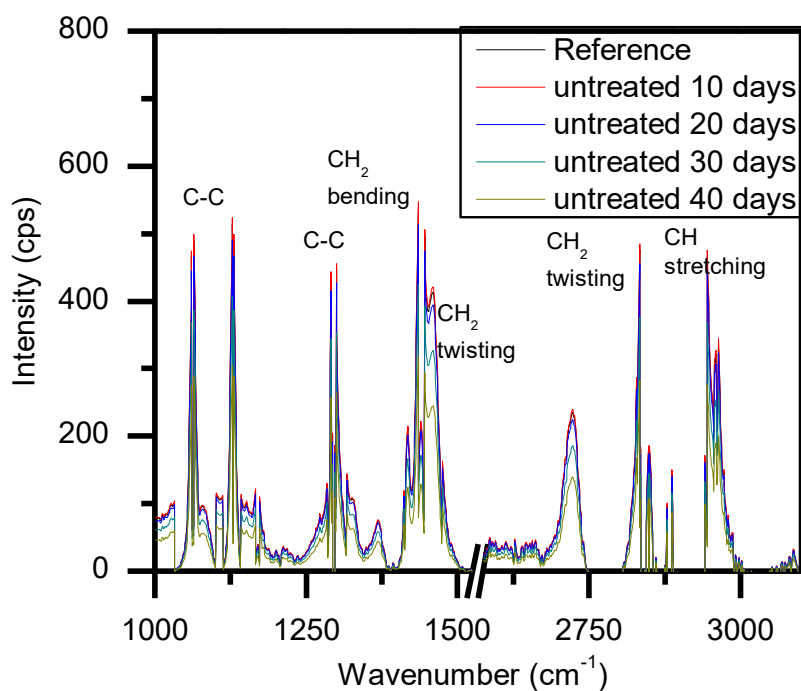
Figure 5.12: Representation of the typical Raman spectra of LDPE and the affiliated carbon bonds to help determine degradation of the samples.

After taking the measurements of all samples with the Raman spectrometer, the reason as to why there were sporadic changes in the weight of treated samples was found. When carrying out the Raman measurements, there was a noticeable difference in the spectra. At either end there was a large curve that continued to skew the results. It was more dominant from 2250 cm^{-1} to 1000 cm^{-1} and can be seen in Figure 5.13 with the untreated sample added as a comparison. The reason for this deviation is fluorescence. Fluorescence can occur for many reasons and may be associated with a contaminated sample, but it can also be due to biological matter being on a sample. Given the use of bacterial cells for degradation of the LDPE samples, and with their

handling being the same as every other sample, it is safe to assume that the fluorescence seen in their spectra is due to the presence of organic matter that is residual of the bacterial cells. By taking this into account, it can be seen why the results from weighing the samples was so sporadic and created an unreliable method to determine the degradation of the samples. Given this, it could be determined that there is much better cell adhesion on the sample surface and thus agrees with previous assumptions and validates the use of plasma to optimise the grafting of bacterial cells to the LDPE samples as a step towards optimised biodegradation. The comparison of fluorescence seen in treated samples compared to the reference sample can be seen in Figure 5.13.
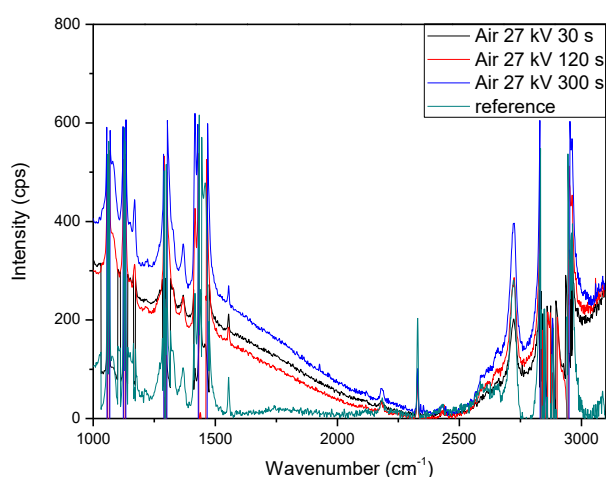
Figure 5.13: Comparison of treated samples to an untreated sample that have undergone 10 days degradation to show the presence of fluorescence due to organic matter adhesion on the sample surface after plasma treatment with ambient air.

After taking into consideration the presence of fluorescence in the treated LDPE samples to explain the weight gains seen in Figure 5.10 and 5.11, the ability to discern the degradation of the polymer samples comes down to the measurement of

the carbon bonds highlighted in Figure 5.12. It can be seen that there is an issue that occurs from the measured fluorescence, and that is an offset of each peak from which needs correction to properly identify the changes that may arise from degradation within the bacterial broth. A polynomial fit was applied to each spectra in order to subtract the best fit baseline in order to analyse the peaks presence for any changes that they may undergo. The full set of Raman measurements for ambient air plasma discharge can be seen in Figure 5.14 and the impact on biodegradation when ~3.8% CO_2 was introduced can be seen in Figure 5.15.

From the results obtained with Raman spectroscopy, it can be clearly seen that there is degradation occurring for each sample. This shows that, even though the weighing of the samples proved ineffective at determining the degradation of the LDPE samples due to the excess bacterial cells adhered onto the polymer surface, the use of Raman spectroscopy highlights the decrease in the carbon bonds of the polymer strips. This shows that with plasma treatment, there is a mixture of good cell grafting onto the samples surface without negatively impacting the degradation of the samples. From Figure 5.14, the change in treatment time allows for higher biodegradation, as does an increase in voltage. However, there is also a beneficial impact on the biodegradation of LDPE when treating the polymer with a working gas containing CO_2, as the samples treated with ~3.8% CO_2 in ambient air showed slightly more biodegradation compared to the sampled treated with solely ambient air. Interestingly, it seems that there is a selectivity in which carbon bonds the bacteria breakdown. This is put forward as the peaks associated with carbon bonds do not seem to decrease at the same rate. There is some proportionality to these changes, but the bacteria may breakdown and process more loosely bound and weaker bonds first, which could give rise to a slightly uneven degradation process across the sample.
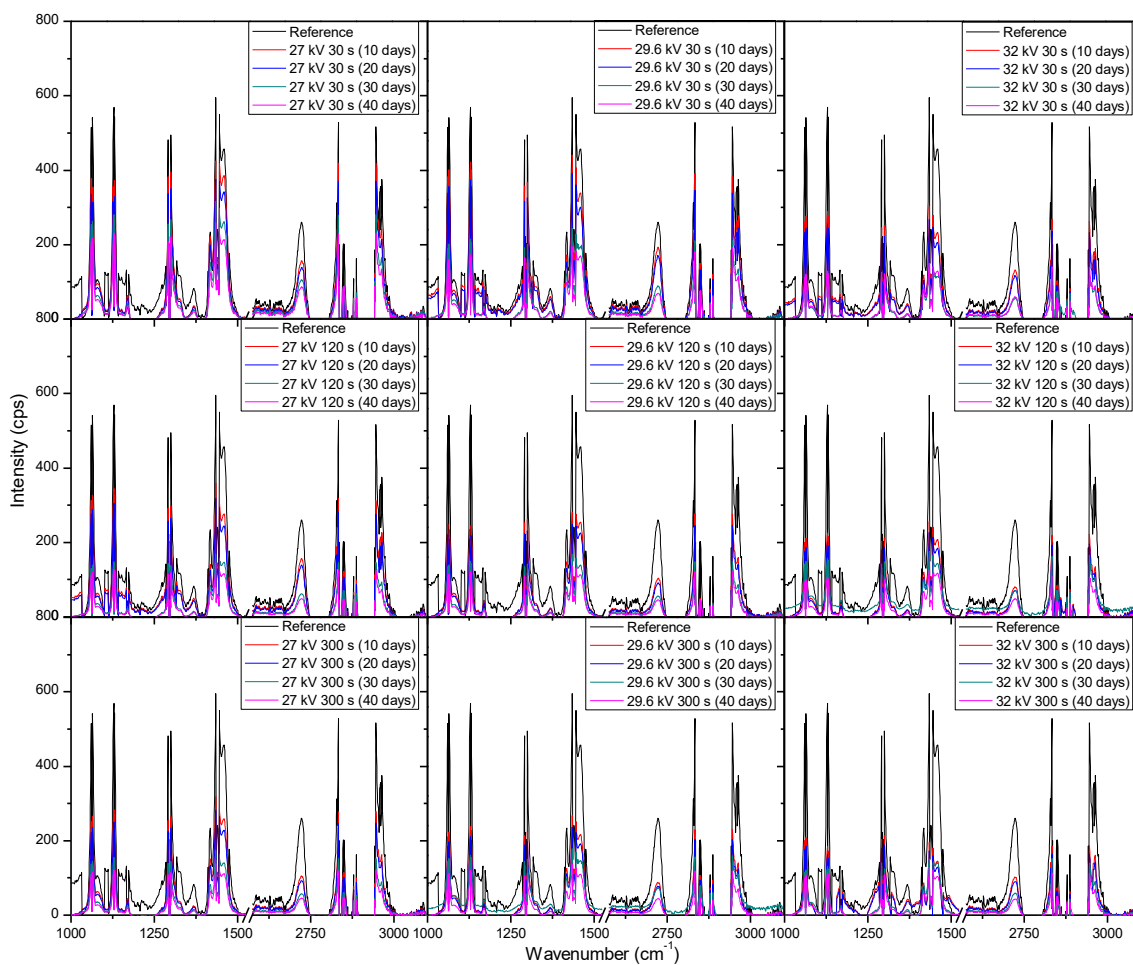
Figure 5.14: Raman spectroscopy measurements of plasma treated LDPE after their introduction into the bacterial broth to obtain biodegradation. The operating gas for plasma discharge was ambient air.
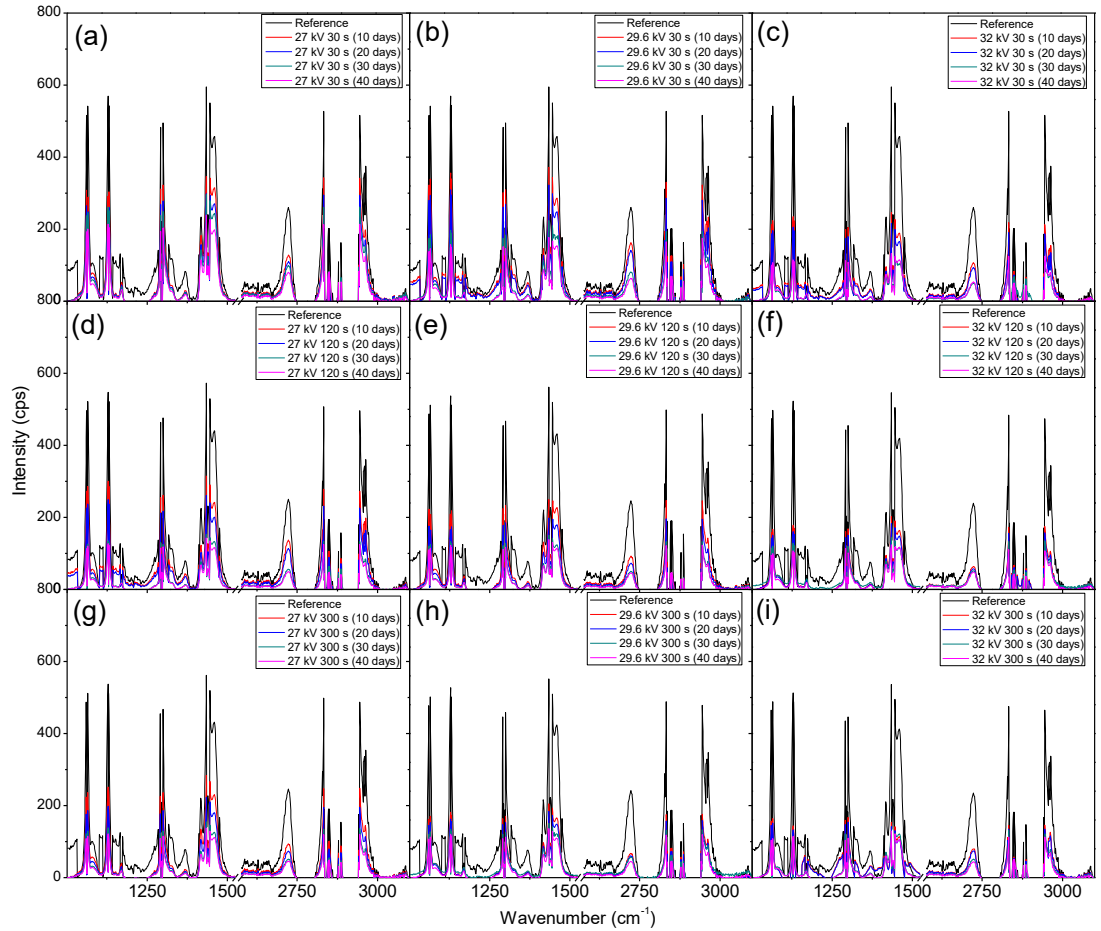
Figure 5.15: Raman spectroscopy measurements of LDPE after their introduction into the bacterial broth to obtain biodegradation to determine the impact ~3.8% CO_2 would have in the plasma discharge.

5.4. Conclusion

It has been found that the use of NTP discharge for the treatment of LDPE strips leads to an increase of its biodegradation in a bacterial broth media containing *Ps. aeruginosa*. The premise of this experiment was to try and optimise a treatment procedure in which biodegradation can be increased. It is well known that NTP discharges in ambient air can generate multiple oxygen containing particles and that these can alter the surface of a sample to have it become more polar. From this, the addition of a slight amount of CO_2 would increase the amount of oxygen containing particles to further the amount of polar functional groups that may form on a treated samples surface. From the results obtained via OES and OAS, this was found to be the case with an increase in O I, OH, and O_3 being obtained when the ambient air contained ~4% CO_2. From this, and comparing the results from the Raman measurements, it was found that this increase in oxidative species in the discharge and polar groups on the sample surface leads to an increase in biodegradation compared to an untreated sample for all treated samples. However, the introduction of CO_2 increased the biodegradation further compared to solely ambient air plasma discharge treated samples which highlights the importance of optical diagnostics in determining the gas chemistry to optimise the application of NTP systems to various areas.

References

A. C. Albertsson, "The Shape of the Biodegradation Curve for Low and High Density Polyethylene in Prolonged Series of Experiments", Eur. Polym. J., 1980, 16, 623–630.

A. L. Andrady, M. A. Neal, "Applications and Societal Benefits of Plastics", Philos. Trans. R. Soc. B. 2009, 364, 1977-1984.

M. Bhatia, A. Girdhar, A. Tiwari, and A. Nayarisseri, "Implications of a Novel Pseudomonas Species on Low Density Polyethylene Biodegradation: An in vitro to in silico Approach", SpringerPlus, 2014, 1, 497.

E, Bodros, I. Pillin, N. Montrelay, C. Baley, "Could Biopolymers Reinforced by Randomly Scattered Flax Fiber be Used in Structural Applications", Compos. Sci. Technol., 2007, 67, 462–470.

I. Cacciari, P. Quatrini, G. Zirletta, E. Mincione, V. Vinciguerra, P. Lupattelli, G. Giovannozzi Sermanni, "Isotactic Polypropylene Biodegradation by a Microbial Community: Physicochemical Characterization of Metabolites Produced", J. of Appl. and Environ. Micro., 1993, 59, 3695–3700.

E. A. Campo and R. U. Halden, "Plastics and Environmental Health: The Road Ahead", Reviews on Environmental Health, **28**, (2013).

F. Cappitelli, C. Sorlini, "Microorganisms Attack Synthetic Polymers in Items Representing Our Cultural Heritage", Appl. Environ. Microbiol., 2008, 74, 564-569.

T. Desmet, R. Morent, N. De Geyter, C. Leys, E. Schacht, and P. Dubruel, "Nonthermal Plasma Technology as a Versatile Strategy for Polymeric Biomaterials Surface Modification: A Review", Biomacromolecules, 2009, 9, 2351–2378.

D. Dobslaw, A. Schulz, S. Helbich, C. Dobslaw, and K. H. Engesser, "VOC Removal and Odor Abatement by a Low-Cost Plasma Enhanced Biotrickling Filter Process", Journal of Environmental Chemical Engineering, **6**, (2017).

A. Esmaeili, A. A. Pourbabaee, H. A. Alikhani, F. Shabani, E. Esmaeili, "Biodegradation of Low-Density Polyethylene (LDPE) by Mixed Culture of Lysinibacillus xylanilyticus and Aspergillus niger in Soil", PLoS ONE, 2013, 8, e71720.

A. Fatimah, "Biodegradation of Synthetic and Natural Plastic by Microorganisms", J. of Appl. & Environ. Microbiol., 2017, 5, 8-19.

A. Gajendiran, S. Krishnamoorthy, J. Abraham, "Microbial Degradation of Low-Density Polyethylene (LDPE) by Aspergillus Clavatus Strain JASKI from Landfill Soil", Biotech, 2016, 6.

N. S. Geweely, S. A. Ouf, "Enhancement of Fungal Degradation of Starch Based Plastic Polymer by Laser-Induced Plasma", African J. of Microbiol. Research, 2011, 5, 3273-3281.

R. Geyer, J. R. Jambeck, K. L. Law, "Production, Use, and Fate of All Plastics Ever Made", Sci. Adv., 2017, 3, e1700782,

M. Haward, "Plastic Pollution of the World's Seas and Oceans as a Contemporary Challenge in Ocean Governance", Nat. Comm., 2018, 9, 667.

N. Hiraishi, J. Y. Yau, R. J. Loushine, S. R. Armstrong, R. N. Weller, N. M. King, D. H. Pashley, F. R. Tay, "Susceptibility of a Polycaprolactone-Based Root Canal-Filling Material to Degradation. III. Turbidimetric Evaluation of Enzymatic Hydrolysis", J. of Endodontics., 2007, 33, 952-956.

J. R. Jambeck, R. Geyer, C. Wilcox, T. R. Siegler, M. Perryman, A. Andrady, R. Narayan, K. L. Law, "Plastic Waste Inputs from Land into the Ocean", Science, 2015, 347, 768–771.

B. M. Kyaw, R. Champakalakshmi, M. K. Sakharkar, C. S. Lim, K. R. Sakharkar, "Biodegradation of Low Density Polythene (LDPE) by Pseudomonas Species", Indian J. Microbiol., 2012, 52, 411-419.

L. Lebreton, B. Slat, F. Ferrari, B. Sainte-Rose, J. Aitken, R. Marthouse, S. Hajbane, S. Cunsolo, A. Schwarz, A. Levivier, K. Noble, P. Debeljak, H. Maral, R. Shoeneich-Argent, R. Brambini, J.; Reisser, "Evidence that The Great

Pacific Garbage Patch is Rapidly Accumulating Plastic", Scien. Rep. 2018, 8, 4666.

J. Li-Na, "Study on Preparation Process and Properties of Polyethylene Terephthalate (PET)", Appl. Mech. And Mater., 2013, 312, 406-410.

I. C. McNeill, L. Memetea, W. J. Cole, "Study of the Products of PVC Thermal Degradation", Polym. Degrad. And Stability. 1995, 49, 181-191.

J. C. Middleton, A. J. Tipton, "Synthetic Biodegradable Polymers as Orthopedic Devices", Biomaterials, 2000, 21, 2335-2346.

Milosavljevi´c, V.; Cullen, P.J. Spectroscopic Investigation of a Dielectric Barrier Discharge in Modified Atmosphere Packaging", European Physics: Journal of Applied Physics, **80**, (2017).

V. Milosavljević, M. Donegan, P. Cullen, D. Dowling, "Diagnostics of an O2-He RF Atmospheric Plasma Discharge by Spectral Emission", J. of the Physical Soc. of Japan, 2014, 83, 014501.

E. J. North, R. U. Halden, "Plastics and Environmental Health: The Road Ahead", Rev. Environ. Health 2013, 28, 1-8.

S. Ochi, "Durability of Starch Based Biodegradable Plastics Reinforced with Manila Hemp Fibres", Materials, 2011, 4, 457-468.

M. R. Prausnitz, " Microneedles for Transdermal Drug Delivery", Adv. Drug Deliver. Rev. 2004, 56, 581-587.

J. M. Restrepo-Flórez, A. Bassi, M. R. Thompson, "Microbial Degradation and Deterioration of Polyethylene – A Review", Int. Biodeterioration & Biodegradation, 2014, 88, 83-90.

M. C. Rillig, "Microplastic in Terrestrial Ecosystems and the Soil?", Environ. Sci. Technol., 2012, 46, 6453–6454.

C. M. Rochman, A. Tahir, S.L. Williams, D. V. Baxa, R. Lam, J. T. Miller, F. C. Teh, S. Werorilangi, S. J. Teh, 2Anthropogenic Debris in Seafood: Plastic Debris and Fibers from Textiles in Fish and Bivalves Sold for Human Consumption2, Scien. Rep. 2015, 5, 14340.

Z. Runye, K. Christian, C. Zhuowei, L. Lichao, Y. Jianming, and C. Jianming, "Styrene Removal in a Biotrickling Filter and a Combined UV–Biotrickling Filter: Steady- and Transient-State Performance and Microbial Analysis", Chemical Engineering Journal, **275**, (2015).

L. Scally, J. Lalor, P. J. Cullen, and V. Milosavljevic, "Impact of Atmospheric Pressure Nonequilibrium Plasma Discharge on Polymer Surface Metrology", Journal of Vacuum Science and Technology A, **3**, (2017).

L. Scally, J. Lalor, M. Gulan, P. J. Cullen, and V. Milosavljevic, "Spectroscopic Study of Excited Molecular Nitrogen Generation Due to Interactions of Metastable Noble Gas Atoms", Plasma Processes and Polymers, **15**, (2018).

M. Seggiani, P. Cinelli, E. Balestri, N. Mallegni, E. Stefanelli, A. Rossi, C. Lardicci, A. Lazzeri, "Novel Sustainable Composites Based on

Poly(hydroxybutyrate-co-hydroxyvalerate) and Seagrass Beach-CAST Fibers: Performance and Degradability in Marine Environments", Materials, 2018, 11, 772.

A. A. Shah, F. Hasan, A. Hameed, S. Ahmed, "Biological Degradation of Plastics: A Comprehensive Review", Biotech. Adv. 2008, 26, 246-265.

A. Sivan, "New Perspectives in Plastic Biodegradation", Current Opinion in Biotech., 2011, 22, 442-426.

Y. Tokiwa, B. P. Calabia, C. U. Ugwu, S. Aiba, "Biodegradability of Plastics", Int. J. of Mole. Sci., 2009, 10, 3722–3742.

P. Tribedi, A. K. Sil, "Low-density Polyethylene Degradation by Pseudomonas sp. AKS2 Biofilm", Environ. Sci. Pollut. Res. Int., 2013, 20, 4146e4153.

N. Tsutsumi, Y. Kono, M. Oya, W. Sakai, M. Nagata, "Recent Development of Biodegradable Network Polyesters Obtained from Renewable Natural Resources", Clean Soil Air Water 2008, 36, 682–686.

S. Veerapandian, C. Leys, N. De Geyter, R. and Morent, "Abatement of VOCs Using Packed Bed Non-Thermal Plasma Reactors: A Review", Catalysts, 2017, 12, 113.

C. Wang, J. Y. Xi, H. Y. Hu, and Y. Yao, "Advantages of Combined UV Photodegradation and Biofiltration Processes to Treat Gaseous Chlorobenzene", Journal of Hazardous Materials, **171**, (2009).

Z. S. Wei, H. Q. Li, J. C. He, Q. H. Ye, Q. R.; Huang, and Y. W. Luo, "Removal of dimethyl sulfide by the combination of non-thermal plasma and biological process", Bioresource Technol., 2013, 146, 451–456.

S. Yoshida, K. Hiraga, T. Takehana, I. Taniguchi, H. Yamaji, Y. Maeda, K. Toyohara, K. Miyamoto, Y. Kimura, K. Oda, "A Bacterium that Degrades and Assimilates Poly(ethylene terephthalate)", Science, 2016, 351, 1196-1199.

P. Zeng, J. Li, D. Liao, X. Tu, M. Xu, and G. Sun, "Performance of a Combined System of Biotrickling Filter and Photocatalytic Reactor in Treating Waste Gases from a Paint Manufacturing Plant", Environmental Technology, **2**, (2015).

Chapter 6 - Diagnostics and Efficacy of a Large Gap Pin-to-Plate Atmospheric Plasma Source for the Treatment of Human Cancer Cell Lines

To be submitted in its entirety for publication

Laurence Scally[1,2], Sean Behan[1*], Andressa Carvalho[1*], Chaitanya Sarngapani[1*], Brijesh Tiwari[4], Renee Malone[1], Hugh J. Byrne[5], James Curtin[1], and Patrick J. Cullen[1,2,6]

Abstract

A novel, large gap pin-to-plate, non-thermal plasma system is shown to exhibit distinct characteristics for fine-tuned gas chemistry control and the ability to treat human cancer cell lines. By implementing optical emission and optical absorption spectroscopy, it has been found that the pin-to-pate plasma system has an optimal discharge frequency of 1000 Hz in ambient air, generating a plasma chemistry containing reactive species such as OH, N_2, N_2^+, and O_3. It has also been shown that, by varying the plasma discharge frequency, the plasma chemistry can be tailored to contain up to 8.85 times higher levels of reactive oxygen species as well as a factor increase of up to 2.86 for levels of reactive nitrogen species. At higher frequencies, however, reactive oxygen species are more dominant than reactive nitrogen species which allows for a more dynamic and well controlled environment for sample treatment without modifying the atmospheric conditions present. When used for treatment of cell culture medium and cultures themselves, variation of the plasma discharge frequency over the range 1000-2500 Hz demonstrated a clear dependence of the responses on this plasma generation parameter, and highest cytotoxic responses for 1000 Hz.

6.1. Introduction

Studies of non-thermal plasma (NTP) have shown that they can be utilised for a very wide range of applications, including; food preservation, wound sterilisation, enhanced crop growth, pollution abatement, volatile organic compound (VOC) removal, polymer functionalisation, and water purification (Thirumdas et al. 2015, Cui et al. 2019, Mahyar et al. 2019, Nageswaran et al. 2019, Tschang et al. 2019). Such a broad variability of applications is due to the large range of gas chemistries that can be generated using NTP systems. By using ambient air, reactive oxygen species (ROS) and reactive nitrogen species (RNS) can be generated to interact with target samples. Examples of ROS include O, O_2^*, O_3, OH, and NO, examples of RNS being N, N_2^*, N_2^+, and N_xO_y. These reactive species can interact with synthetic and/or biological samples and, when the plasma conditions are appropriately tailored, can cause alterations within cells that can lead to cancer cell death (Lin et al. 2019). The plasma chemistry can be altered by introducing different gases into the system environment at varying percentages and ratios. For example, adding a small percentage of CO_2 into a system that is running predominantly on ambient air can lead to higher levels of O_3 formation, which can be further optimised with the introduction of other secondary gases such as Ar (Moss et al. 2017, Scally et al. 2018a, Xu et al. 2018). Introducing inert gases such as Ar and He gives rise to the production of inert excited species that can bombard and interact with sample surfaces and give rise to more binding sites or can aid in the formation of other reactive species, such as OH and N_2^*, through synergistic energy transfers (Scally et al. 2018b).

An emerging research focus in the applications of plasma science is the treatment of cancer cells to create better alternatives to conventional therapeutic approaches (Yan et al. 2017). Interest in the use of NTP sources for cancer treatment

has arisen due to their ease of use, the potential for minimising treatment side effects, and reducing damage to healthy cells by more specifically targeting cancerous cells. This potential comes from the versatile chemistry produced by NTP discharges. Numerous *in vitro* studies have shown that cytotoxicity can be induced through the generation of ROS, causing a disruption of various cell functions (Dubuc et al. 2018, Yan et al. 2018). Claims as to which reactive species are responsible for cancer cell death identify H_2O_2, OH, O_2^-, O_3 and NO_x as important candidates (Dubuc et al. 2018, Yan et al. 2018). There are a host of possible chemical reactions and pathways that occur within plasma discharges and the sample boundaries to which they are exposed, but some samples are more resilient to particular reactive species, while being susceptible to others. Specific assays can be carried out to determine which species and reaction pathways are most likely to induce cytotoxicity in cancer cells. Through different comparative methods, studies have shown that the presence of ROS, such as peroxides and superoxides, causes intracellular stress to a greater extent than RNS, for *in vitro* treatments of various human cell lines, including glioblastomas, brain, lung, blood, cervical, melanoma, and breast cancer (Kurake et al. 2016, Dubuc et al. 2018). The use of NTP discharges can be employed to disrupt the growth of various cancer cells, with lower cytotoxic impact on normal host cells, due to preferential ROS interactions that can initiate cell cycle disruption and apoptosis in cancerous cells (Babington et al. 2015, He et al. 2018).

Given that the gas chemistry interactions of the plasma discharge are the most important factors in plasma processing techniques, there are many variables that need to be considered in order to optimise NTP systems for specific applications. Some factors include voltage, resonant frequency, discharge frequency, duty cycle, discharge gap, electrode geometry, and dielectric material selection. It is well known

that varied input power to a system (voltage, current, and pulse) gives rise to more intense, and possibly differing modes of, plasma discharges (Rajasekaran et al. 2010). Recently, focus on electrode designs has allowed NTP systems to become much more versatile, efficient, and to create more homogeneous discharges for more equal surface interactions (Takaki et al. 2004, Johnson et al. 2015, Edelblute et al. 2016, Malik et al. 2016, Brandenburg et al. 2017). One of the designs that has been developed and investigated is pin-to-plate based electrodes. By creating an array of pins that are connected to a high voltage source and allowing a plate electrode to act as the ground, a stable and efficient plasma can be achieved (Zhang et al. 2014). The efficiency can be seen in the relatively lower values of power consumption compared to purely plate-to-plate dielectric barrier discharge systems, resulting in a more diffusive nature of the discharge over sample surfaces (Liu et al. 2013, Zhang et al. 2014). Utilising pin type electrodes can enable finer control over the distribution of the electric field, which leads to a focusing effect that produces a more energetic and dense plasma. This can then result in a higher number of streamer channels which form higher levels of reactive species due to higher gas collision and excitation rates. It has also been shown that each pin within such pin-to-plate systems creates a diffusive discharge that has an area much larger than the area of the pin tip (Zhang et al. 2014). These qualities create an environment that allows for more interactions between reactive species and samples being treated, thus enabling better coverage of sample surface areas, speeding up treatment processes, and aiding in larger scale plasma discharges to be generated.

In this work, a novel pin-to-plate NTP system is characterised, and the dependence of its efficacy for cell death on plasma generation conditions is demonstrated in a human cancer cell line. In order to gain more insights into the interactions of non-thermal plasma discharges and how they create an environment

conducive to higher levels of reaction mechanisms, the plasma discharge is initially characterised and optimised by a combination of optical absorption spectroscopy (OAS) and optical emission spectroscopy (OES). The effect of the plasma discharge conditions on the generation of reactive species in cell culture medium is then investigated. Finally, it is demonstrated that optimised plasma discharge conditions can lead to enhanced cell death rates in human cancer cells, in vitro.

6.2. Materials and Methods

6.2.1 System Configuration

A large gap pin-to-plate electrode was employed, which facilitated the insertion of well plates into the plasma discharge. The 88-pin stainless steel electrode was supplied by PlasmaLeap Technologies (Dublin, Ireland). In order to create a plasma discharge that is as homogeneous as possible throughout the discharge volume, the pins are arranged in a slightly convex manner. This is done by varying the length of the pins on the high voltage plate such that they are gradually set closer to the ground plate from the edge of the pin array to the centre, leaving the central pins the closest to the ground plate. By using this geometry, the electric field is distributed so as to minimise the losses at the edge and corners of the high voltage plate. The electrode configuration was powered by an AC supply (Leap100, PlasmaLeap Technologies, Dublin, Ireland). The design facilitated the control of resonance frequency (30-125 kHz), discharge frequency (50 – 3000 Hz), power (50 – 400 W), with a discharge gap of a maximum of 55 mm. For this study, the duty cycle was set at 54, 72, or 90 µs. The resonant frequency was set at 55.51 kHz, and the discharge frequency was varied in the range 100 – 2500 Hz. The discharge gap was kept at 40 mm, the samples prepped for

treatment being placed in the centre of the system on the ground plate. Figure 6.1 shows how the system was set up for sample treatment.
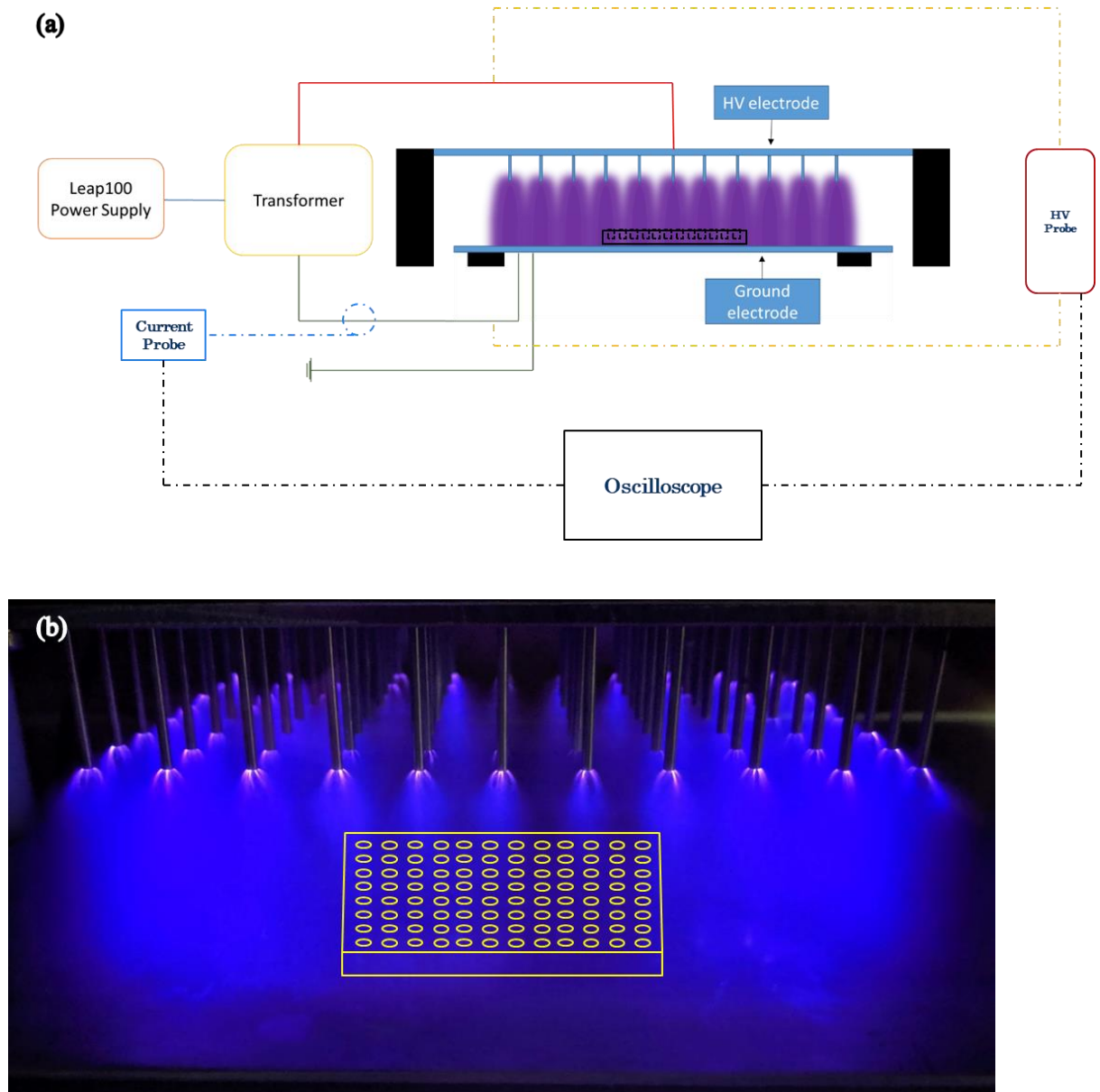
Figure 6.1: (a) Schematic of the Leap100 system setup used to carry out the experiments of this work with a simple 96 well plate placed to coincide with the sample placements (b) Schematic showing plasma discharge throughout the system volume and how the placement of treatment samples into the device

6.2.2 Electrical Characterisation

The electrical characterisation of the system was performed by connecting a passive probe (CP6990-NA Cal Test Electronics, Yorba Linda, CA, USA) to the ground wire in order to measure the current and by having a high voltage probe (VD-100 North Star, Bainbridge Island, WA, USA) connected in parallel to the high voltage and ground plate to measure the applied voltage. By measuring the output voltage and current from the transformer, the power needed to generate the plasma discharge can be measured and maintained for continuous use and better repeatability. Current measurements can also be used to ascertain the behaviour of the plasma discharge as the fluctuation in current represents changes in electron energetics.

6.2.3 Optical Diagnostics

6.2.3.1 OES

In order to determine the gas chemistry of the plasma discharge and the interactions that may occur at the sample boundary of the cell culture media during treatment, OES and OAS were used to monitor and characterise the reactive species formed in the discharge. Both of these measurement techniques were carried out by using an Edmund Optics CCD spectrometer that has a wavelength range of 200 – 850 nm. To record the spectra during the measurement processes, for both OES and OAS, the software BWSpec^{TM} was used. The spectral resolution for this particular spectrometer is between 0.6 and 1.8 nm and is wavelength dependent. Due to the limited spectral resolution, there may be overlap of emission lines of certain species, which leads to a need for a deconvolution process. However, in this study, the spectral lines that are studied are separated by large enough ranges that the peaks of interest have no overlap with those of other emissive species. OES measurements were carried out at 15 points

on the NTP system used in this study. The first point was set at a (0, 0) coordinate at the ground plate, below where the first row of pins began, and the subsequent points were set at 4 cm intervals up to 16 cm to the right of the initial position. These were set at 2 cm and 4 cm above the ground plate to give a full spatial interpretation of the plasma discharge. The acquisition of each spectrum was carried out with an integration time of 2000 ms and the time between each spectrum was 5.5 s. In order to carry out these measurements, a fibre optic cable was used that had an adjustable lens attached to the end and was directed perpendicular to the system. The species that were detected with OES were OH at 300 nm, N_2 from the second positive system (SPS) from 315-380 nm, and N_2^+ from the first negative system (FNS) at 391 nm. After finishing the OES measurements, the spectra were analysed by integrating the area under each peak of interest to calculate the value of the total intensity, in arbitrary units.

From the OES data obtained, a line ratio method was used to determine the distribution of electron energies within the discharge (Scally et al. 2018b). Given that the spectrometer used gives the intensity results in arbitrary units, the method employed only gives an indication as to whether there is a higher density of low or high energy electrons. From this, the most probable reaction mechanisms and how certain species are formed can be asserted. By using the total emission intensity of N_2 at 337 nm and the total emission intensity of N_2^+ at 391 nm, the line ratio shown in equation 1 can be used. It has been demonstrated in other works that the dominant route for the excitation of these two species is from direct electron excitation (Naveed et al. 2006, Begum et al. 2013). The excitation energy of N_2 at 337 nm is 11.01 eV and the excitation for N_2^+ at 391 nm is 18.8 eV. From this, the line ratio gives a good indicator as to the electron energy distribution function (EEDF) and what energetics

can be expected within the plasma discharge with respect to the spatial and temporal evolution of the gas chemistry.

$$EEDF = \frac{I(337 \text{ nm})}{I(391 \, nm)} = \frac{I(N_2)}{I(N_2^+)} \qquad (1)$$

6.2.3.2 OAS

With regards to OAS measurements, there may be an overlap of different light absorbing reactive species, as there can be a large band of absorbed wavelengths with a resonant absorption wavelength. Of interest in this study was O_3, which has a strong absorbance in the UV-region of the spectrum. There are, however, other reactive species that may absorb in this region, such as NO_2. In order to determine whether or not there would be any influence and interference from this, Dräger tubes were used to detect whether there was any concentration of NO_2 after plasma discharge. From this, there was found to be no detectable amounts of NO_2 and the emission spectrum in Figure 6.4(d) shows no detectable amounts of NO that are typically found between 240 - 260nm. The gas chemistry that has been measured, and that is explained in greater detail in section 3, gives an insight into the reaction mechanisms giving rise to the generation of reactive species. On this basis, the evaluation of O_3 became the main objective of the OAS measurements.

In order to carry out the OAS measurement of the generated plasma, two fibre optic cables were used. Both had adjustable lenses to optimise the focal point of detection. They were placed perpendicular to one another at a distance of 25 cm and had a direct line-of-sight between them. One fibre optic cable was connected to a

deuterium-tungsten UV-Vis-NIR light source and the other to the CCD spectrometer to detect the incoming light. By referencing the incoming light from the plasma discharge, the average optical density of different absorbing species can be determined. The spectra were measured with an integration time of 550 ms at intervals of 1450 ms between each measurement. OAS measurements were analysed by using equation 2 to find the average spatial density of O_3 during the plasma discharge and post-discharge. In equation 2, $D(t)$ is the average spatial density (cm^{-3}), L is the optical path (cm), $I(0)$ is the reference intensity with no plasma discharge (A.U.), $I(t)$ is the measured intensity (A.U.) during and after plasma discharge, and $\sigma(\lambda)$ is the wavelength dependent absorption cross-section for the species of interest. For O_3, the wavelength of optimal absorption is taken as 253.7 nm which gives an absorption cross-section value of 1.154×10^{-17} cm^2 (Scally et al. 2018a)

$$D(t) = \frac{1}{\sigma(\lambda)L} ln \frac{I(0)}{I(t)} \tag{2}$$

6.2.4 Chemical Analysis of Reactive Species in cell culture medium

Nitrite concentrations in the plasma treated water and Dulbecco's modified eagle's cell culture medium (DMEM) samples were quantified by employing the Griess reagent (N-(1-naphthyl) ethylenediamine dihydrochloride) spectrophotometric method. This was accomplished by the addition of 100 μl sample, trichloroacetic acid and Griess reagent. The reaction mixture was incubated at 37 °C for 30 min, after which the absorbance was determined at a wavelength of 548 nm using a UV–visible spectrophotometer (Shimadzu UV-1800, Shimadzu Scientific Instruments Kyoto, Japan). A calibration curve was prepared using a standard solution of sodium nitrite. Nitrate concentrations were determined according to the procedure of Lu et al. (2017) Hydrogen peroxide concentrations were determined using the titanium oxysulfate

colorimetric method (Boehm et al. 2016). For this purpose, a total of 10 µl TiOSO$_4$ solution were added to 100 µl of treated samples. After 10 min incubation, absorbance was read on a spectrophotometric plate reader at a wavelength of 405 nm.

6.2.5 Cancer Cells Cytotoxicity

6.2.5.1 Cell Culture

Human glioblastoma multiform (U373MG-CD14) cells were obtained from Trinity College Dublin, Ireland. Human epithelial carcinoma (A431) cells were purchased from ATCC European Distributor (LGC Standards, Teddington, UK). Cells were cultivated with DMEM-F12 medium without pyruvate (Sigma-Aldrich, Arklow, Ireland) and supplied with 10% FBS (Sigma-Aldrich) and 1% penicillin/streptomycin (Sigma-Aldrich). U373MG cells were maintained in a humidified incubator containing 5% CO$_2$ at 37 °C.

6.2.5.2 Cell viability assay

U373MG cells were seeded at a density of 2 x 10^3 into 96 `U` shaped wells plates (Sarstedt, Ltd., Wexford, Ireland) and allowed to seed overnight. 80 µL of medium were removed before treatment, leaving 20 µL of medium in each well. In order to determine the optimal discharge frequency for sample treatments, the cytotoxic effects of the pin-to-plate device on U373MG human multiforme glioblastoma cells were measured at discharge frequencies of 1000, 2000, and 2500 Hz at 240 V and 72 µs. Plates were then treated with the pin-to-plate discharge at 7 different times (5, 10, 20, 40, 80, 160, 320 – (s)) using a duty cycle of 72 µs, 240v and frequency of 1000 Hz. Fresh medium was added to the wells after treatment and cells were then incubated at 37 ºC for 96h.

Cell viability was analysed using the Alamar Blue Cell Viability Reagent (Thermo Fisher, Dublin, Ireland), a resazurin-based solution that functions as a cell health indicator by using the reducing power of living cells to quantitatively measure viability. Cells were washed once with PBS and incubated for 3h at 37 °C with a 10% Alamar Blue solution. Fluorescence was measured using an excitation wavelength of 530 nm and an emission wavelength of 595 nm on a Varioskan Lux multi-plate reader (Thermo Fisher).

All experiments were performed at least three independent times with a minimum of 24 replicates per experiment. Cytotoxicity data was fitted to determine the Inhibitory Concentration (IC50) using a 4 parameter Hill equation of the form $f(x) = min + (max-min)/(1+(x/IC50)^n)$, where n is the Hill slope.

6.3 Results and Discussion

A combination of electrical and optical measurements were employed to identify the optimum operating parameters for the pin-to-plate discharge reactor. Following optimisation of the parameters, these were then used for the treatment of U373MG human glioblastoma multiforme cells.

### 6.3.1 Electrical Characterisation

Varying the voltage, duty cycle, and discharge frequency and measuring the changes in the actual current and voltage across the system in response to parameter changes gave insights into the dynamics that occur within the discharge. The resonant frequency was maintained at a value of 55.51 kHz.

The discharge frequency was initially varied to determine which frequency was optimal for generating a plasma discharge. Figure 6.2(a) shows that, between 100

– 300 Hz, the discharge voltage increases and reaches a plateau at 600 Hz, at which point it begins to steadily decline. Figure 6.2(b) highlights changes in the current measured with respect to the discharge frequency. Overall, the current decreases significantly, but has plateaux from 100 – 500 Hz and from 2000 – 2600 Hz. The effects observed can be explained by the interaction of the electric field and the impact it has on electron excitation and, therefore, plasma ignition. There are two main instabilities that occur and cause premature quenching of the plasma: One at low discharge frequencies and the other at higher discharge frequencies. When the discharge frequency is too low, electrons accumulate rapidly and cause the opposing electric field to increase too quickly and suppress that rise of the applied voltage. On the other hand, when the discharge frequency is too high, the electrons that are formed in the plasma bulk become trapped within the inner electrode space and are unable to reach the electrodes to form the opposing electric field. Both events prematurely quench the plasma discharge (Deng et al. 2004). Therefore, the discharge frequency must allow for high energetics to create a strong plasma discharge that has a higher level of electron kinetics, but not so much that they induce a self-quenching event. The optimum discharge frequency for this work was found to be 1000 Hz, which was further validated by the optical results.
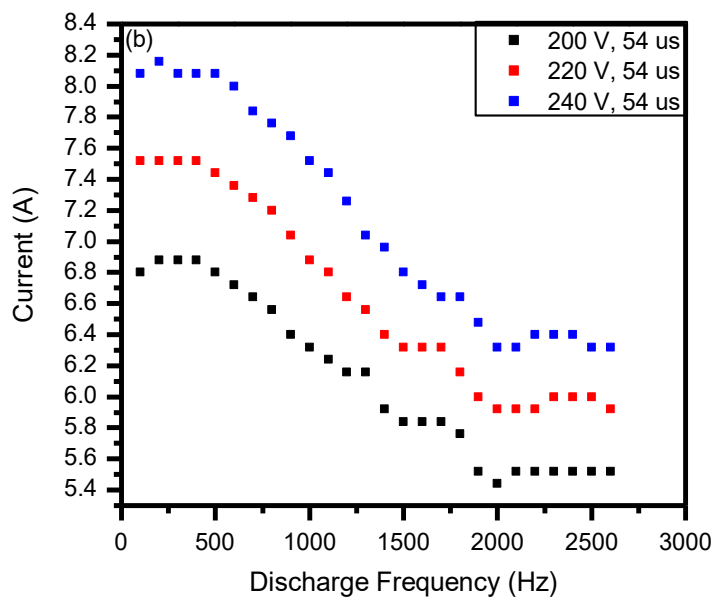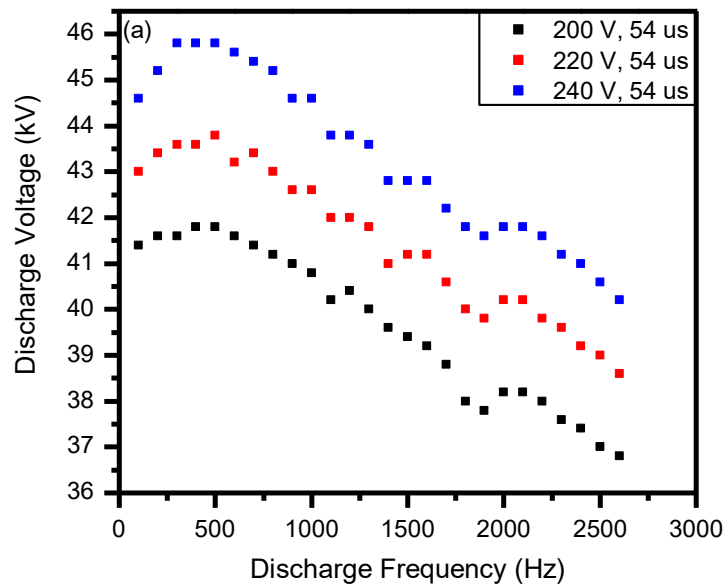
Figure 6.2: (a) the changes in discharge voltage with change in frequency and (b) the change in current with respect to discharge frequency. For each of these graphs, the duty cycle on the power unit display was kept at 54 μs and the voltage was set at 200, 220, and 240 V.
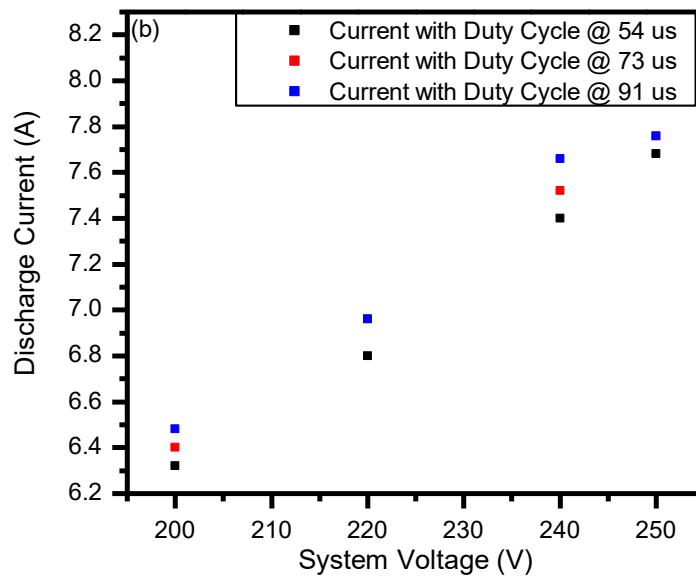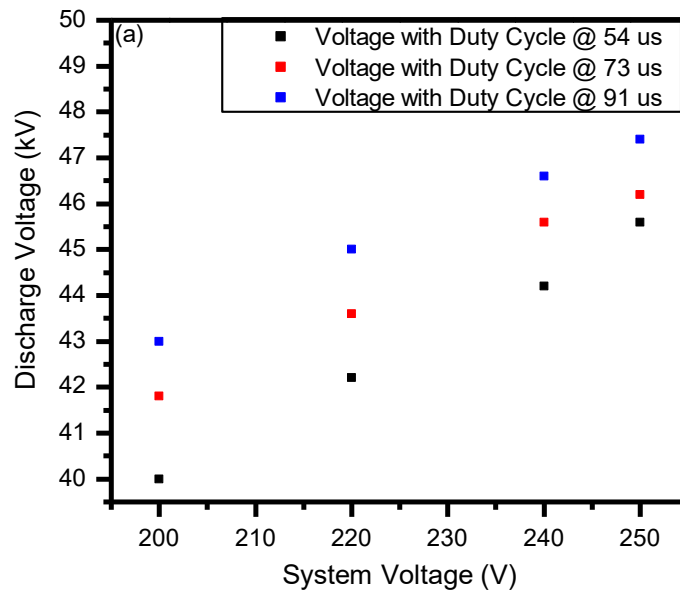
Figure 6.3: (a) changes in discharge voltage with variation in system voltage and duty cycle and (b) the change in current with variation in system voltage and duty cycle. For each of these graphs, the discharge frequency was kept at 1000 Hz.

6.3.2 Optical Diagnostics

6.3.2.1 Parameter Optimisation

OES and OAS were used to measure the formation of different reactive species over time as a function of voltage, duty cycle, and discharge frequency. As can be seen in Figure 6.4(a), the optimum discharge frequency for the formation of N_2 at 337 nm, and by association of the SPS group, given the similar excitation energies, is 1000 Hz. Although there are comparable levels detected at 1300 Hz, there is a larger fluctuation over the timescale of the measurement (1-70 sec). In Figure 6.4(b), it can be seen that the largest formation of N_2^+ occurs at the lower frequencies (600 and 800 Hz) and at 1300 Hz. The higher levels of N_2^+ detected at the lower frequencies is due to the higher energetics of the electrons. Although not quite self-quenching at this point, there is still an issue of initiating a large cascade event to form more reactive species, and so the kinetic transfer of energy through collisional means excites N_2 to N_2^+. This is evident when noting that low levels of excited N_2 at 337 nm are seen at these lower frequencies. However, there is a relatively large amount of N_2^+ generated at 1000 Hz. Given that there is a higher and consistent level of N_2 from 337 nm (and the SPS) at 1000 Hz and a relatively high level of N_2^+ formed at the same discharge frequency, it seems optimal to use this value for cellular treatments.
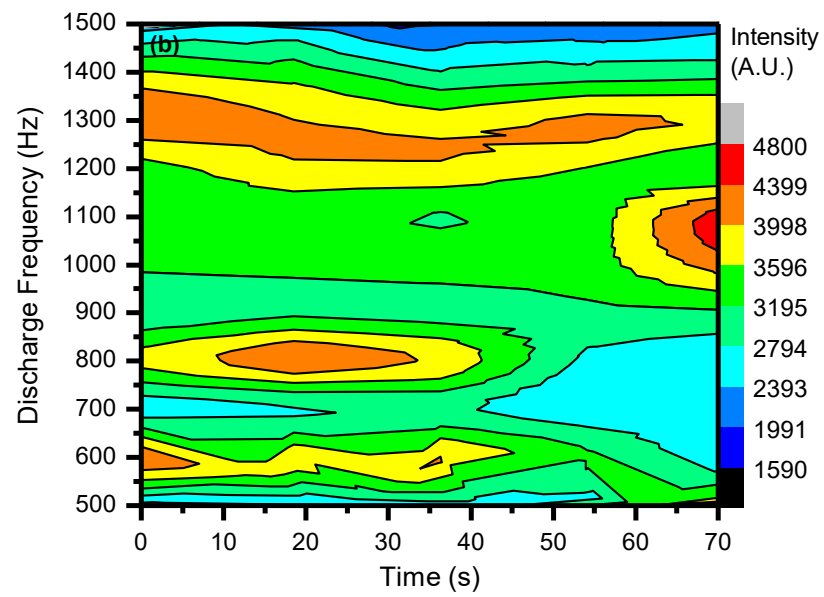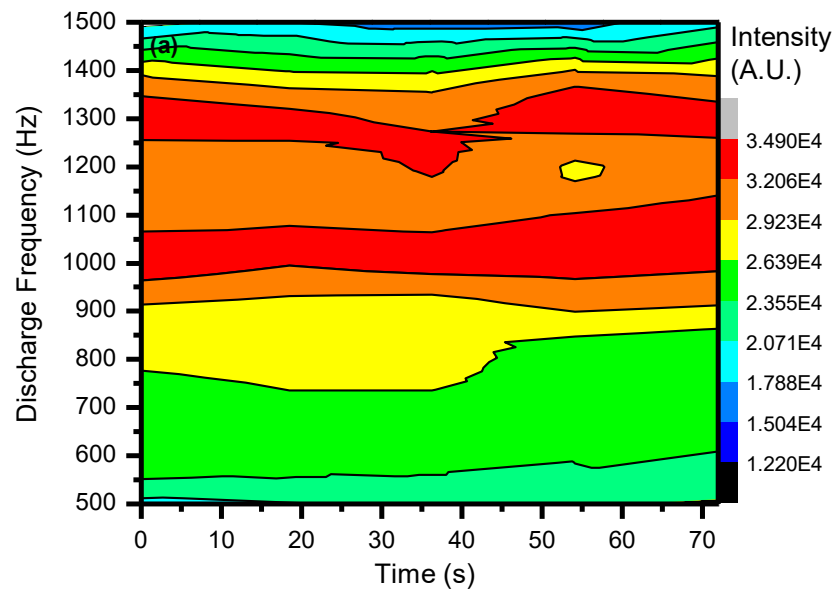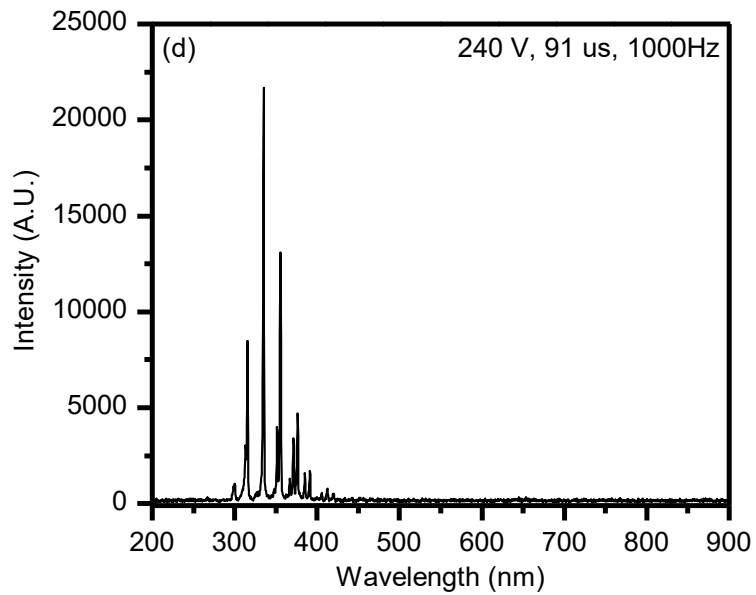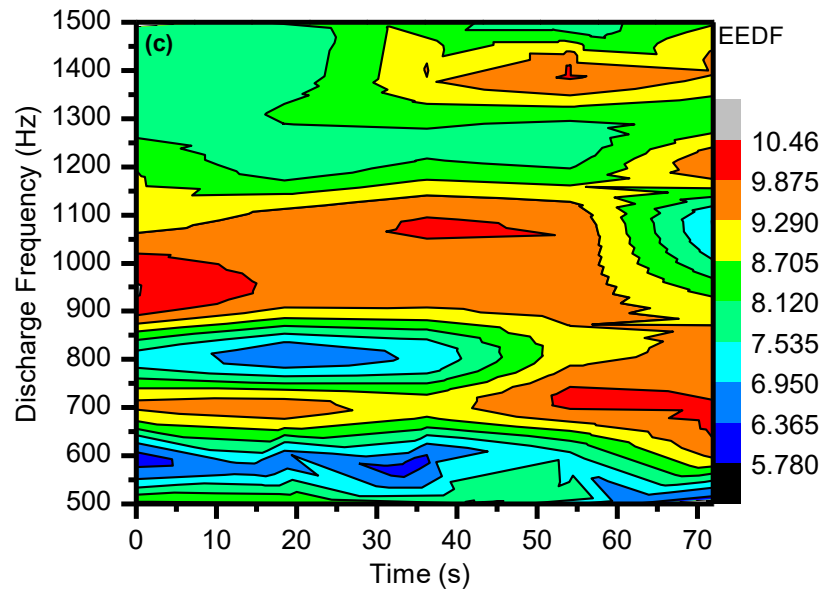
Figure 6.4: Changes seen in (a) N_2-337 nm (b) N_2^+-391 nm and (c) the EEDF calculated from the line ration of (337 nm/391 nm) (d) single spectrum of all detected emission species.
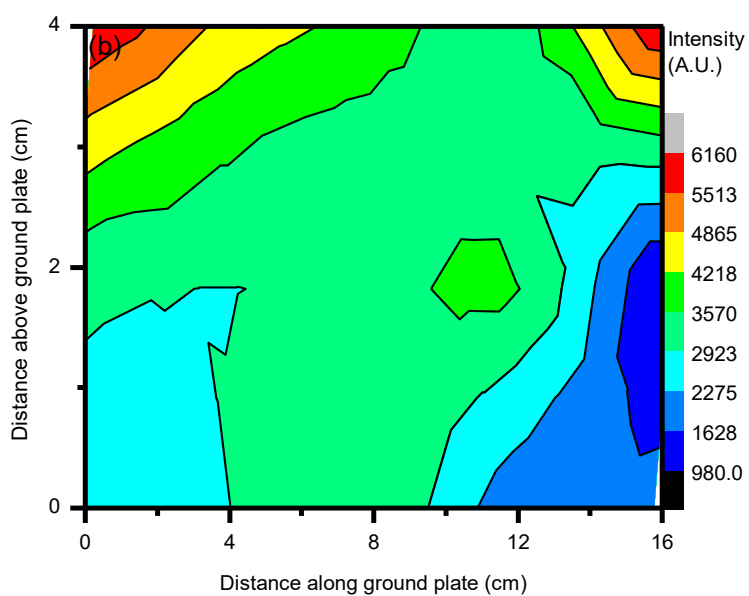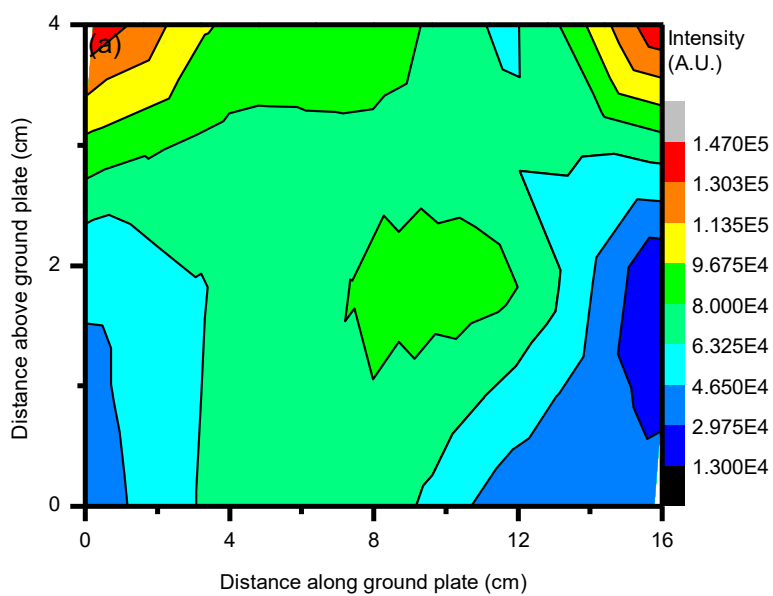
OAS data can be employed to support the evidence that 1000 Hz is the optimum discharge frequency. As can be seen in Figure 6.5, the average spatial density of O_3 increases with the plasma discharge time. It is also observed that the lifetime of O_3 is considerable and there is a substantial density left within the discharge zone when the plasma discharge has ceased. This allows for the option of leaving samples within the system for a period post discharge. Although there is a range of frequencies within which the highest amount of O_3 is formed, the optimum is again suggested to be 1000 Hz, as this allows for an equally high generation of N_2 and N_2^+.
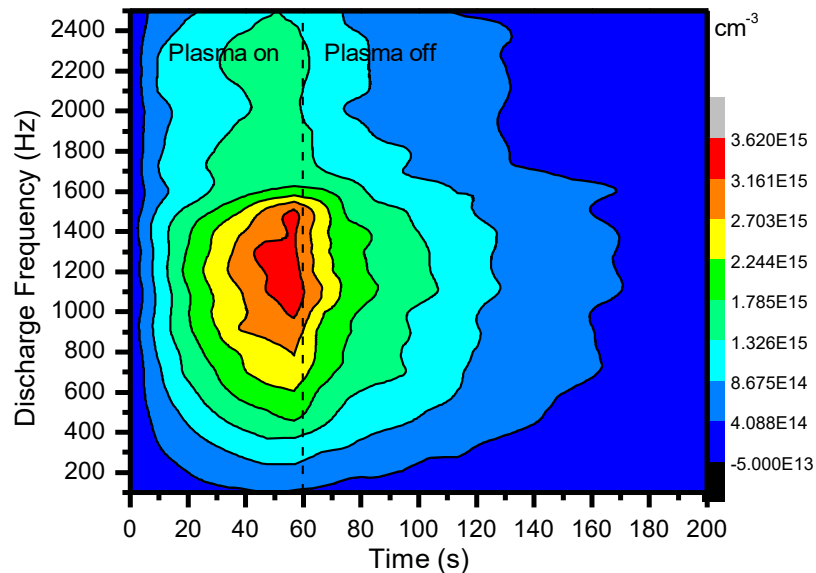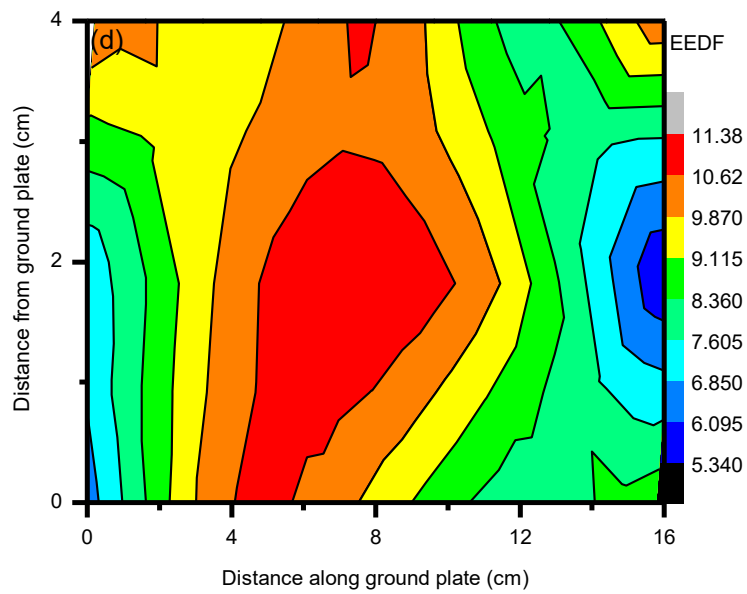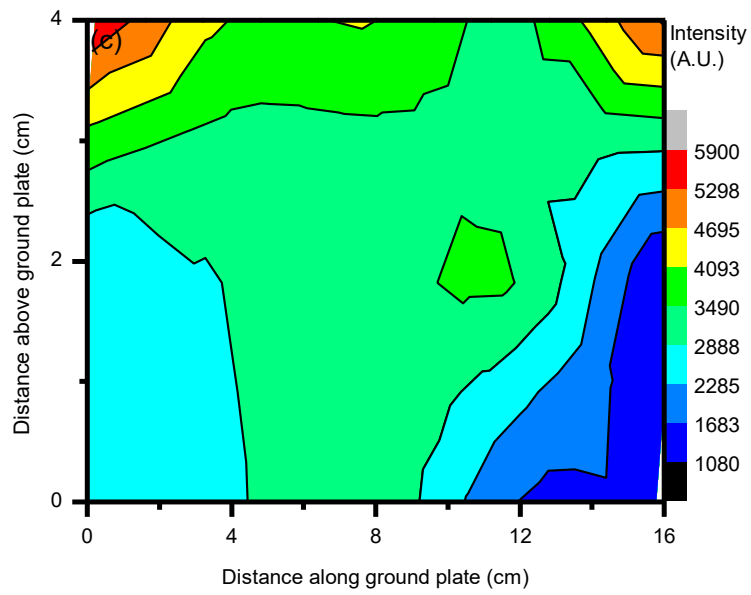

Figure 6.5: The variation of the average spatial density of O_3 with respect to the discharge frequency and temporal evolution. The plasma discharge was set to run for 60 s and the total measurement time was 200 s. This was to allow for measurement of O_3 during and post-discharge.

6.3.2.2 Spatial Characterisation

The spatial evolution of the total intensity of N_2 from the SPS is shown in Figure 6.6(a). This was measured by investigating each peak found in this group, being 315, 337, 357, and 380 nm. Each was found to follow the same trend as shown for N_2-337nm in Figure 6.4(a). The maximum values were found to be at the tip of the edge pins, where the electric field is highest. and where the border of the discharge zone meets the surrounding ambient air. Greater levels of N_2 are expected to be formed at the boundary, as there is lower quenching as a result of reduced reaction rates due to the electronegativity of other reactive species (i.e. O_3). The intensity of N_2^+, the only emission detected that belongs to the FNS, is shown in Figure 6.6(b). It follows a similar trend to that seen for N_2 of the SPS and the same reasoning can be applied. Figure 6.6(c) shows that the OH values are highest around the pin region and are relatively consistent throughout the rest of the discharge volume. This may be due to the interactions that occur between O, O_2, O_3, and H_2O. Although there is no detection of atomic oxygen, it is reasonable to assume that the majority of O_2 and O are converted to O_3. What remains from these reactions may still be in a sufficiently energetic state to dissociate H_2O due to its low excitation levels and give rise to the formation of more OH, as shown in equations 1-3, in which M is a third chemical constituent. In ambient air, M may be N_2^*, O, NO, NO_2, or OH. Figure 6.6(d) shows the EEDF of the system using the line ratio of (N_2-337 nm/N_2^+-391 nm) and highlights that the central locations are dominated by lower energy species when compared to N_2^+. These include N_2(SPS) and OH, which have excitation energies of 11 eV and 4.17 eV, respectively. This could be due to the quenching of N_2^+ in the interactions and mechanisms that form O_3, reducing the amount of detected emissions from this energetic species, due loss of energy through more collisional processes.

$$O_2 + e_{fast} \rightarrow O^* + O^* + e_{slow} \qquad (1)$$

$$O^* + H_2O \leftrightarrow 2OH \qquad (2)$$

$$O^* + O_2 + M^* \rightarrow O_3 + M \qquad (3)$$

Figure 6.6: OES measurements that show the spatial evolution of the emission species that were detected in this experiment and are (a) total intensity from the SPS (b) intensity of N_2^+ at 391 nm (c) intensity of OH measured at 300 nm and (d) the EEDF from the line ratio of (391/337) based on the values from (a) and (b).

Figure 6.7 shows the spatial evolution of O_3 and its average spatial density. It is shown that the highest values of O_3 are along the pin tips and throughout the central portion of the system, towards the ground plate. The likely reasons for this are twofold. Firstly, the edge of the system has high fluctuations of O_3, as it is at the boundary edge of the system, and the direct electric field. This gives less time for the reactive species to dwell within the electric field and maintain high energetic levels, and any O_3 generated is easily be dissociated through collisional processes with other atomic and molecular species, transferring its gained energy in the resulting kinetics. Secondly, the central part of the system will most likely have a better electric field distribution, exciting species to higher levels and allowing them to maintain such energetic states by allowing them to have a longer residence time in the direct electric field.
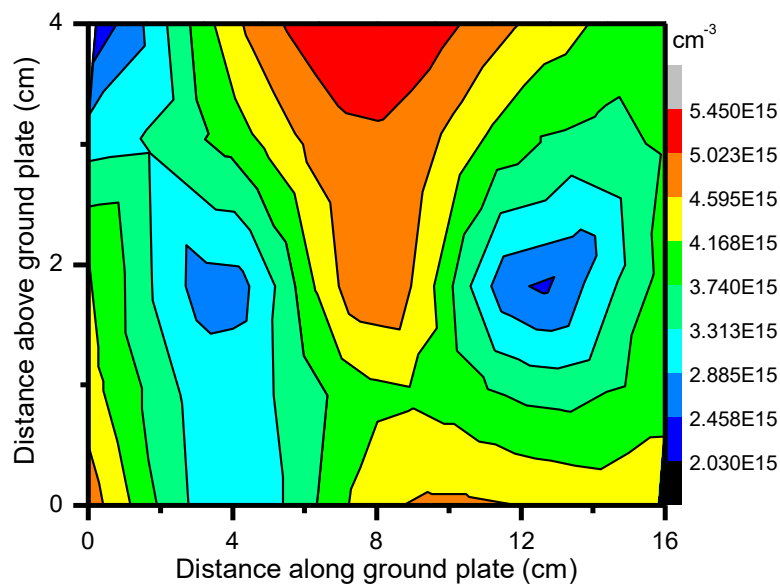
Figure 6.7: Spatial evolution of O_3 using the maximum value found after 300 s of discharge with the voltage set at 240 V and the duty cycle at 91 μs.
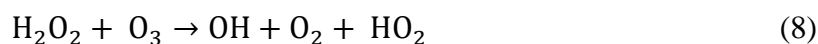
6.3.3 Reactive Species Formation in Liquids

The analysis of section 6.3.2.1 suggests that the characteristics of the plasma discharge are dependent on the discharge frequency, and that the optimal operation frequency is ~1000Hz. In terms of applications for treatment of cell cultures, the performance optimisation was therefore checked by monitoring the effects of the treatment on cell culture medium, by monitoring the production of several metastable species, namely nitrite, nitrate, and hydrogen peroxide in both deioinised (DI) water and DMEM cell culture medium. This was carried out as a function of discharge frequency at a fixed time of 5 minutes and also as a function of time at a fixed frequency of 1000 Hz. Figure 6.8 shows that the values of all species were highest at 1000Hz. Figure 6.9(a) indicates that this concentration increases monotonically over the exposure time of 0-320sec. For the case of nitrate species, the measurement similarly shows a maximum measured value at 1000 Hz, and an evolution which is continuing to increase after 320 sec exposure, as shown in Figure 6.9(b). A similar trend is shown for H_2O_2 generation. However, it can be seen that the production rate is maximum at the early stages of exposure and begins to saturate after 1-2 minutes. The results of the analysis further confirm the importance of discharge frequency for applications such as the treatment of biological samples.
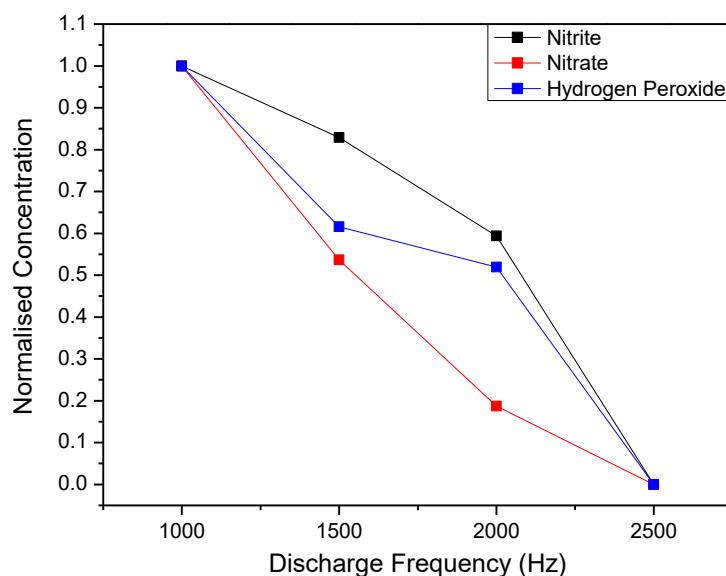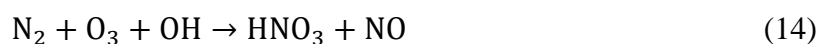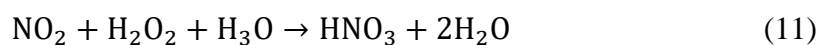
Figure 6.8: Normalised concentration values of the reactive species measures within media shows an optimisation of the plasma discharge at 1000 Hz.

The reactive species generated during plasma treatment undergo several chemical reactions to form ROS, such as OH and H_2O_2. The concentrations of H_2O_2 were seen to increase gradually with increased treatment time, up to ~140 uM after 320s treatment, in both deionised water and DMEM. Due to its short lifetime ($3.7{\times}10^{-9}$s), OH radicals diffusing from the plasma zone to the liquid interface undergo recombination to form hydrogen peroxide (oxidation potential 1.77 V)(Yan et al. 2015). Hydrogen peroxide in the sample solutions can be directly or indirectly generated via various reaction mechanisms (e.g., dissociation, photolysis), as described by Equations 4-8.

$$O_3 + OH \rightarrow HO_2 + O_2 \tag{4}$$

$$OH + OH \rightarrow H_2O_2 \tag{5}$$

$$O_2 + H \rightarrow HO_2 \tag{6}$$

$$H + HO_2 \rightarrow H_2O_2 \tag{7}$$

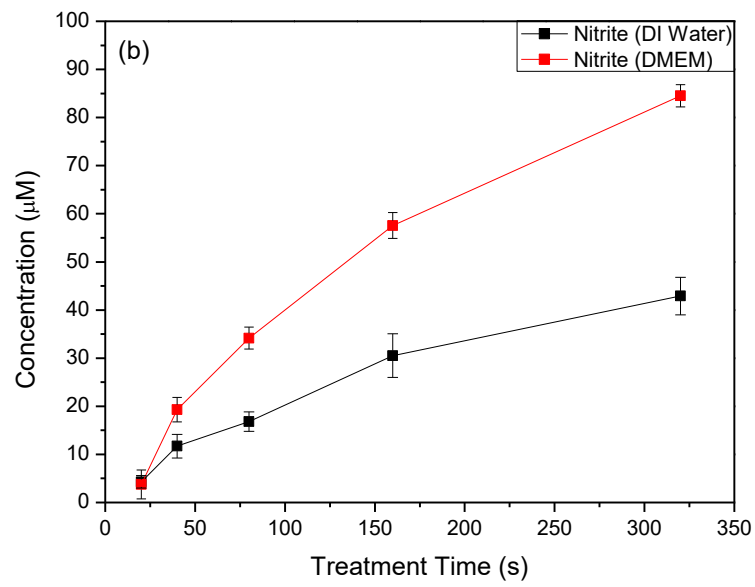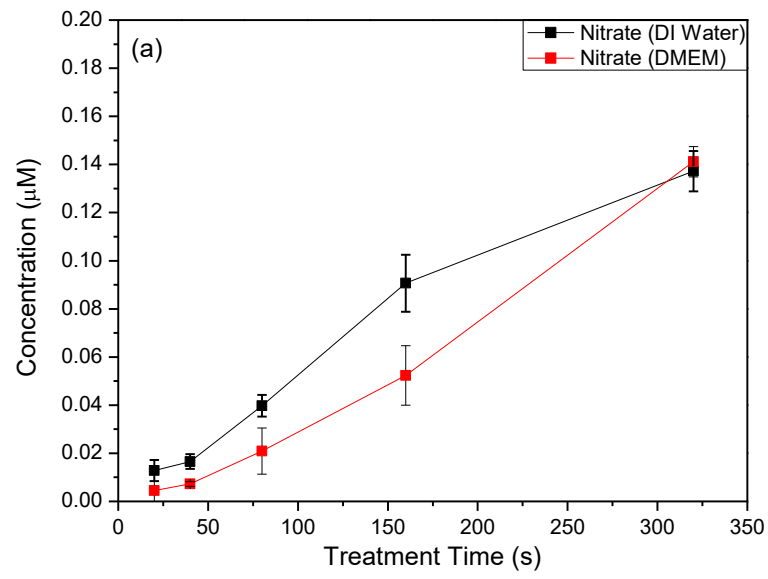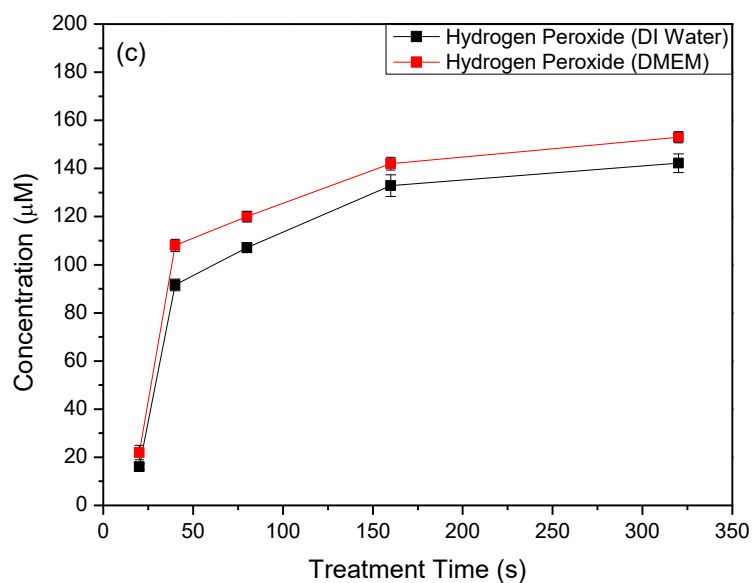$$H_2O_2 + O_3 \rightarrow OH + O_2 + HO_2 \tag{8}$$

As can be observed in Figure 6.9, there is an increase in the concentration of nitrates and nitrites in both deionised water and DMEM, which can significantly change both the fluid pH and electrical conductivity. The dissolution of nitrate to form nitric acid can be explained by reaction mechanisms 9 to 14. During plasma treatment, the production of NO mainly follows the Zeldovich mechanism (Yan et al. 2015). The NO formed can be oxidised to NO_2. NO and NO_2 can subsequently dissolve in water to form nitrates and nitrites (HNO_3, NO_3, and NO_2)(Lu, et al. 2017). Given that there was no emission detected for NO and there were no levels of NO_2 detected through the use of Dräger detection tubes, they either form and interact immediately with other species and have their lifetime reduced or are generated predominantly at the plasma-media boundary. From the concentrations measured, the reaction pathways that generate H_2O_2 may be the most dominant interactions at the boundary. Reaction mechanisms 15 - 16 are then suggested as possible pathways.

$$N_2 + e \rightarrow 2N + e \tag{9}$$

$$N + 2O \rightarrow NO_2 \tag{10}$$

$$NO_2 + H_2O_2 + H_3O \rightarrow HNO_3 + 2H_2O \tag{11}$$

$$HNO_3 + 2H_2O \rightarrow NO_3 + H_3O \tag{12}$$

$$NO_2 + OH \rightarrow HNO_3 \tag{13}$$

$$N_2 + O_3 + OH \rightarrow HNO_3 + NO \tag{14}$$

$$HNO_3 + OH \rightarrow H_2O_2 + NO_2 \tag{15}$$

$$HNO_3 + O_2 \rightarrow H_2O_2 + NO_3 \tag{16}$$

$$HNO_3 + O_2 \rightarrow H_2O_2 + NO_3 \tag{16}$$

Figure 6.9: Changes in the formation of reactive oxygen and reactive nitrogen species over time in deionised water and DMEM with settings at 240 V, 74 µs, and 1000 Hz

6.3.4 Cancer cell cytotoxicity

From the optical plasma diagnostics data and chemical analyses of plasma treated DI water and DMEM, the optimal frequency for generating the gas chemistry with the highest concentration of both ROS and RNS is 1000 Hz. Varying the voltage and duty cycle can be shown to significantly affect the levels, but, comparably, the discharge frequency has the largest impact for plasma discharge optimisation.
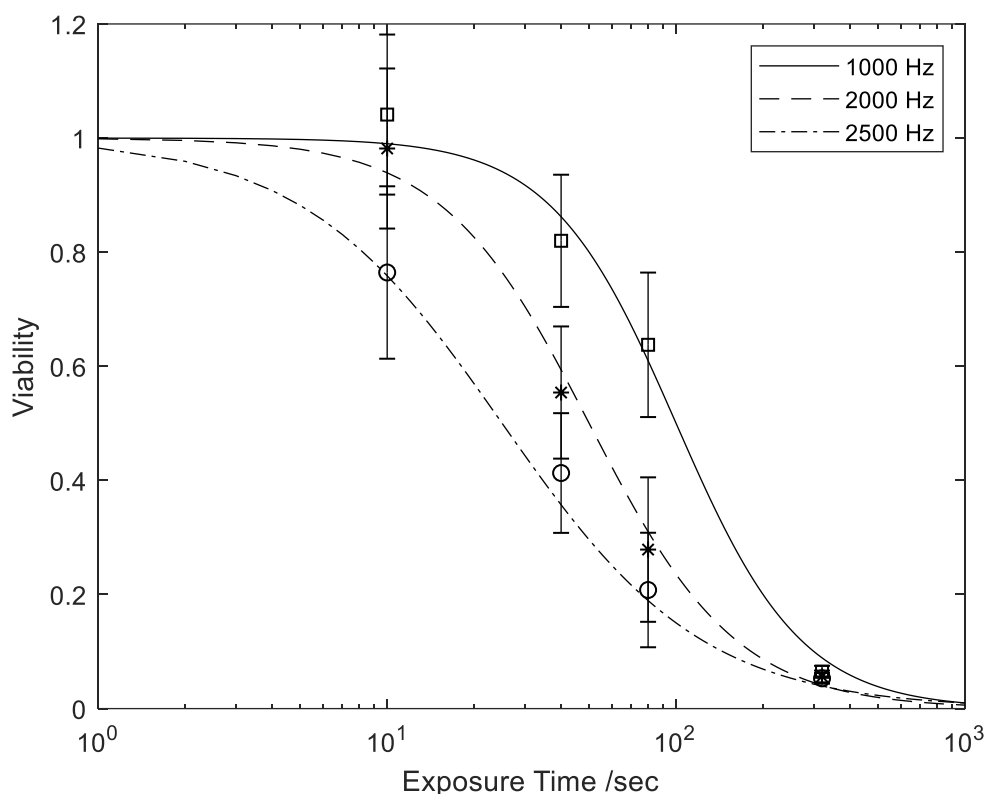
Figure 6.10: Cytotoxic effects of the pin-to-plate device on U373MG human multiforme glioblastoma cells with different discharge frequencies.

To confirm these findings, U373MG human multiforme glioblastoma cells were exposed to plasma generated at 240V, of discharge frequency varied from $1000-2500$ Hz and a duty cycle of 72 µs, for between 0s and 320s. In all cases, a dose dependent cytotoxicity is evident after 96 hours, when measured using the Alamar Blue cell viability assay. In terms of cancer cell line treatment, it can be seen from Figure 6.10 that the use of a plasma discharge frequency of 1000 Hz has the highest cytotoxic impact. Using a 4-parameter nonlinear logistic equation, the IC_{50} in pyruvate-free media was measured to be ~25 sec. The observations are consistent with the observations of Section 6.3 (Figure 6.8), that a discharge frequency of 1000Hz produced the higher amount of all reactive species measured within the culture

medium, and that these generated amounts increased monotonically over the timescale 0-320sec.

6.4 Conclusion

The optical diagnostics of the large gap atmospheric plasma discharge demonstrated that the discharge frequency plays a vital role in the formation of the reactive species. As the frequency was increased, it was found that the optimal discharge frequency was 1000 Hz, as this produced the greatest combination of RNS and ROS within the plasma. However, at higher frequencies, the emission intensities recorded through OES diminished and were not easily detected above 1500 Hz. This was not the case for the detection of O_3, as large levels were still generated even when approaching a discharge frequency of 2500 Hz. This allows for a tailoring of the gas chemistry to produce relatively higher ROS levels over RNS without changing the atmospheric conditions or gas, allowing for dynamic settings to be used for sample treatments or to highlight which reactive species plays a dominant role for different effects. It has also been shown that, although there were higher emission intensities found at the edge of the pin region, a greater density of O_3 was measured in the central region of the system, the area above the placement of the 96-well plate had little variance and allows for a consistent and homogeneous treatment at the sample/plasma boundary. It has been demonstrated that the generation of RNS and ROS in cell culture medium by the plasma is also highly dependent on the plasma discharge frequency, as is the cytotoxicity to human cancer cell lines. The study demonstrates the importance of appropriate plasma diagnostics and the impact of the plasma generation conditions for potential biomedical applications of this highly promising emerging technology.

Acknowledgements

Author Contributions

L.S., P.C. and J.C. conceived the project and designed the experiments. L.S., S.B., and A.C. performed the experiments, and collected and analysed the data. B.J, R.M., P.C, H.B. and J.C. co-wrote the paper. All authors discussed the results and reviewed the manuscript.

Conflict of interest

Author PJ Cullen is CEO of PlasmaLeap Technologies, the supplier of the plasma equipment used in this study.

References

P. Babington, K. Rajjoub, J. Canady, A. Siu, M. Keidar, and J. H. Sherman, *"Use of Cold Atmospheric Plasma in the Treatment of Cancer"*, AVS: Biointerphases, **10**, (2015).

A. Begum, M. Laroussi, and M. R. Pervez, "*Plasma Jet: Breakdown Process and Propagation Phenomenon*", AIP Advances, **3**, (2013).

D. Boehm, C. Heslin, P. J. Cullen, and P. Bourke, *"Cytotoxic and Mutagenic Potential of Solutions Exposed to Cold Atmospheric Plasma"*, Scientific Reports, **6**, (2016).

R. Brandenburg, "*Dielectric Barrier Discharges: Progress on Plasma Sources and on the Understanding of Regimes and Single Filaments*", Plasma Sources, Science, and Technology, **26**, (2017).

H. Chugh, D. Sood, I. Chandra, V. Tomar, G. Dhawan, and R. Chandra, "*Role of Gold and Silver Nanoparticles in Cancer Nano-Medicine*", Artificial Cells, Nanomedicine, and Biotechnology, **46**, (2018).

S. Cui, R. Hao, and D. Fu, "*Integrated Method of Non-Thermal Plasma Combined with Catalytical Oxidation for Simultaneous Removal of SO$_2$ and NO*", **246**, Fuel, Elsevier, (2019).

X. T. Deng and M. G. Kong, "*Frequency Range of Stable Dielectric-Barrier Discharges in Atmospheric He and N2*", IEEE Transactions on Plasma Science, **22**, (2004).

List of Publications

L. Scally, J. Lalor, P. J. Cullen, and V. Milosavljević, "Impact of atmospheric pressure nonequilibrium plasma discharge on polymer surface metrology"Journal of Vacuum Science and Technology A: Vacuum, Surfaces, and Films 35, 105 (2017).

L. Scally, J. Lalor, M. Gulan, P. J. Cullen, and V. Milosavljević, "Spectroscopic study of excited molecular nitrogen generation due to interactions of metastable noble gas atoms", Plasma Processes and Polymers. 2018;e1800018.

L. Scally, M. Gulan, L. Weigang, P. J. Cullen, V. Milosavljevic, "Significance of a Non-Thermal Plasma Treatment on LDPE Biodegradation with Pseudomonas Aeruginosa", MDPI Materials, 11, 1925, (2018).

P. J. Cullen, J. Lalor, L. Scally, D. Boehm, V. Milosavljević, P. Bourke, and K. Keener, "Translation of plasma technology from the lab to the food industry", Plasma Processes and Polymers, 2017;e1700085.

J. Lalor, L. Scally, P. J. Cullen, and V. Milosavljević, "Impact of plasma jet geometry on residence times of radical species", Journal of Vacuum Science and Technology A: Vacuum, Surfaces, and Films, **36**(5), (2018).

Conferences and poster presentations

Poster presentation: L. Scally (Presenter), J. Lalor, M. Gulan, P. J. Cullen, and V. Milosavljević, "Deriving a correlation between the emission intensities of molecular nitrogen species and the metastables of argon and helium using optical spectroscopy", IOP Quantum, Atomic, and Molecular Physics 2017 (QUAMP 2017).

Oral presentation: V. Milosavljević (Presenter), L. Scally, J. Lalor, and P. J. Cullen, "Fundamental characterization of a low frequency, ambient air, plasma jet discharge", AVS 63rd International Symposium & Exhibition, Nashville, Tennessee, USA, PS+AS+SE+MoM3 p.14-15 (2016).

Oral presentation: V. Milosavljević (Presenter), J. Lalor, L. Scally, and P. J. Cullen, "Study of atmospheric-pressure kHz multi-jet plasma system", AVS 64th International Symposium & Exhibition, Tampa, Florida, USA, PS+AS+SE-MoM1 p.14 (2017).